Characterization of the RCF1 Q-X3-R-X-R-X3-Q Motif and Its Role in Supporting Oxidative Phosphorylation Enzyme Complexes

Joshua Garlich
Marquette University

CHARACTERIZATION OF THE RCF1 Q-X3-R-X-R-X3-Q MOTIF AND ITS ROLE IN SUPPORTING OXIDATIVE PHOSPHORYLATION ENZYME COMPLEXES

By

Joshua Garlich

A dissertation submitted to the Faculty of the Graduate School,

Marquette University,

in Partial Fulfillment of the Requirements for

the Degree of Doctor of Philosophy

Milwaukee, Wisconsin

December 2016

ABSTRACT
CHARACTERIZATION OF THE RCF1 Q-X3-R-X-R-X3-Q MOTIF AND ITS ROLE IN SUPPORTING OXIDATIVE PHOSPHORYLATION ENZYME COMPLEXES

Joshua Garlich

Marquette University, 2016

Mitochondrial respiratory complexes are critical components of cellular energy production that require tight regulation to ensure optimal function. Rcf1 and Rcf2 are mitochondrial proteins that can physically associate with the yeast respiratory complexes III and IV, and the higher-ordered III-IV respiratory supercomplex that also contains the ADP/ATP translocase, AAC. Rcf1 can physically associate with both complex III and IV independently, and can be chemically crosslinked to AAC, indicating a close physical proximity to a predominant regulator of energy flux within the cell. It was therefore hypothesized that Rcf1, through its physical association with complexes III and IV, and its close proximity to AAC, may possess the capacity to communicate with multiple components of supercomplexes, a feature which may be important for coordinated regulation of the respiratory enzymes.

The goal of this dissertation was to characterize the importance of an evolutionarily conserved motif, referred to here as the Q-X3-R-X-R-X3-Q (QRRQ) motif, within Rcf1 that defines it as a member of the Hypoxia-induced gene 1 (Hig1) protein family. To investigate the functional significance of the QRRQ motif, His-tagged Rcf1 proteins harboring mutations in the QRRQ motif were generated and expressed these in a yeast strain devoid of Hig1 proteins (*Δrcf1Δrcf2*). The importance of the QRRQ motif for the function of yeast Rcf1 was explored. I was found that mutations in conserved residues of the QRRQ motif affect the organization of the III-IV supercomplex and lead to the assembly of a novel Rcf1-complex IV subpopulation that displays altered enzymatic properties. The QRRQ motif impacts the ability of Rcf1 to associate with assembled complex IV and newly-synthesized unassembled Cox3, a core subunit of complex IV. Additionally, it was determined that Rcf1 exists in close physical proximity to Cox2, a catalytically important subunit of complex IV. It was found that the QRRQ motif influences the molecular environment of Rcf1 including its relationship to AAC proteins and possibly the cardiolipin-remodeling enzyme TAZ. Based on these findings, a model of the Rcf1-complex IV binding site is proposed and it is speculated that Rcf1 functions to modulate the complex IV enzyme activity and supercomplex organization.

ACKNOWLEDGEMENTS

Joshua Garlich

I would like to begin by expressing my sincere gratitude to my doctoral supervisor, Dr. Rosemary Stuart, for accepting me as a student in her lab and guiding my development as a scientist. Rosemary's encouragement, patience, and intellectual stimulation were pivotal to my development as an independent researcher. She provided me the space to grow intellectually, while constantly challenging me to expand my thinking when interpreting results. Her contributions in shaping and editing this written dissertation were invaluable, and I am indebted to her for all of her thoughtful guidance.

I would like to thank the members of my dissertation committee; Dr. Allison Abbott, Dr. Stephen Downs, Dr. Dale Noel, and Dr. Martin St. Maurice. Their guidance and direction enriched the breadth and depth of my dissertation research and I am sincerely grateful for the intellectual contributions that they provided during my dissertation study.

I would like to thank the members of the Stuart lab, both past and present, for patiently teaching me new techniques, offering their time and talents to discuss experimental design and results, and for the genuine camaraderie and friendship that they have offered. I would like to express my sincere gratitude to the current lab members, Vera Strogolova, Jodie Box and Jessica Anderson, and to acknowledge past members Sneha Potdar, Hanting Tsai, Dr. Jasvinder Kaur, Micaela Robb Bowers, Katelin Krenzke, Jonathan Scheel and Dr. Angela Tollefson. In particular, I would like to acknowledge the exceptional work that Phoebe (Hanting) Tsai contributed to this dissertation study as a

student in the lab. Phoebe generated the mutations in the Rcf1 PXVPXG motif and characterized the resulting Rcf1 mutant derivatives.

I am grateful for the friendships that I have developed among both faculty and students within the Department of Biological Sciences. I would like to acknowledge in particular Vera Strogolova and Dr. Zac Lunak for their friendship and for being constant sources of intellectual stimulation. Our conversations greatly contributed to my analytical thinking about this dissertation study.

I would like to acknowledge the following collaborators and colleagues: Dr. Ilka Wittig (Goethe-Universität, Frankfurt Germany), Dr. Steven Claypool (Johns Hopkins University School of Medicine), Dr. Alexander Tzagoloff (Columbia University), Dr. Maria Bohnert (Universität Freiburg, Freiburg Germany), Dr. Kathleen Noon (Medical College of Wisconsin) for providing mass spectrometry analysis, lipid analysis, yeast strains and antibodies.

I would like to thank the Arthur J. Schmitt Foundation for a generous fellowship, as well as the opportunity to grow as a leader and mentor.

I would like to thank my family. My parents, Don Garlich and Robyn Parker have been a constant source of love and encouragement throughout my life, and its because of their support, patience, and wisdom that I am here today. I want to thank my sisters, Emily and Laura, for their love and support.

Finally, I would like to acknowledge Jackie Garlich, who I am beyond proud to call my wife. Jackie has encouraged and supported me, especially during my time at Marquette while completing my PhD. Her genuine, selfless commitment to others is evident in each of the many roles that she seamlessly weaves between, from committed

practitioner, to loving wife, and devoted mother to our beautiful children, Cal and Naomi. This dissertation is dedicated to Jackie, Cal and Naomi.

TABLE OF CONTENTS

ACKNOWLEGEMENTS…….....i

LIST OF TABLES……x

LIST OF FIGURES……... xi

CHAPTER 1: INTRODUCTION……...1

1.1 Chapter Overview…….. 1

1.2 Origin and Function of Mitochondria…… 2

1.3 Oxidative Phosphorylation…….3

1.4 Complex IV……7

1.4.1 Complex IV Overview……7

1.4.2 Complex IV Polypeptide Composition……...7

1.4.3 Heme and Copper Reactive Centers of Complex IV……..... 10

1.4.4 Complex IV Assembly……...11

1.4.5 General Functions of Complex IV……13

A. Oxidation/Reduction Reactions of complex IV…… 13

B. Proton Pumping by complex IV……14

1.5 The Complex III–Complex IV Supercomplex……...15

1.5.1 Respiratory Supercomplex Overview ……15

1.6 Respiratory Supercomplex Factor 1 (Rcf1) Characterization…….... 19

1.6.1 Rcf1 Protein Overview…….. 19

1.6.2 Identification of *Saccharomyces cerevisiae* Rcf1 as a Respiratory Supercomplex-associated Protein ……..20

1.6.3 Characterization of Rcf1 Membrane Topology…… 21

1.6.4 Hypoxia induced gene family domain of Rcf1……..21

1.6.5 Yeast Hig1 Homologs Rcf1 and Rcf2 Contain……. 23
Overlapping Function

A: Identification of Rcf2……23

B: The Absence of *S. cerevisiae* Hig1-type 2 Proteins……..24
Rcf1 and Rcf2 Results in a Respiration-based
Growth Deficiency

C: Rcf1 and Rcf2 Cooperatively Influence the Activity…....24
of Complex IV, and their Absence Results in an
Aerobic Growth Deficiency that Cannot be
Explained by Complex IV Impairment
Alone

D: Mitochondria from the Δ*rcf1;*Δ*rcf2* Strain Appear…….. 25
to Contain Hyperactive O_2 Consumption Rates
Despite a Reduction in Complex IV Protein

E. Rcf1 Associates with Complex IV and Complex III…… 27
Independently, Likely Through an Association with
Newly-synthesized Cox3

F. The Assembly of Complex IV and its Association……29
with Complex III is Altered in the Absence of Rcf1
and Rcf2

G. Rcf1 Associates with AAC Proteins, and Rcf1 and……..31
AAC Exhibit a Close Physical Relationship

H. Rcf1 and Rcf2 Have Been Reported to Function in……. 32
Cellular Mediation of Oxidative Stress

1.7 Yeast as a Model System……33

1.8 Dissertation Study Aims…… 34

CHAPTER 2: MATERIALS AND METHODS……... 35

2.1 Chapter Introduction……... 35

2.2 Molecular and Cellular Biology Methods……. 35

2.2.1 Polymerase Chain Reaction (PCR) and PCR-mutagenesis……35

2.2.2 Restriction Digestion and Transformation into *E. coli*…….. 40

2.2.3 Isolation of Plasmid DNA……. 41

2.2.4 Plasmid DNA Linearization and Transformation into Competent Yeast Cells……...41

2.2.5 Cloning of Human Hig1-1A and Hig1-2A…… 42

2.2.6 Isolation of Mitochondria: Long, and Quick-Long, and Quick Preparation……48

2.2.7 Serial Dilution Growth Analysis……50

2.3 Protein Biochemistry and Physiology Methods…….51

2.3.1 Protein Determination (Bradford Method)…… 51

2.3.2 SDS-PAGE……..52

2.3.3 Western Blotting: Transfer of SDS-PAGE Gel to Nitrocellulose Membrane…… 52

2.3.4 Western Blotting: Immuno-decoration of Nitrocellulose Membrane….. 53

2.3.5 BN-PAGE and 1D BN-PAGE/2D SDS-PAGE……. 54

2.3.6 Steady State Analysis of Mitochondrial Proteins…….. 56

2.3.7 Ni-NTA Affinity Purification of His-tagged Proteins…….. 56

2.3.8 Chemical Cross-linking……..57

2.3.9 Mitochondrial *In organello* Labeling of Mitochondrial Translation Products…… 59

2.3.10 Silver Staining of SDS-PAGE Gels……...60

2.3.11 Cytochrome *c* oxidase ‘In Gel’ Activity Assay……. 61

2.3.12 Oxygen Consumption Rates (OCR)……...62

2.4 Miscellaneous…… 62

2.4.1 Yeast Strains and Growth Conditions……62

2.4.2 Preparation of Yeast and Bacterial Competent Cells…….64

2.4.3 Maintenance of Yeast and Bacterial Strains…….. 65

2.4.4 Primer Design and Sequence Analysis…….. 65

2.4.5 Sequence Alignment…….. 66

2.4.6 Structure Modeling…… 66

CHAPTER 3: MUTATIONAL ANALYSIS OF THE HIG1-TYPE 2 QRRQ MOTIF IN *S. CEREVISIAE* RCF1 …….. 67

3.1 Introduction……67

3.2 Chapter 3 Results……... 72

3.2.1 Expression of Rcf1 QRRQ Mutant Derivatives…….72

3.2.2 Expression of *rcf1*$_{\text{His}}^{\text{R67A}}$ Alters the Complex IV…….. 74
Assembly State

3.2.3 The QRRQ Motif Influences the Association of Rcf1 with…….. 82
Complex IV, in Particular with the Cox12 and
Cox3 Subunits

3.2.4 The complex IV in Mitochondria Harboring the *rcf1*$_{\text{His}}^{\text{R67A}}$ …… 86
Derivative Displays Altered Enzymatic Properties

3.2.5 Rcf1 May be Involved in Post-translational Modification…… 91
of Complex IV

3.2.6 Rcf1 Associates with a Cardiolipin-binding Protein of …… 94
Complex III

3.2.7 Comparative Analysis of Hig1-type1 and Hig1-type2……..... 96
Proteins and their Association with
Complex IV

3.2.8 Analysis of the Molecular Environment of the Rcf1 QRRQ Motif 101

3.2.9 Investigation of the Protonation State of R67 in Influencing the Molecular Interactions of the Rcf1 Protein 107

3.3 Chapter 3 Summary 115

CHAPTER 4: CHARACTERIZATION OF THE MOLECULAL ENVIRONMENT OF RCF1 AND AAC 117

4.1 Introduction 117

4.2 Chapter 4 Results 129

4.2.1 Independent Verification of the $Rcf1_{His}$-AAC MBS Cross-link Via LC-MS/MS 129

4.2.2 Characterization of N-terminal Amino Acid Residues of Rcf1 and their Influence on the Molecular Environment of Rcf1 and AAC 130

4.2.3 The Integrity of the Rcf1 QRRQ Motif Alters the Molecular Interaction Between Rcf1 and AAC 134

4.2.4 The Bio-Energetic State of the Mitochondria Influences the Ability of Rcf1 and AAC Proteins to be Cross-linked 136

4.2.5 The Ability of Rcf1 to be Cross-linked to AAC is Dependent Upon the Conformational State of AAC 137

4.2.6 The Molecular Environment of Rcf1 and AAC is Altered in the Absence of Cardiolipin 140

4.2.7 The Native Gel Mobility of AAC is Influenced by the Presence of Rcf1 and Rcf2 143

4.3 Chapter 4 Summary 145

CHAPTER 5: DISCUSSION 148

5.1 Introduction……148

5.2 The Role of Rcf1 in Supporting Complex IV Activity……. 142

5.3 The Role of Rcf1 in Supporting AAC……... 151

5.4 Rcf1 and the Lipids Associated with Complex IV and AAC…… 154

5.5 The Role of the Rcf1/Hig1 QRRQ Motif…….. 158

5.6 Comparison of Hig1-type 1 and -type 2 Isoforms……. 166

5.7 The Role of Hig1 Proteins in Hypoxia and Stress Conditions……...169

5.8 Model of the Proposed Role of Rcf1/Hig1 Proteins…….. 174

REFERENCES ……....175

LIST OF TABLES

TABLE 1 SEQUENCE OF PCR PRIMERS USED IN THIS STUDY……36

TABLE 2 YEAST STRAINS USED IN THIS STUDY ……... 63

LIST OF FIGURES

FIGURE 1 Overview of the Mitochondrial Structure…….. 4

FIGURE 2 The Mitochondrial Oxidative Phosphorylation Enzyme……... 6
Complexes

FIGURE 3 Cytochrome *c* oxidase (Complex IV) is a Multi-subunit……...8
Enzyme Complex

FIGURE 4 Respiratory Supercomplex Factor 1 (Rcf1) is an Integral……. 22
Inner Mitochondrial Membrane Protein

FIGURE 5 The Yip351 Plasmid Featuring a Single BsteII Site and……... 44
LEU2 Gene

FIGURE 6 The pDNR-LIB Plasmid Featuring Single Xba1 and Pst1…… 45
Sites

FIGURE 7 The pOTB7 Plasmid Featuring Single Xba1 and Pst1…….. 46
Sites

FIGURE 8 Rcf1 is an Inner Mitochondrial Membrane Protein and a……. 73
Member of the Hig1-type 2 Protein Family that Contain
a Conserved QRRQ Motif

FIGURE 9 Mutation of the Rcf1 QRRQ Motif Affects the Stability…….. 75
But Not the Assembly of Complex IV

FIGURE 10 Compositional Analysis of the Complex IV** Subpopulation……..79

FIGURE 11 2 Dimension (1D BN-PAGE/2D SDS-PAGE) Analysis of the…….81
Complex IV** Subpopulation

FIGURE 12 Mutation of the QRRQ Motif Affects the Association of Rcf1…….83
With Cox3 and Complex IV

FIGURE 13 Mutation of the QRRQ Motif Affects the Association of Rcf1…….85
With Newly-synthesized Cox3

FIGURE 14 Complex IV in *rcf1*$_{\text{His}}^{\text{R67A}}$ Mitochondria Displays Altered……... 88
Catalytic Properties

FIGURE 15 The *rcf1*$_{His}^{R67A}$ Mutant Derivative Associates With the…… 90
Cardiolipin Remodeling Enzyme, Taz1

FIGURE 16 Mutation of the QR Pairs in the QRRQ Motif in Rcf1 Affects……. 92
the Stability of Rcf1, But Complex IV Assembles

FIGURE 17 Mutation of the QR Pairs in the QRRQ Motif in Rcf1 Does…….95
Not Negatively Affect the Catalytic Activity of Complex IV

FIGURE 18 Rcf1 Associates with the Complex III Cardiolipin-associated……..97
Subunit, Cytochrome c_1

FIGURE 19 Hig1-type 1 and –type 2 Proteins Display Contrasting Levels……..99
of Association with Complex IV

FIGURE 20 Cysteine Mutation of Residues Within, and Adjacent to, the……102
Rcf1 QRRQ Motif

FIGURE 21 Cysteine-based Scanning Analysis of the Molecular…….104
Environment of the Rcf1 QRRQ Motif

FIGURE 22 Liquid Chromatography- (tandem) Mass Spectrometry…… 106
Identification of an Rcf1-Rcf1 Dimer

FIGURE 23 Charge-altering Mutations in Rcf1 R67 Do Not Negatively……. 108
Affect the Assembly State of Complex IV or the
Assembly of Complex IV with Complex III, in
Contrast to the Size-altering R67A Mutation

FIGURE 24 Charge-altering Mutations in Rcf1 R67 Affect the Association…...110
of Rcf1 with Complex IV

FIGURE 25 A Charged Rcf1 R67 Residue Affects the Catalytic Properties…… 112
of Complex IV

FIGURE 26 Mutation of R67 Affects the Molecular Environment of Rcf1……..114
and Cox2

FIGURE 27 Inhibitors of AAC Lock the Translocase in Specific ……119
Conformational States

FIGURE 28 The Yeast ADP/ATP Carrier, Aac2……...121

FIGURE 29 Rcf1 Cysteine Residues Influence the Molecular Environment…… 132
of Rcf1 and AAC

FIGURE 30 Rcf1 R67 Influences the Molecular Environment of Rcf1 and AAC 135

FIGURE 31 The Bio-energetic State of the Mitochondria Influences the Ability of Rcf1 and AAC Proteins to be Cross-linked 138

FIGURE 32 The Ability to Cross-link Rcf1 and AAC is Dependent Upon the Structural Conformation of the AAC Protein 139

FIGURE 33 The Molecular Environment of Rcf1 and AAC is Altered in the Absence of Cardiolipin 142

FIGURE 34 The Native Gel Mobility of AAC is Altered in the Absence of Rcf1 and Rcf2 144

FIGURE 35 Predicted Model and NMR Structure of the *S. cerevisiae* Rcf1 Protein 160

FIGURE 36 Proposed Role of the QRRQ Motif in Influencing the conformation of Rcf1 162

FIGURE 37 Proposed Rcf1-Complex IV Interface 172

FIGURE 38 Model of Speculated Rcf1 Function 173

CHAPTER 1: INTRODUCTION

1.1 Chapter Overview

Cytochrome *c* oxidase (complex IV) is the terminal enzyme complex of the mitochondrial electron transport chain and couples the reduction of oxygen to water to the pumping of protons across the inner mitochondrial membrane. In yeast, as in many eukaryotic taxa, cytochrome *c* oxidase can assemble into higher ordered structures termed supercomplexes with other respiratory enzymes. Respiratory supercomplex factor 1 (Rcf1) was recently described as an integral inner mitochondrial membrane protein that influences the activity of complex IV, the assembly state of complex IV-containing respiratory supercomplexes, and the mitigation of mitochondrial oxidative damage. Rcf1 is a member of a highly conserved sub-set of homologous proteins that contain a hypoxia-induced protein conserved region (Hig1) domain, and are functionally related in their regulation of complex IV activity and supercomplex organization. However, the molecular basis underlying the conserved functions of Hig1 proteins is not understood. To gain insight into the molecular underpinnings of Hig1 proteins, the conserved Hig1 domain region and the molecular environment of Rcf1 were characterized in this dissertation. Conserved regions of Rcf1 were analyzed to determine their contribution to Rcf1 interactions and function. Additionally, the relationship between Rcf1 and the mitochondrial ADP/ATP carrier protein was explored in this study. To that end, this chapter will provide background information regarding complex IV and complex IV - containing supercomplexes, as well as a short review on the Rcf1 protein and the larger Hig1 domain protein family in order to aid in understanding this dissertation study.

1.2 Origin and Function of Mitochondria

Mitochondria are essential eukaryotic organelles that are enclosed by a double membrane system. The inner membrane separates the center of the mitochondria, referred to as the matrix, from the intermembrane space that lies between the inner and outer membranes (Figure 1). As most cellular organelles contain a single-layered membrane, the double-membrane compartmental architecture is a unique feature of mitochondria and is directly related to its most well known function, the aerobic production of cellular energy through respiration.

It is generally accepted that mitochondria arose from an alpha-proteobacterium engulfed by an ancestral eukaryotic precursor cell during a critical time period when the earth was becoming increasingly oxygenated (Lane and Martin, 2010). It is proposed that this atmospheric transitional period for earth was uniquely optimal for the transformation of endosymbiotic bacteria, going from an oxygen "scavenging" partner to a permanent cellular organelle that functions as an oxygen-utilizing specialist in energy production. During evolution, much of the bacterial genome was transferred to the nucleus of the eukaryotic cell, but mitochondria have retained a small circular genome of deoxyribonucleic acid (mtDNA) that encodes for a small, but critical subset of OXPHOS complex subunits.

Mitochondria perform a diversity of functions that include steps in the catalytic pathways of heme biosynthesis, urea cycle, Krebs cycle, fatty acid metabolism and the biosynthesis of phospholipids, amino acids and nucleotides (Nunnari and Suomalainen, 2012; Saraste, 1999; Scheffler, 2001). Moreover, mitochondria have been shown to play an important role in ageing, apoptosis, cancer, cellular Ca^{2+} flux, ROS homeostasis, and

the assembly of iron-sulfer clusters (Cui et al., 2012; Demaurex et al., 2009; Lill and Mühlenhoff, 2008; Wallace, 2005). However, these functions are often eclipsed by mitochondria's most prominent role as the primary means of aerobic energy production by a process known as oxidative phosphorylation.

1.3 Oxidative Phosphorylation

Oxidative phosphorylation (OXPHOS) couples the establishment of an electrochemical proton gradient to the generation of adenosine triphosphate (ATP). The mechanistic underpinnings of this critical cellular process were first proposed through the chemiosmotic coupling theory, in a series of seminal papers by Peter Mitchell (Mitchell, 1961, 1966, 1968). The chemiosmotic theory posits that enzymes of the electron transfer chain facilitate the unidirectional movement of protons across a membrane, establishing an electrochemical gradient ($\Delta pH + \Delta\Psi$) that drives the synthesis of ATP from adenosine diphosphate (ADP) and inorganic phosphate (Pi) by ATP-synthase (Mitchell, 1966). The enzymes involved in this cellular energy pathway, referred to as complexes I-IV, include: NADH-ubiquinoe oxidoreductase (complex I), succinate dehydrogenase (complex II), cytochrome bc_1 reductase (complex III); and cytochrome *c* oxidase (complex IV). Yeast, the model organism of this study, does not contain the traditional complex I, but rather, has alternative internal and external NADH dehydrogenases. Respiratory enzyme complexes are embedded within the inner mitochondrial membrane and facilitate the oxidation of reducing equivalents Nicotinamide Adenine Dinucleotide, reduced (NADH) and Flavin adenine dinucleotide, reduced ($FADH_2$)(Figure 2). In the final steps of this

A.

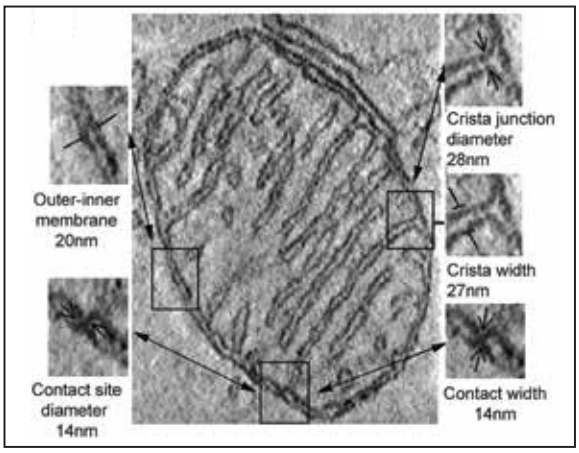

B.

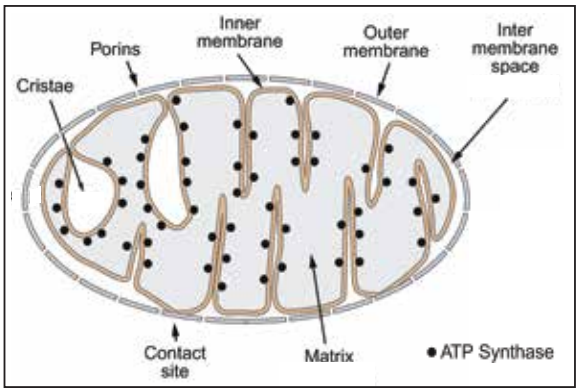

Figure 1. Overview of the Mitochondrial structure. (A) Transmission electron microscopy image of a mitochondrion, highlighting the ultrastructure and measurmements of unique features of the double-membrane system. (Nicholls and Ferguson, Bioenergetics, Academic Press, 4th Edition, 2013). **(B)** Mitochondria are double membraned organelles and the architecture of the inner membrane divideds the mitochondrion into separate compartments of the intermembrane space and matrix (Modified from Nicholls and Ferguson, Bioenergetics, Academic Press, 4th Edition, 2013).

process, the soluble iron-containing electron carrier, cytochrome *c*, mediates the transfer of electrons from complex III to complex IV, which donates electrons to molecular oxygen (O_2) forming water (Fontanesi et al., 2008; Mick et al., 2011; Schägger, 2002; Tsukihara et al., 1996) Complex III and complex IV (in addition to the traditional complex I enzyme) couple electron transfer to the translocation of protons across the inner mitochondrial membrane from the mitochondrial matrix to the intermembrane space (IMS), resulting in an electrochemical gradient within the IMS (Brandt , 1994; Hatefi, 1985; Wikstrom, 1977). The proton gradient is utilized by the F_1F_O -ATP synthase, and provides the energy necessary to generate ATP from ADP and inorganic phosphate (Pi) (Saraste, 1999).

Mitochondrial OXPHOS is the preeminent source of ATP for the vast majority of cellular processes. Not surprisingly, mitochondrial O_2 dysregulation and oxidative stress are distinct features of diverse pathologies including cancer, aging, ischaemic heart disease and diabetes (Fernyhough et al., 2010; Jarrett et al., 2010; Ren et al., 2010; Sas et al., 2010; Wallace, 2005). Additionally, mitochondrial dysfunction and reduced bioenergetic capacity underlie numerous muscular and neurological diseases (Ferreira et al., 2010; Kawamata and Manfredi, 2010; Kones, 2010; Waldbaum and Patel, 2010). Therefore, understanding how mitochondria regulate OXPHOS is paramount to understanding health and disease at the cellular level.

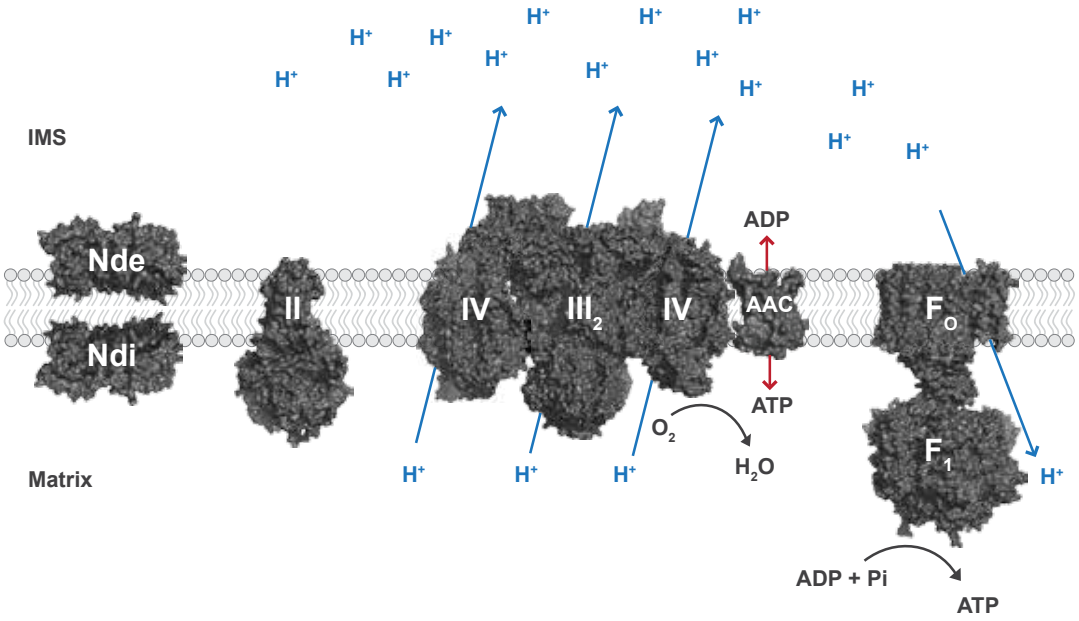

Figure 2. The mitochondrial oxidative phosphorylation enzyme complexes. Respiratory enzyme complexes embedded in the inner mitochondrial membrane establish an electrochemical proton gradient by coupling the oxidation of reducing equivalents to the pumping of protons across the inner membrane into the inner membrane space (IMS). The F_1F_O ATP synthase couples the energy of the electrochemical gradient to the production of ATP in the process of oxidative phosphorylation. Enzyme complex structures generated from structures deposited in the protein data base (PDB) 4G9K (Ndi,Nde), 1NEK (II), 1KYO (III), 1OCC (IV), 4C9G (Aac), 1E79 (F1), 1C17 (FO).

1.4 Complex IV

1.4.1 Complex IV Overview

Complex IV is an oligomeric enzyme complex that couples the reduction of molecular oxygen to the translocation of protons across the bacterial membrane or the inner mitochondrial membrane (Figure 3). As the terminal enzyme in the mitochondrial electron transport chain, complex IV is a pivotal component of cellular respiration. Therefore, characterizing the mechanistic underpinnings of complex IV has been the focus of substantial effort in the fields of biochemistry and bioenergetics. Underlying the mechanism of complex IV reactions are fundamental chemical reactions, termed reduction and oxidation (redox) reactions. These reactions are characterized by the transfer of negatively charged subatomic particles known as electrons between different molecules, and in cytochrome *c* oxidase these are carried out by four redox active metal sites, Cu_A, heme *a*, heme a_3 and Cu_B, within the enzyme.

Deficiency in complex IV accounts for the majority of human OXPHOS defects, and defects in the assembly or function of complex IV underlie multiple diseases associated with mitochondrial dysfunction (Barrientos et al., 2002; Bratton et al., 2003). Therefore, characterizing the factors that regulate complex IV assembly and function is paramount to understanding the molecular underpinnings of diseases associated with mitochondrial dysfunction.

1.4.2 Complex IV Polypeptide Composition

Knowledge of complex IV has benefited greatly from the crystal structure, first described in bacterial and bovine complex IV (Iwata et al., 1995; Tsukihara et al., 1995).

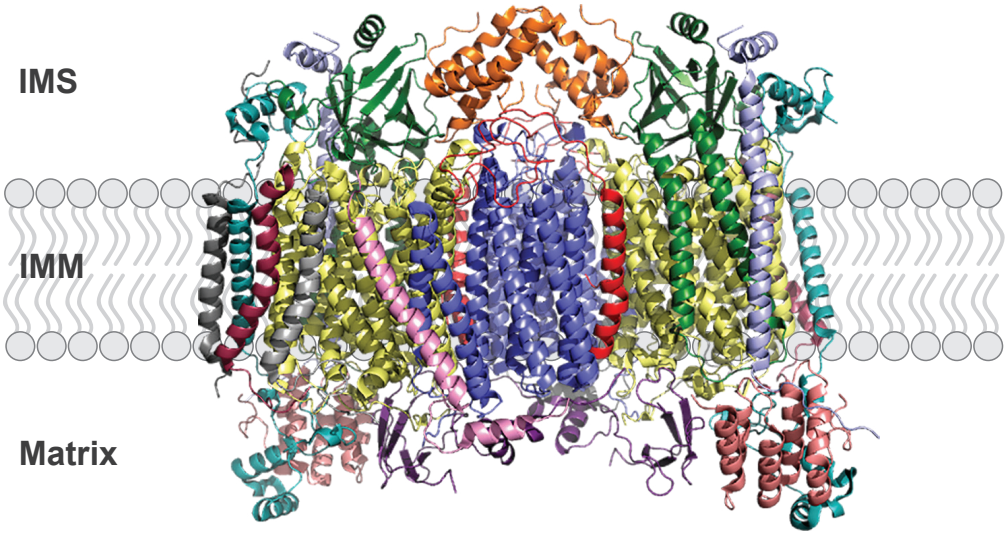

Figure 3. Cytochrome *c* oxidase (Complex IV) is a multi-subunit enzyme complex. Complex IV is embedded in the inner mitochondrial membrane (IMM) where it couples the oxidation of cytochrome *c* and the reduction of oxygen to the translocation of protons across the IMM and into the inner membrane space (IMS). Depicted is bovine complex IV PDB 2DYR (Shinazawa-Itoh et al., 2007). Individual mammalian (m-prefix) polypeptide subunits and their yeast homologs in parenthesis are; mCox1 (Cox1) yellow, mCox2 (Cox2) forrest green, mCox3 (Cox3) slate blue, mCox4-1 (Cox5a) teal, mCOX5a (Cox6) salmon, mCOX5b (Cox4) purple, mCOX6a (Cox13) red, mCOX6b (Cox12) orange, mCOX6c (Cox9) light blue, mCOX7a (Cox7) pink, mCOX7b (no yeast homolog identified) dark grey, mCOX7c (Cox8) light grey, mCOX8 (no yeast homolog identified) maroon.

The reduction of oxygen is coupled to the translocation of protons, and the enzymatic mechanisms involved are highly conserved features of complex IV. However, the number of individual polypeptide subunits varies between different organisms, ranging from 3 to 5 in the aa_3-type complex IV in bacteria, to at least 12 and 13 subunits in yeast and humans, respectively (Lucas et al., 2011; Mick et al., 2011). The yeast *Saccharomyces cerevisiae* (*S. cerevisiae*) contains a 12- subunit complex IV enzyme that is genetically mosaic in origin. Three large, highly hydrophobic transmembrane proteins, Cox1, Cox2, and Cox3, form the catalytic core of the enzyme, are encoded by mtDNA, and are homologous to the three subunits that comprise bacterial complex IV (Das et al., 2004; Fontanesi et al., 2008; Tsukihara et al., 1996). The mtDNA-encoded core subunits are synthesized by mitochondrial ribosomes, and inserted into the inner mitochondrial membrane. While specific assembly chaperones have been identified for Cox1 and Cox2 proteins, no assembly partner for Cox3 has yet been identified (Fontanesi et al., 2008; Mick et al., 2011; Tsukihara et al., 1996). The remaining 9 nuclear-encoded subunits are synthesized by ribosomes in the cytosol, imported into the mitochondria by the translocase of the outer membrane (TOM) and translocase of the inner membrane (TIM), and assembled in a coordinated multistep manner with Cox1, Cox2 and Cox3 (Das et al., 2004; Fontanesi et al., 2008; 2011; Fornuskova et al., 2010; Mick et al., 2011; 2007). Nuclear–encoded subunits, while not enzymatically active, are necessary for the assembly and stability of the holo-enzyme, as well as its predicted dimerization (Fontanesi et al., 2008). Additionally, non-catalytic subunits of complex IV can modulate catalytic activity of the enzyme in response to external cues. In *S. cerevisiae*, Cox5a and Cox5b are isoforms expressed alternately in response to oxygen levels, with the

expression of Cox5b resulting in complex IV that is capable of functioning under low oxygen conditions. Additionally, the peripheral Cox13 subunit has been suggested to be important to protect respiratory enzyme complexes from dysfunction and the generation of reactive oxygen species (ROS) under hypoxic conditions (Vukotic et al., 2012).

1.4.3 Heme and Copper Reactive Centers of Complex IV

Mitochondrial complex IV contains 4 redox active functional heme and copper groups that serve as the reactive centers, and catalyze the transfer of electrons from cytochrome *c* to molecular oxygen. Both hemes, heme *a* and heme a_3, are located within the Cox1 (bacterial subunit 1) protein moiety. The low-spin heme *a* facilitates the transfer of electrons from the soluble electron carrier cytochrome *c* to the high-spin heme a_3. Heme a_3, together with a copper atom (Cu_B) form a binuclear reactive center that functions as the site of molecular O_2 reduction. A second copper center (Cu_A) consisting of two copper atoms is located within the protein moiety of Cox2 (bacterial subunit II). Cu_A is believed to be the primary acceptor of electrons from the soluble electron carrier, cytochrome *c* (Lucas et al., 2011).

Biosynthesis of heme A occurs within the mitochondrial inner membrane and involves successive farnesylation and oxidation steps that are catalyzed by the enzymes Cox10 and Cox15, respectively (Barrientos et al., 2002; Barros et al., 2001; Saiki et al., 1993; Tzagoloff et al., 1993). Heme A is unique in that it is present only in cytochrome *c* oxidase (Barrientos et al., 2002). Copper that is destined for assembly into cytochrome *c* oxidase enters *S. cerevisiae* through a combination of high affinity (Ctr1/3) or low affinity (Fet4/Smf1) permeases, and the high affinity metalloreductase Fre1. Following copper translocation into the mitochondria, the metallation of cytochrome *c* oxidase is

facilitated by a number of accessory factors and is required for the maturation of Cox1 and Cox2. The insertion of copper into nascent Cox1 and Cox2 proteins is believed to occur within the intermembrane space (IMS) and is dependent upon the soluble, IMS-localized donor molecule Cox17, together with the co-metallochaperones Cox11 and Sco1, both located in the inner membrane and containing a globular domain that projects into the IMS (Cobine et al., 2006). The insertion of copper is required for the maturation of Cox1 and Cox2

The formation of the Cu_B site is believed to occur in parallel to the assembly of heme a_3 in Cox1, and that the formation of the heme a_3 - Cu_B reactive center occurs via a co-translational process with nascent Cox1, prior to its assembly with Cox2 (Cobine et al., 2006). Similarly, the transfer of copper to Cox2 occurs prior to the assembly of Cox2 into complex IV.

1.4.4 Complex IV Assembly

The translation of mitochondrial- encoded complex IV protein subunits is tightly regulated and requires specific regulators for the translation and maturation of mitochondrial- encoded Cox1 Cox2 and Cox3.

Cox1 translation is dependent upon the translational regulators Mss51 and Pet309. Together with an assembly-regulating Cox14-Coa1-Coa3 complex, Cox1 translational regulators control Cox1 synthesis, thereby regulating the assembly of the complex IV holo-enzyme (Barrientos et al., 2004; Soto et al., 2012). It has been suggested that the Cox1 protein serves as a core platform for complex IV assembly, whereby a regulatory feedback loop would connect the translation of Cox1 to the assembly of complex IV (Barrientos et al., 2004).

The translation of Cox2 is regulated by Pet111 and results in a Cox2 precursor (pCox2) that contains an amino-terminal 15 amino acid extension (Mulero and Fox, 1993; Poutre and Fox, 1987). The subsequent insertion of Cox2 into the membrane is thought to occur co-translationally in a process that involves the assembly factors Oxa1, Cox18 and Mss2 (Fiumera et al., 2007; Herrmann and Funes, 2005; Mick et al., 2011). Following Cox2 membrane insertion, the Cox2 specific chaperone Cox20 facilitates the cleavage of the 15 amino acid leader sequence by the mitochondrial inner membrane peptidase subunit 1 (Imp1) protease and maintains Cox2 in an assembly-competent state (Hell et al., 2000; Jan et al., 2000; Nunnari et al., 1993).

Three translational activators are required for the synthesis of Cox3 in *S. cerevisiae*, Pet54, Pet122, and Pet494 (Costanzo et al., 1986; Kloeckener-Gruissem and McEwen, 1988). Interestingly, it was shown that one of the factors regulating Cox3 translation, Pet54, is also required for the synthesis of Cox1, suggesting an additional level of co-translational regulation between the catalytic core subunits of complex IV (Shingú-Vázquez et al., 2010).

The mechanistic underpinnings that define how the highly hydrophobic Cox3 protein is inserted into the inner mitochondrial membrane, as well as its integration into complex IV assembly intermediates and the identification of Cox3 specific chaperones remain unknown. Along with Cox1 and Cox2, the Cox3 protein completes the catalytic core of complex IV. However, unlike Cox1 and Cox2, Cox3 does not contain a redox reactive prosthetic group. Yet the Cox3 protein is a highly conserved core subunit of complex IV and the conserved sequence identity of Cox3 between the bacteria *Rhodobacter sphaeroides* and *Homo sapiens* is as high as that of Cox1 in the same

species (Varanasi et al., 2006). It is thought that Cox3 functions, in part, to stabilize the core, as the absence of Cox3 results in the loss of detectable Cox1 and Cox2 proteins in the mitochondrial membrane (Barrientos et al., 2004).

Mitochondrial encoded subunits of complex IV are assembled together with nuclear-encoded subunits in a tightly regulated process. The study of yeast deletion mutants has aided the identification of complex IV assembly intermediates, and has shed light on the assembly process (Barrientos et al., 2009; Mick et al., 2011). Following the synthesis of Cox1, Cox2 and Cox3 in the mitochondria, Cox1 associates with nuclear encoded subunits Cox5 and Cox6 (Fontanesi et al., 2008; Horan et al., 2005; Stiburek et al., 2005). It is unclear whether the assembly of Cox2 and Cox3 into the Cox1-Cox5-Cox6 intermediate occurs independently or concurrently. However, Cox2 or Cox3 containing intermediates have been identified in Cox3 or Cox2 mutants, respectively (Horan et al., 2005; Tiranti et al., 2000). The subsequent steps of complex IV assembly see the integration of Cox7, Cox8 and Cox9 along with the peripheral, non-essential subunits Cox12 and Cox13. However, little is know about the assembly of these subunits.

1.4.5 General Functions of Complex IV

A. Oxidation/Reduction Reactions of complex IV

Complex IV couples the complete reduction of molecular oxygen to water with the translocation of 4 protons into the IMS (Wikstrom, 1977). The heme a_3-Cu_B O_2 reduction site sequentially receives electrons from cytochrome *c*. Following the electrostatic binding of reduced cytochrome *c* to the Cox2 subunit, electrons are transferred from Cu_A and heme *a* metal centers to the heme a_3-Cu_B O_2 reduction site. The

O_2 -binding heme a_3-Cu_B center is located in the Cox1 protein moiety and lies within the interior of the complex IV enzyme (Bloch et al., 2004; Yoshikawa et al., 2011).

B. Proton Pumping by complex IV

Subsequently, substrate protons that are used to generate water molecules are pumped into the interior-located heme a_3-Cu_B O_2 reduction site from the mitochondrial matrix through two proton-pumping pathways, referred to as the K- and D-pathways (Yoshikawa et al., 2011). Mutational analyses of key residues within the K and D channels suggest that these pathways are involved in both the channeling of substrate protons used in the catalytic cycle as well as the coupled translocation of protons from the mitochondrial matrix to the IMS. An additional proton –translocation pathway, referred to as the H-pathway, has been proposed to exist in bovine complex IV (Yoshikawa et al., 2011). The proton pumping pathways of complex IV are comprised of a hydrogen bond network within the Cox1 subunit that facilitates the channeling of 4 protons per catalytic cycle through the tightly-assembled complex IV holo-enzyme. The energy necessary to drive the active, gated, translocation of protons from the mitochondrial matrix to the IMS is driven by the exergonic reduction of O_2 enzyme (Rich and Marechal, 2013). Therefore, the ability of mitochondria to generate ATP through the proton motive force, is dependent upon the translocation of protons by complex IV and is functionally connected to the ability of complex IV to channel O_2 and substrate protons to the heme a_3-Cu_B binuclear center.

1.5 The Complex III–Complex IV Supercomplex

1.5.1 Respiratory Supercomplex Overview

The structural organization of respiratory enzyme complexes within the mitochondrial electron transport chain represents a widely debated point of contention within the field of mitochondrial biology. For more than 20 years, two predominant and opposing models of respiratory enzyme complex organization, referred to as the 'solid' and 'fluid' models, divided the field. The 'solid model' predicted that respiratory enzyme complexes are rigidly bound together in a framework that represents a functional unit capable of carrying out efficient electron transfer and OXPHOS (Chance et al., 1963; Keilin and Hartree, 1937). Two important findings preceded the subsequent proposed alternative to the solid state model. The first was Mitchell's chemiosmotic theory that proposed the electrochemical gradient drives the synthesis of ATP by ATP-synthase, in a system that does not require the physical interaction between complex V and the other mitochondrial respiratory enzyme complexes (Mitchell, 1961). The second was the isolation and reconstitution of enzymatically functional forms of mitochondrial respiratory enzyme complexes I-IV (Hatefi et al., 1962). Based partly on these findings, it was proposed that electron transfer between mitochondrial respiratory enzyme complexes occurs through the dual modes of intracomplex electron transfer between solid state components and intercomplex electron transfer mediated by the diffusion of co-substrates such as the electron carriers coenzyme Q (CoQ) and cytochrome *c* (Green and Tzagoloff, 1966). These findings led to the proposal of a new model termed the random collision model often referred to as the 'fluid model' (Hackenbrock et al., 1977, Hackenbrock et al., 1986). While its predecessor, the 'solid model, suggested mitochondrial respiratory

enzyme complexes were physically associated in an architecture that ensures high catalytic activity, the fluid model posited that the mitochondrial respiratory enzyme complexes are arranged as independent complexes positioned in close proximity to one another within the inner mitochondrial membrane (IMM) and that electron transfer occurs laterally through long-range diffusion (Hackenbrock et al., 1986). The first demonstration of the existence of higher ordered organization of OXPHOS complexes came from the characterization of the dimeric F_1F_O ATP-synthase, where it was proposed that function of so-called 'supracomplex' formation was to optimize the activity of the enzymes and enhance their stability (Arnold et al., 1998). Two studies that further challenged the then widely-accepted fluid model were published in 2000 when Cruciat et al. reported the isolation of a III-IV 'supracomplex' from yeast mitochondria and proposed that supracomplex assembly was a critical regulatory or enhancement feature of the OXPHOS system (Cruciat et al., 2000). At the same time, Schägger and Pfeiffer described the BN-PAGE isolation of supramolecular structures of respiratory enzyme complexes that included the III-IV 'supercomplex' in yeast, and the mammalian I-III-IV assembly that, together, informed a higher-ordered 'respirasome' model of respiratory chain complex organization (Schägger and Pfeiffer, 2000). In isolating higher-ordered assemblies of eukaryotic respiratory enzyme complexes, these two seminal papers were the first to demonstrate that different OXPHOS complexes organize into supramolecular structures, thereby challenging the fluid model paradigm. Subsequently, it was shown that the higher-ordered organization of OXPHOS complexes is interdependent, and the organizational state of one complex can influence the assembly of a separate enzyme into supercomplexes. Specifically, the stoichiometry of III-IV supercomplex formation was

altered and despite normal levels of complex IV, its activity was reduced when the ability of F_1F_O ATP-synthase to assemble as a dimer was inhibited (Saddar et al., 2008). Additionally, the assembly of dimeric F_1F_O ATP-synthase was shown to influence the biogenesis of the IMM, where the IMM cristae structure was adversely affected in the absence of ATP-synthase dimerization-dependent subunits (Paumard et al., 2002). These findings highlighted an additional layer of complexity in the organizational state of OXPHOS enzyme complexes into oligomeric supercomplexes.

Despite initial opposition to the existence of supercomplexes, an overwhelming amount of experimental evidence has confirmed the presence of catalytically functional respiratory supercomplexes across diverse eukaryotic taxa. Respiratory supercomplexes have been detected by BN-PAGE in mitochondria from plants (Eubel et al., 2003; Krause et al., 2004; Pineau et al., 2013); fungi (including yeast) (Arnold et al., 1998; Brandner et al., 2005; Cruciat et al., 2000; Nübel et al., 2009; Schägger and Pfeiffer, 2000); invertebrates (Suthammarak et al., 2009) and vertebrates (Acín-Pérez et al., 2008; D'Aurelio et al., 2006; McKenzie et al., 2006; Schägger and Pfeiffer, 2000). Remarkably, the compositional organization of these complexes was found to be similar across different species, suggesting an evolutionarily conserved mechanism for the formation of supercomplexes with defined stoichiometric composition (Enríquez, 2016). Despite skepticism suggesting that supercomplexes might represent an artifact of detergent solubilization, respiratory supercomplexes were also found to be stable in the absence of detergent (Althoff et al., 2011). The structural characterization of purified respiratory supercomplexes by transmission electron microscopy and single-particle tomography has yielded important information regarding the conformation of the I_1III_2 supercomplex

from *Arabidopsis thaliana* (Dudkina et al., 2005) and *Bos taurus* (Schäfer et al., 2006), the $I_1III_2IV_1$ from *B taurus* (Althoff et al., 2011; Dudkina et al., 2011; Schäfer et al., 2006) and the III_2IV_2 supercomplex from *S. cerevisiae* (Mileykovskaya et al., 2012).

Respiratory supercomplexes are stabilized by both AAC and the signature mitochondrial phospholipid cardiolipin (CL), with the loss of either affecting the stability of supercomplexes (Dienhart and Stuart, 2008; Zhang et al., 2002). Aac itself contains 3 cardiolipin molecules that have been shown to be required for transport in reconstituted vesicles (Klingenberg, 2009). The importance of cardiolipin for the stability of supercomplexes is a function that is conserved from yeast to humans (Mileykovskaya and Dowhan, 2014; Pfeiffer et al., 2003). Yeast strains deficient in CL (*Δcrd1*) have a reduction in assembled complex IV, lack stably assembled III-IV supercomplexes and have a concomitant reduction in respiratory growth. (Jiang et al., 2000; Mileykovskaya et al., 2005; Pfeiffer et al., 2003; Zhang et al., 2002; 2005). In model systems and tissue from patients with Barth Syndrome, an X-linked mutation in the CL remodeling acyltransferase gene *TAZ* associated with cardioskeletal myopathy, there is a reduction in the organization of respiratory complexes into higher ordered supercomplexes. (reviewed by (Mileykovskaya and Dowhan, 2014).

Since the initial reports of respiratory supercomplexes in the literature, a number of reviews have been written on the topic of supercomplexes (Barrientos and Ugalde, 2013; Boekema and Braun, 2007; Enríquez, 2016; Lenaz and Genova, 2009; Schägger and Pfeiffer, 2000; Stuart, 2008).

In the yeast *S. cerevisiae*, respiratory supercomplex factors 1 and 2 (Rcf1 and Rcf2) are nonessential components of complex IV and impact the stability of complex

IV, and therefore, the stoichiometry of III-IV supercomplexes. The following section will provide an in-depth review of the known functions and molecular interactions of Rcf1 and Rcf1-homologs.

1.6 Respiratory Supercomplex Factor 1 (Rcf1) Characterization

1.6.1 Rcf1 Protein Overview

Rcf1 was originally identified as an 18 kilodalton (kDa) mitochondrial protein of unknown function in a number of large-scale, computationally driven studies with broad and diverse goals (Helbig et al., 2009; Hess et al., 2009; Reinders et al., 2006; Sickmann et al., 2003). Nearly a decade after its identification, Rcf1 was characterized and its role in OXPHOS supercomplex function and complex IV function was described in three independent publications in 2012, (Chen et al., 2012; Strogolova et al., 2012; Vukotic et al., 2012).

The Rcf1 protein was first identified in a large-scale tandem mass spectrometry analysis to identify the *S. cerevisiae* mitochondrial proteome (Sickmann et al., 2003). Rcf1 was subsequently discovered in a screen designed to identify gene products that alter mitochondrial biogenesis and inheritance in *S. cerevisiae,* and thus, was originally named Aim31 for *altered inheritance* of *mitochondria* (Hess et al., 2009). Concurrently, in an approach that combined 1-D blue native polyacrylamide electrophoresis (BN-PAGE) with quantitative mass spectrometry, it was discovered that Rcf1 (then Aim31) co-migrated with complex IV and was thus identified as a putative novel complex IV interacting partner (Helbig et al., 2009). In 2012, three papers described *S. cerevisiae* Rcf1 as a member of the conserved hypoxia-induced gene (Hig1) protein family and an integral inner mitochondrial membrane protein that stably associates with complex IV

and complex III, is required for the efficient assembly of complex IV and III-IV supercomplexes, and plays an important role in hypoxic growth. The deletion of Rcf1 led to altered complex III- complex IV supercomplex assembly, a reduction in complex IV activity, impaired respiration, and elevated oxidative stress (Chen et al., 2012; Strogolova et al., 2012; Vukotic et al., 2012). Rcf1 was found to display a strong association with the Cox3 protein and was characterized as being in close proximity to AAC. Additionally, it was shown that Rcf1 contains overlapping function with a second Hig1 protein in *S. cerevisiae*, Rcf2. The absence of Rcf1 and Rcf2 results in a respiration-based growth deficiency that is not observed when only one Hig1 protein, Rcf1 or Rcf2, is absent (Strogolova et al., 2012). Rcf1 contains homologs in varied and diverse eukaryotic taxa, including humans. In contrast, although Rcf2 shares limited sequence homology to Rcf1 and Hig1 proteins, it contains no homologs outside of fungal species. The following sections will provide a detailed description of current Rcf1 findings that preceded and were published during this dissertation.

1.6.2 Identification of *Saccharomyces cerevisiae* Rcf1 as a Respiratory Supercomplex-associated Protein

The initial functional characterization of Rcf1 and its role in supporting III-IV assembly was reported in three independent publications (Chen et al., 2012; Strogolova et al., 2012; Vukotic et al., 2012). Analysis of the complex III-Complex IV (III-IV) respiratory supercomplex by BN-PAGE and affinity chromatography identified a novel protein, 18 kDa in size that co-purified with the supercomplex (Strogolova et al., 2012; Vukotic et al., 2012). Mass spectrometry analysis indicated that this protein was Aim31, encoded by the nuclear gene YML030w in *S. cerevisiae*. Aim31 was subsequently

renamed respiratory supercomplex factor 1 (Rcf1), to reflect its characterization as a supercomplex -associated protein.

1.6.3 Characterization of Rcf1 membrane topology

Statistical modeling programs indicate the presence of two predicted transmembrane segments within the Rcf1 protein. Using protease accessibility and alkaline extraction assays, it was proposed that Rcf1 was an integral IMM protein with an N_{out}-C_{out} orientation (Chen et al., 2012; Strogolova et al., 2012; Vukotic et al., 2012) (Figure 4).

1.6.4 Hypoxia-induced gene family domain of Rcf1

Sequence analysis indicated that Rcf1 is a member of the conserved "hypoxia induced gene 1 (Hig1)" family of proteins, conserved from bacteria to diverse eukaryotic taxa. The conserved region, referred to as the *hypoxia induced protein conserved region* (Pfam PF04588: *HIG_1_N*), encompasses Rcf1 amino acids 28-81 and spans from the N-terminal intermembrane space region through the first transmembrane segment (TM1), the matrix loop and the majority of the second transmembrane segment (TM2). While preliminary data indicate that Hig1 proteins may be involved in stress response, the function of these proteins remains largely unknown. Hig1 family members are divided into two similar, but distinct, groups based on sequence. Hig1-type 1 proteins were identified in several screens designed to identify genes whose expression was enhanced during a number of cellular stresses including, but not limited to, hypoxia, low glucose, and oxidative stress (Bedo et al., 2005; Denko et al., 2000; Gracey et al., 2001; Shen et al., 2005; Wang et al., 2006). Hig1-type 2 proteins were identified primarily through

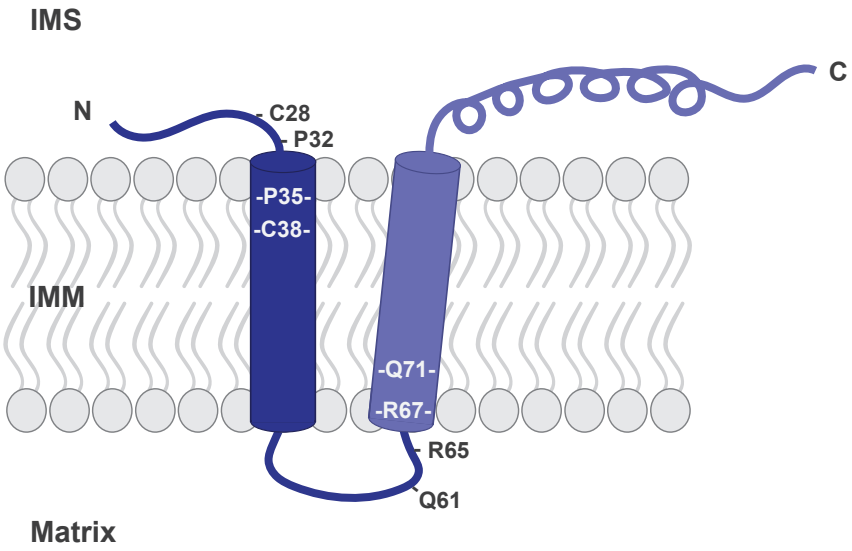

Figure 4. Respiratory supercomplex factor 1 (Rcf1) is an integral inner mitochondrial membrane protein. The predicted Rcf1 structure contains two putative transmembrane segments and is predicted to adopt an N_{out}-C_{out} orientation within the inner mitochondrial membrane. Labeled amino acids represent residues that were targeted for alanine mutagenesis in this study.

their high degree of sequence homology with Hig1-type 1 proteins and potentially represent constitutively expressed members of the Hig1 family. A number of Hig1-type 2 proteins from different species, including *S. cerevisiae* Rcf1, represent a highly conserved sub-set of homologous proteins that contain a Hig1 domain and are functionally related in their regulation of complex IV activity and respiratory supercomplex organization.

1.6.5 Yeast Hig1 homologs Rcf1 and Rcf2 contain overlapping function

A. Identification of Rcf2

In addition to Rcf1, a blastp database search indicated that *S. cerevisiae* contains a second Hig1 protein, Rcf2, that bears limited sequence similarity with Rcf1 and Hig1-type 2 proteins (Strogolova et al., 2012). Rcf1 and Rcf2 each contain a Hig1 domain and are functionally related in their regulation of complex IV activity and supercomplex organization. While Rcf1 is evolutionarily conserved and contains homologs in alpha-proteobacteria, plants, nematodes and mammals, Rcf2 is a fungal-specific protein.

In the same *S. cerevisiae* altered mitochondrial inheritance screen that identified Rcf1, Rcf2, formerly Aim38 (Hess et al., 2009) was also identified. Additionally, both Rcf1/Aim31 and Rcf2/Aim38 were identified as putative novel complex IV interacting partners through a combination of BN-PAGE and quantitative mass spectrometry (Helbig et al., 2009). Rcf2 is a 25 kDa mitochondrial protein that is predicted to contain 2 transmembrane segments.

B. The absence of *S. cerevisiae* Hig1-type 2 proteins Rcf1 and Rcf2 results in a respiration-based growth deficiency

In *S. cerevisiae*, Rcf1 and Rcf2 cooperatively play a critical role in respiration-based growth and the activity of complex IV (Strogolova et al., 2012). The deletion of either the *RCF1* or *RCF2* gene individually, results in a modest decrease in respiration-based growth on non-fermentable carbon sources (Chen et al., 2012; Strogolova et al., 2012; Vukotic et al., 2012). In contrast, a pronounced growth defect is observed in yeast in which both Rcf1 and Rcf2 are absent (Δ*rcf1;*Δ*rcf2*) and the expression of his-tagged forms of either Rcf1 ($Rcf1_{His}$) or Rcf2 ($Rcf2_{His}$) complement this growth defect (Strogolova et al., 2012). However, the underlying defect(s) that results in the growth deficiency of the Δ*rcf1;*Δ*rcf2* mutant strain remains unknown.

C. Rcf1 and Rcf2 cooperatively influence the activity of complex IV, and their absence results in an aerobic growth deficiency that cannot be explained by complex IV impairment alone

The deletion of *RCF1* or *RCF2* alone does not appear to result in a reduction of the protein levels of complex IV, yet partially compromises complex IV enzymatic activity (measured spectrally by the oxidation of cytochrome *c*) (Strogolova et al., 2012; Vukotic et al., 2012). In contrast, the protein levels and enzyme activity of complex IV are reduced in the Δ*rcf1;*Δ*rcf2* mutant, and both are approximately 50% of the wild type levels. Comparatively, the levels of the NADH dehydrogenase, and complexes II and III were not reduced in Δ*rcf1;*Δ*rcf2* mutant mitochondria, suggesting that deficiencies in complex IV activity in the absence of Rcf1 and Rcf2 could underlie the growth deficiency of the double mutant. However, a number of independent studies, including those from our lab, indicate that complex IV enzyme levels do not become limiting to

supporting respiration-based growth until they dip below a threshold of 20-30% of wild type levels. Thus, the respiration-based growth deficiency of the Δ*rcf1;*Δ*rcf2* mutant cannot be explained solely by the reduction in complex IV. Therefore, additional factors that might contribute to the respiration-based growth deficiency, including defects in other OXPHOS enzymes, must be considered.

D. Mitochondria from the Δ*rcf1;*Δ*rcf2* strain appear to contain hyperactive O_2 consumption rates despite a reduction in complex IV protein

Respiration can be evaluated in intact mitochondria by measuring O_2 consumption in response to the presence of oxidizable substrates (NADH or succinate). Upon the addition of substrate alone, a low level of O_2 consumption can be measured that is referred to as state 4 respiration. The electron transport chain (ETC) is regulated through a feed back mechanism by the proton gradient that it generates. State 4 respiration has been proposed to reflect the level of 'basal' activity that is necessary to compensate for proton leak across the IMM, thereby maintaining a sufficient level of proton motive force. It has been reported that up to 2/3 of basal proton leak can be attributed to intrinsic uncoupling activity of AAC proteins. When ADP is added in the presence of substrate (i.e. NADH or succinate + ADP), the H^+ transport activity of the F_1F_O -ATP synthase is induced, resulting in the dissipation of the Δp gradient and subsequent stimulation of ETC activity referred to as state 3 respiration. The O_2 consumption rate is elevated during state 3 respiration, compared to state 4 respiration, and the ratio of state 3 to state 4 O_2 consumption rates (state 3/ state 4) - referred to as respiratory control ratio (RCR)- is a value that is commonly used to determine the level of coupling in evaluating mitochondrial defects. Furthermore, the isolated complex IV activity can also be

determined by measuring the O_2 consumption rate in the presence of the exogenously added electron donor ascorbate/TMPD. Mediated by TMPD, ascorbate donates electrons directly to cytochrome *c* that are subsequently passed to complex IV, thus bypassing other enzymes of the ETC and providing a method to evaluate the bio-energetically isolated complex IV O_2 consumption rate. When the O_2 consumption rate by ascorbate/TMPD is measured in the presence of the protonophore CCCP, which dissipates the Δp resulting in a compensatory increase in complex IV enzyme activity, the maximum complex IV O_2 consumption capacity can be measured.

Using a Clark electrode, O_2 consumption rates were measured in wild type and Rcf mutant mitochondria Δ*rcf1* and Δ*rcf1;*Δ*rcf2*. Interestingly, when the state 4 O_2 consumption rate was measured in Δ*rcf1;*Δ*rcf2* mitochondria (measured using NADH as substrate), the rates were found to be similar to those measured in wild type mitochondria. However, when the maximum complex IV O_2 consumption capacity (i.e. ascorbate/TMPD in the presence of CCCP) was measured in Δ*rcf1;*Δ*rcf2* mitochondria, it was found to be approximately 50% of wild type mitochondria. These results suggest that in Δ*rcf1;*Δ*rcf2* mitochondria, where the abundance of complex IV is substantially reduced, the OXPHOS system is working twice as hard as that of the wild type, in order to achieve similar state 4 O_2 consumption rates. These results together, could potentially be explained by the thermodynamics of H^+ pumping, whereby when complex IV is limiting (as in Δ*rcf1;*Δ*rcf2* mitochondria) an increased effort is required to maintain Δp under state 4 conditions. Alternatively, the degree of H^+ leak across the IMM might be elevated in the absence of Rcf1 and Rcf2.

When the Δ*rcf1* single mutant was analyzed in parallel to the Δ*rcf1;*Δ*rcf2* double mutant, the state 4 respiration and maximum complex IV O_2 consumption rates were found to be similar between the single and double null mutant mitochondria. However, unlike the Δ*rcf1;*Δ*rcf2* double null mutant, the Δ*rcf1* single null strain retains the ability to support aerobic growth, adding further evidence that complex IV activity alone, cannot completely explain the aerobic growth deficiency of the Δ*rcf1;*Δ*rcf2* double mutant strain.

Analysis of state 3 respiration (addition of ADP in the presence of NADH) was carried out in parallel in Δ*rcf1* single and Δ*rcf1;*Δ*rcf2* double null mutant mitochondria and indicates that, compared to wild type mitochondria, the Δ*rcf1;*Δ*rcf2* double null mutant but not the single mutant (Δ*rcf1*) may contain impaired adenine nucleotide transport or ATP synthesis. The respiratory control ratio (RCR, state 3 rate/state 4 rate) is a determinant of the 'coupled' state of the mitochondria, and a reduced RCR can indicate an underlying impairment of ADP/ATP transport, ATP synthesis and/or excessive H^+ leak. The RCR of Δ*rcf1;*Δ*rcf2* mitochondria was reduced compared to both wild type mitochondria and the Δ*rcf1* single null mutant, suggesting that in the absence of Rcf1 and Rcf2 additional mitochondrial defects could contribute to the aerobic growth deficiency of the Δ*rcf1;*Δ*rcf2* strain.

E. Rcf1 Associates with complex IV and complex III independently likely through an association with newly-synthesized Cox3

Rcf1 co-purifies with the III-IV supercomplex and partitions with complex IV. Rcf1 (both a newly imported radiolabeled species as well as endogenous Rcf1) was found to co-fractionate with the III-IV supercomplex, as revealed by mass spectrometry analysis

of the III-IV supercomplex (Strogolova et al., 2012). Likewise, using tagged Rcf1 and Rcf2 proteins combined with affinity purification under digitonin solubilization conditions, subunits of the III-IV supercomplex were found to independently co-purify with Rcf1 and Rcf2 (Chen et al., 2012; Strogolova et al., 2012; Vukotic et al., 2012). However, Rcf1 did not co-purify Rcf2, and vice-versa, suggesting that Rcf1 and Rcf2 are not found together in the same III-IV, but rather, independently associate with III-IV supercomplexes (Strogolova et al., 2012). It was found that the peripheral subunits Cox12 and Cox13 do not appear to be present at the same level as they are in a $Cox5a_{His}$-purified III-IV supercomplex, suggesting that the III-IV associating with Rcf1 could be a late-stage III-IV assembly intermediate, where the assembly of peripheral subunits Cox12 and Cox13 is not yet complete.

When Rcf1 and Rcf2 were purified following Triton X-100 or n-dodecyl β-D-maltoside (DDM) mitochondrial solubilization - detergent conditions that disrupt III-IV arrangement – Rcf1 was found to co-purify with complex IV, whereas Rcf2 did not co-purify with complex IV (or complex III). Thus, Rcf2's association with complex III and/or IV appears to be labile to Triton X-100 (and DDM) detergent, and therefore it cannot be determined whether Rcf2 partitions with one complex or the other. When a *C.elegans* Hig1 protein is expressed in the Δ*rcf1;*Δ*rcf2* yeast strain, an increased association of Cox12 with the complex IV that co-purified with *C.elegans* Hig1 was observed, highlighting the conserved capacity of Hig1 proteins to associate with complex IV and a potential role in the assembly or stability of Cox12.

Additionally, Rcf1 was found to directly interact with the newly-synthesized mitochondrial-encoded Cox3 protein prior to its assembly into complex IV (Strogolova et

al., 2012). Thus it was concluded that Rcf1 displays a higher affinity to the complex IV aspect of the III-IV supercomplex, presumably through its high affinity to the Cox3 protein.

Finally, evidence was also presented to indicate that Rcf1 displays the capacity to independently associate with complex III. When Rcf1 was purified from mutants deficient in the assembly of complex IV under the mild detergent conditions of digitonin, the co-purification complex III protein subunits was also observed (Chen et al., 2012; Strogolova et al., 2012).

F. The assembly of complex IV and its association with complex III is altered in the absence of Rcf1 and Rcf2

Rcf1 and Rcf2 display overlapping function in their ability to support the correct assembly of complex IV and its association with complex III. In the current assembly model of complex IV, the core protein subunits (Cox1, Cox2, and Cox3) together with Cox5 and Cox6, form the early structural framework for the assembly of the complete complex IV holoenzyme (Mick et al., 2011). If complex IV assembly is hindered, the core complex IV protein subunits are highly susceptible to proteolytic turnover. Therefore, the assembly state of complex IV can be determined by examining the steady-state protein levels of complex IV subunits. In Δ*rcf1* mitochondria, the steady-state levels of complex IV subunits are reduced to approximately 50% of wild type levels, and a similar level of reduction was observed in the Δ*rcf1;*Δ*rcf2* double mutant. In contrast, the levels of other OXPHOS enzyme subunits were unaffected by the presence of Rcf1 or Rcf2 (Strogolova et al., 2012). These results indicated that the presence of Rcf1 is required to stabilize the core complex IV subunits. Additionally, the association of

conserved structural complex IV subunits, Cox12 and Cox13, is specifically impaired in the absence of Rcf1 and Rcf2. The Δ*rcf1*;Δ*rcf2* double mutant displays a strong reduction in the association of Cox12 and Cox13 with complex IV, in contrast to wild type mitochondria and single mutants (Δ*rcf1* or Δ*rcf2*), where there does not appear to be a significant impairment in Cox13 assembly, and a only a modest decrease in Cox12 association is observed in the Δ*rcf1* single null mutant (Strogolova et al., 2012).

The importance of Rcf1 and Rcf2 for the association of Cox12 and Cox13 with complex IV, together with the enhanced association of Cox12 with complex IV observed in the presence of the *C. elegans* Hig1 homolog, suggests that Rcf1/Hig1 proteins may regulate a dynamic association of Cox12 with complex IV, and that the cycling off of Cox12 from complex IV may be impaired when *C. elegans* Hig1 is present in yeast.

In wild type mitochondria, nearly all of complex IV is associated with complex III in III_2-IV_2 and to a lesser extent III_2-IV supercomplex forms. In the absence of Rcf1 and Rcf2, respiratory complexes III and IV can still associate, however the levels of III_2-IV_2 and III_2-IV are reduced and an additional accumulation of free III_2 is observed (Strogolova et al., 2012). However, the reduction in supercomplexes is likely due to lowered levels of complex IV in the absence of Rcf1 and Rcf2, where complex IV levels are limiting for III_2-$IV_{(1\text{-}2)}$ formation.

Together, these results indicate that Rcf1 and Rcf2 cooperatively influence the assembly state of complex IV, thereby influencing the organization of respiratory supercomplexes.

G. Rcf1 associates with AAC proteins, and Rcf1 and AAC exhibit a close physical relationship

Rcf1 was found to associate with AAC, and these proteins exist in close physical proximity within the mitochondrial inner membrane. The purification of a His-tagged AAC derivative under digitonin solubilization conditions resulted in the co-purification of Rcf1 (Strogolova et al., 2012). Likewise, the reciprocal purification of tagged Rcf1 was reported to co-purify AAC, as determined by mass spectrometry (Chen et al., 2012).

Wild type Rcf1 and his-tagged derivatives were shown to crosslink to all isoforms of AAC via MBS, an amine-sulfhydryl cross-linker with a 7.3 Å spacer length (Strogolova et al., 2012). Moreover, when crosslinking was performed in mitochondria isolated from mtDNA deficient yeast strains (rho^0), crosslinking between Rcf1 and AAC was enhanced, suggesting that the interaction between Rcf1 and AAC occurs independent of assembled complexes III or IV.

Furthermore, a genetic interaction has been reported to exist between Rcf1 and AAC, where a double null Δ*rcf1;*Δ*aac2* mutant strain displayed a survival defect during stationary phase that was not observed in either single mutant strain (Δ*rcf1* or Δ*aac2*) (Chen et al., 2012).

Together, these results suggest that Rcf1 and AAC co-exist in close proximity and that the interaction between Rcf1 and AAC occurs independent of assembled complexes III or IV.

H. Rcf1 and Rcf2 have been reported to function in cellular mediation of oxidative stress

The mediation of oxidative stress is a conserved feature among Hig1 proteins, including Rcf1 and Rcf2 (Ameri et al., 2015; Chen et al., 2012; Fischer et al., 2016; Vukotic et al., 2012). In the Rcf1 null yeast strain (Δ*rcf1*), a hypoxic (1% O_2) growth deficiency was reported on both fermentable and non-fermentable (respiration) carbon sources (Vukotic et al., 2012). Furthermore, it was reported that yeast lacking Rcf1 or Rcf2 (Δ*rcf1* or Δ*rcf2* strains) contain an elevated level of mitochondrial dysfunction that results in the increased production or accumulation of reactive oxygen species (ROS), oxidative damage and an elevated susceptibility to exogenous oxidative stress (Chen et al., 2012; Vukotic et al., 2012). These results suggest that one potential role of Rcf1 (and Rcf2) might be to modulate respiration through regulation of complex IV thereby mediating mitochondrial dysfunction.

Recent studies have demonstrated that Rcf1 homologs (from a number of different fungal, nematode and mammalian species) contain evolutionarily conserved functions, including the ability to: associate with complex IV, support respiration-based growth and complex IV activity, influence the assembled state of complex IV and complex IV-containing supercomplexes, and mitigate ROS production or damage (Ameri et al., 2015; Chen et al., 2012; Fischer et al., 2016; Hayashi et al., 2015; Strogolova et al., 2012; Vukotic et al., 2012). However, a unifying molecular basis for the conserved functions of Hig1 domain proteins remains unknown.

Notably, it has been reported that the physical binding of isolated Higd1A to purified complex IV induces structural changes that increase the enzymatic activity of

complex IV (Hayashi et al., 2015). The authors of this study propose a model in which the binding of Higd1a induces structural changes that increase the activity of complex IV through modulation of the proton-pumping pathway (Hayashi et al., 2015). Importantly, the aforementioned study provides evidence that a Hig1 domain protein can induce structural changes within complex IV that modulate activity. However, a common molecular underpinning by which Hig1 proteins modulate complex IV activity remains unknown.

1.7 Yeast as a Model System

The research detailed in this dissertation is focused on understanding the role of Rcf1 in the function of the mitochondrial respiratory chain complexes and supercomplexes. The process of OXPHOS and the components involved have been shown to be highly conserved throughout eukaryotic evolution, from single cell organisms such as yeast, to more complex organisms such as humans. I have adopted a variety of genetic and biochemical approaches to address the role of the Rcf1/Hig1 protein in the function of complex IV. To do so, I have studied OXPHOS function and molecular interactions in the yeast S. cerevisiae as a eukaryotic model system. In addition to performing aerobic respiration, yeast can live by fermentation, which enables the propagation and analysis of mutants, deficient areas of aerobic metabolism, thus making yeast an ideal model organism to study mitochondrial function. Furthermore, yeast cells are relatively easy to genetically manipulate and the entire genome has been sequenced now for a number of years, which simplified many aspects of this research. Isolation of large quantities of mitochondria from wild type and mutant yeast cells is very

straightforward and thus enabled me to perform detailed biochemistry on the mitochondrial OXPHOS complexes and their individual protein components.

1.8 Dissertation Study Aims

The goal of this dissertation study is to characterize the role of Rcf1/Hig1 proteins in cellular energy production by oxidative phosphorylation. Chapter 3 is focused on characterizing the role of the conserved Rcf1/Hig1 QRRQ motif in the interaction between Rcf1 and Cox3/complex IV, and the importance of this motif for Rcf1's role in supporting complex IV stability, activity and association with complex III in the III-IV supercomplex. Included in this analysis is the analysis of the molecular environment of the Rcf1 QRRQ motif. Additionally, potential functional differences between Hig1-type1 and Hig1-type2 proteins were investigated. The aim of Chapter 4 is the characterization of the Rcf1-AAC interaction, and includes an investigation into the functional relationship between Rcf1 and AAC by identifying the molecular and bio-energetic conditions that promote or obstruct their interaction.

CHAPTER 2: MATERIALS AND METHODS

2.1 Introduction

This chapter is divided into two sections and provides a detailed description of the molecular and cellular biology, protein chemistry and physiology methods that were used in this dissertation work to study the function and molecular interactions of the Rcf1 and Hig1 proteins. The first section is comprised of the molecular and cellular techniques that were used to make point mutations in the Rcf1 protein, express the Rcf1 mutant derivatives and Human Hig1 isoforms in yeast, and the isolation of the mitochondria from the resulting strains. The second section includes the protein chemistry and physiological methods that were used to analyze the function of the Rcf1 and Hig1 proteins and to characterize the Rcf1 mutant derivatives.

2.2 Molecular and Cellular Biology Methods

2.2.1 Polymerase Chain Reaction (PCR) and PCR-mutagenesis

Point mutations in Rcf1 (YML030W gene) were generated in the wild type yeast YML030W gene encoding the Rcf1 Open Reading Frame (ORF) that has been previously isolated from the wild type (W303-1A) yeast strain, PCR amplified to encode a histidine$_{12}$ epitope, and cloned into the Yip351 plasmid down-stream of the galactose-inducible GAL-10 promoter (Figure 5) (Strogolova et al., 2012). In this study, mutations were made in the predicted matrix loop/TM2 region and within the N-terminal/TM1 region of the Rcf1 protein using a two-step PCR mutagenesis strategy and incorporating

the mutated sequence into forward and reverse primers (TABLE 1). To generate the Q61A/Q71A mutant derivative, residues Gln-61 and Gln-71 were mutated to Ala at the

TABLE 1
Sequence of PCR Primers Used in This Study

Primer #	Name	Sequence of PCR Primer 5' to 3'
ST746	YipSeq For	5' GGTGGTAATGCCATGTAATATG 3'
ST757	YipSeq Rev	5' GACGTTGTAAACGACGGCCAGTG 3'
2ST093	Rcf1 C28A For	5' GGCGAAAGGATTATATACCATGCGAAGAAACAG CCATTGGTACCCATTGGG 3'
2ST094	Rcf1 C28A Rev	5' CCCAATGGGTACCAATGGCTGTTTCTTCGCATG GTATATAATCCTTTCGCC 3'
2ST221	Rcf1 P32A For	5' GGATTATATACCATTGTAAGAAACAGGCTTTGGT ACCCATTGGGTGCTTGC 3'
2ST222	Rcf1 P32A Rev	5' GCAAGCACCCAATGGGTACCAAAGCCTGTTTCTT ACAATGGTATATAATCC 3'
2ST225	Rcf1 P35A For	5' CCATTGTAAGAAACAGCCATTGGTAGCTATTGG G TGCTTGCTGACTACAGG 3'
2ST226	Rcf1 P35A Rev	5' CCTGTAGTCAGCAAGCACCCAATAGCTACCAAT G GCTGTTTCTTACAATGG 3'
2ST095	Rcf1 C38A For	5' GCCATTGGTACCCATTGGGGCGTTGCTGACTACA GGAGCTGTCATTCTGGC 3'
2ST096	Rcf1 C38A Rev	5' GCCAGAATGACAGCTCCTGTAGTCAGCAACGCC CCAATGGGTACCAATGGC 3'
2ST181	Rcf1 W58C For	5' GCTCAAAATGTTCGTCTTGGTAATAAATGTAAAG C

		TCAGTACTACTTCCGT 3’
2ST182	Rcf1 W58C Rev	5’ ACGGAAGTAGTACTGAGCTTTACATTTATTACCAA GACGAACATTTTGAGC 3’
2ST183	Rcf1 A60C For	5’ CGTCTTGGTAATAAATGGAAATGTCAGTACTACTT CCGTTGGCG 3’
2ST184	Rcf1 A60C Rev	5’ CGCCAACGGAAGTAGTACTGACATTTCCATTTATT ACCAAGACG 3’
ST836	Rcf1 Q61A For	5’ CGTCTTGGTAATAAATGGAAAGCTGCGTACTACT TCCG 3’
ST837	Rcf1 Q61A Rev	5’ CGGAAGTAGTACGCAGCTTTCCATTTATTACCAA GACG 3’
2ST243	Rcf1 Q61A For2	5’ CGTCTTGGTAATAAATGGAAAGCTGCGTACTACT TCGC 3’
2ST244	Rcf1 Q61A Rev2	5’ GCGAAGTAGTACGCAGCTTTCCATTTATTACCAA GACG 3’
ST875	Rcf1 R65A For	5’ GCTCAGTACTACTTCGCTTGGCGTGTGGGTCTA CAAGCG 3’
ST876	Rcf1 R65A Rev	5’ CGCTTGTAGACCCACACGCCAAGCGAAGTAGTA CTGAGC 3’
ST877	Rcf1 R67A For	5’ GCTCAGTACTACTTCCGTTGGGCTGTGGGTCTA CAAGCGGCC 3’
ST878	Rcf1 R67A Rev	5’ GGCCGCTTGTAGACCCACAGCCCAACGGAAGTA GTACTGAGC 3’

2ST189	Rcf1 R67Q For	5’ GCTCAGTACTACTTCCGTTGGCAAGTGGGTCTA CAAGCGGCC 3’
2ST190	Rcf1 R67Q Rev	5’ GGCCGCTTGTAGACCCACTTGCCAACGGAAGTA GTACTGAGC 3’
2ST191	Rcf1 R67E For	5’ GCTCAGTACTACTTCCGTTGGGAAGTGGGTCTA CAAGCGGCC 3’
2ST192	Rcf1 R67E Rev	5’ GGCCGCTTGTAGACCCACTTCCCAACGGAAGTA GTACTGAGC
2ST193	Rcf1 R67K For	5’ GCTCAGTACTACTTCCGTTGGAAGGTGGGTCTA CAAGCGGCC 3’
2ST194	Rcf1 R67K Rev	5’ GGCCGCTTGTAGACCCACCTTCCAACGGAAGTA GTACTGAGC 3’
2ST195	Rcf1 R67H For	5’ GCTCAGTACTACTTCCGTTGGCATGTGGGTCTA CAAGCGGCC 3’
2ST196	Rcf1 R67H Rev	5’ GGCCGCTTGTAGACCCACATGCCAACGGAAGTA GTACTGAGC 3’
2ST185	Rcf1 V68C For	5’ GCTCAGTACTACTTCCGTTGGCGTTGTGGTCTAC AAGCGGCCACACTAGTCGC 3’
2ST186	Rcf1 V68C Rev	5’ GCGACTAGTGTGGCCGCTTGTAGACCACAACGC CAACGGAAGTAGTACTGAGC 3’
2ST187	Rcf1 G69C For	5’ GCTCAGTACTACTTCCGTTGGCGTGTGTGTCTAC AAGCGGCCACACTAGTCGC 3’
2ST188	Rcf1 G69C Rev	5’ GCGACTAGTGTGGCCGCTTGTAGACACACACGC

		CAACGGAAGTAGTACTGAGC 3’
ST838	Rcf1 Q71A For	5’ GCGTGTGGGTCTAGCAGCGGCCACACTAGTCG CACTAGTCGC 3’
ST839	Rcf1 Q71A Rev	5’ GCGACTAGTGCGACTAGTGTGGCCGCTGCTAGA CCCACACGC 3’
2ST245	Rcf1 Q71A For2	5’ GGCTGTGGGTCTAGCAGCGGCCACACTAGTCG CACTAGTCGC 3’
2ST246	Rcf1 Q71A Rev2	5’ GCGACTAGTGCGACTAGTGTGGCCGCTGCTAGA CCCACAGCC 3’
2ST189	HsHig1-1A For	5’ GGGTCTAGAATGTCAACAGACACAGGTGTTTCC C 3’
2ST005	HsHig1-1A Rev2	5’ GGGCTGCAGTTAGTGGTGATGATGGTGGTGATG ATGGTGGTGATGATGAGGCTTAGGTTTTGCCCA 3’
ST885	HsHig1-2A For	5’ GGGTCTAGAATGGCGACTCCCGGCCCTGTG 3’
ST886	HsHig1-2A Rev	5’ GGGCTGCAGTTAGTGGTGATGATGGTGGTGATG ATGGTGGTGATGATGGGGTCGAGACTTCATAGC 3’

For = Forward primer (binds to 5’ region of ORF)
Rev = Reverse primer (binds to 3’ region of ORF)

same time. Rcf1 P32A, P35A, C38A, R65A and R67A (Q/H/K/E) derivatives were made by mutating Pro-32, Pro-35, Cys-38, Arg-65 or Arg-67 individually. The Rcf1 Q/R pair mutants (Q61A/R65A and R67A/Q71A) were made using the R65A and R67A mutant derivatives as the template to mutate Gln-61 or Gln-71, respectively. Likewise, the C28A/C38A mutant was made by using the C38A mutant as the template to mutate Cys-28 to Ala. The reaction mixture for the PCR was prepared according to standard protocols and contained; template DNA [100 ng], forward (or reverse) primer [0.25 μM],

1x *Pfu* Buffer, dNTP mix [200 μM], *Pfu* DNA polymerase (1.25 units). Forward and reverse priming reactions were performed separately, an in parallel to a control reaction that did not contain DNA polymerase. Following a hot start that was performed at 95°C for 50 s, three cycles of denaturation (95°C for 50 s), annealing (55°C for 50 s) and extension (68°C for 15 m) were performed. Corresponding forward and reverse reactions were then combined into a single tube and an additional 1.25 units of *Pfu* DNA polymerase was added. This was followed by a hot start performed at 95°C for 50 s, and 24 cycles of denaturation (95°C for 50 s), annealing (55°C for 50 s) and extension (68°C for 15 m). Amplified DNA was subsequently analyzed by agarose gel electrophoresis (Sambrook et al. 1989). Following PCR amplification, DpnI restriction digestion of template DNA was performed using 1 unit of the Dpn1 restriction endonuclease (New England BioLabs). The reaction mixture was incubated at 37°C for 3 hours. Following heat inactivation of the enzyme at 80°C for 20 min. 1 μl of the reaction was transformed into the E. coli cells as described in section 2.1. Positive E.coli transformants, which harbored the plasmid containing the ampicillin resistant gene, were selected based on their ability to grow on LB media containing ampicillin. The plasmid DNA of successful transformants was purified (as decribed in section 2.1.3) and subjected to DNA sequencing to verify the incorporation of the correct mutation.

2.2.2 Restriction Digestion and Transformation into *E. coli*

Plasmid DNA (e.g. the DpnI digested product described in section 2.1.1)(1 μl) was transferred to a 0.1 cm electroporation cuvette and transformed into 40 μl of TOP10 chemically competent *E. coli*. by electroporation using a Biorad Gene MiroPulser (3 kV, 400 Ω, 25 μF). Following the pulse, 1 ml of LB (Luria-Bertani) medium was immediately

added to the cuvette and the mixture was incubated at 37°C for 1 hour shaking at 225 rpm. Cells were recovered by a short (~1 min) centrifugation and plated on selective medium (LB-Amp) for 16 hours at 37°C.

2.2.3 Isolation of Plasmid DNA

Positive bacterial transformant colonies were manually isolated from the initial selection (LB-AMP) plate and inoculated in 5 ml LB-Amp medium overnight at 37°C. Plasmid DNA was isolated from selected colonies using a plasmid isolation kit according to the manufacturers specifications (Qiagen). Following isolation, DNA was eluted in H_2O and stored at 4°C. DNA was then subjected to sequencing to verify the incorporation of the correct mutation.

2.2.4 Plasmid DNA Linearization and Transformation into Competent Yeast Cells

Plasmid DNA of yeast integrating plasmids (e.g. Yip351-based palsmids) was linearized using the restriction endonuclease BstEII (New England BioLabs) and the reaction was performed in the recommended buffer supplied by the manufacturer (New England BioLabs). BstEII cuts at a unique position in the LEU2 gene of the Yip351 plasmid. Purified plasmid DNA (15 µl, concentration varied) was digested using 10 units of BstEII at 60°C for 2 hours during which the mixture was vortexed every 20 min. Approximately 1 hour into the incubation, an additional 10 units of enzyme was added. Following incubation in restriction enzyme, 3M NaAc (pH6.0) and Ethanol (p.a.) were added to the digested (linearized) product and the mixture was stored at -20°C overnight.

Following linearization, recombinant plasmids were integrated into the yeast genome at the *leu*2 gene locus. To prepare DNA for transformation into yeast, linearized

DNA was pelleted by centrifugation at 15,000 rpm for 15 min at 4°C, washed in 70% Ethanol and pelleted again prior to drying using a SpeedVac vacuum concentrator. To the dried pellet, 15 µl of H_2O was added and DNA was stored at -20°C. Approximately 5 µl of linearized DNA was mixed with 50 µl of yeast competent cells (W303-1A) by gentle pipetting up and down. Cold PEG (300 µl)(100 mM LiAc, 10 mM Tris-HCl (pH 8.8), 1 mM EDTA/NaOH, 40% PEG 3350) was added to the mixture and gently mixed by pipetting up and down prior to incubation at 30°C for 30 min under constant shaking. Following incubation, DMSO (40 µl) was added and the mixture was incubated at 42°C for 10 min. The yeast competent cells were pelleted by centrifugation at 2,000 rpm for 3 min, and washed once in H_2O prior to being pelleted again in a final volume of 200 µl H_2O. Approximately 100 µl of yeast cells were plated onto selective medium (SD-Leu) and grown for approximately 3 days at 30°C. Leucine-positive transformants were isolated and grown overnight in 5 ml of YP-lactate containing galactose (2%) prior to isolation of the mitochondria by the *Quick Preparation Procedure* described in section 2.1.6. for further characterization by SDS-PAGE (section 2.2.2), western blotting (section 2.2.3), and immune-decoration (section 2.2.4) with an anti-His antibody.

2.2.5 Cloning of Human Hig1-1A and Hig1-2A

Clones of human Hig1 isoforms, Hig1-1A (*NP_054775*) and Hig1-2A (*NP_620175*), were purchased from a manufacturer (ATCC, Manassas, VA) and individual clones were provided in respective cloning vectors (pDNR-LIB-Hig1-1A (pOTB7- Hig1-2A) that had been transformed into *E. coli* (Figure 6, Figure 7).

PCR amplification of Hig1-1A/2A ORF

Bacterial clones were grown overnight at 37°C in selective medium (LB-chloramphenicol). Following overnight growth, plasmid DNA was isolated as described above in section 2.1.3. PCR amplification of the human Hig1 DNA was performed using primers (TABLE 1) that were designed to amplify the Hig1 ORFs as Xba1-Pst1 fragments, and included 12 histidine residues prior to the stop codon. The PCR-amplified DNA was purified using a DNA isolation kit according to the manufacturers specifications (GeneJET®, Fermentas) and excess ethanol was evaporated from the purified plasmid DNA using a SpeedVac vacuum concentrator.

Restriction Digest and Gel purification of Hig1-1A/2A DNA fragments

The insert (Hig1-1A or Hig1-2A) was excised by restriction digestion, performed in the recommended buffer supplied by the manufacturer (New England BioLabs) and 1 unit of each endonuclease (Xba1 and Pst1). The reaction mixture, containing 25 µl of purified DNA, was incubated at 37°C for 2 hours. Following heat inactivation of the enzyme at 80°C for 20 min, the digested product was loaded onto a 1% agarose gel and electrophoresis was performed for 1 hour at 50 V. DNA fragments were visualized using a UV illuminator and identified by their respective sizes (Hig1-1A, approximately 350 kDa and Hig1-2A, approximately 400 kDa). The purified DNA fragments were excised from the gel using a sterile razor blade and kit purified according to the manufacturers specifications (QIAquick®, Qiagen).

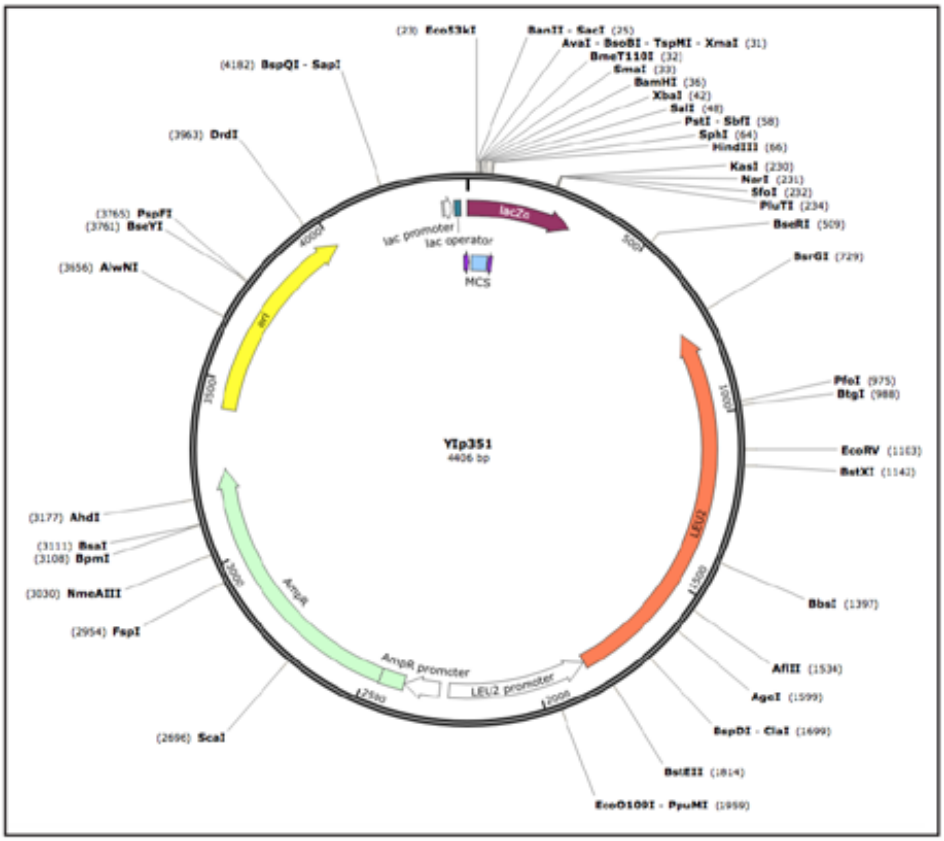

Figure 5. The Yip351 plasmid featuring a single BstEII site and LEU2 gene. Image source: SnapGene

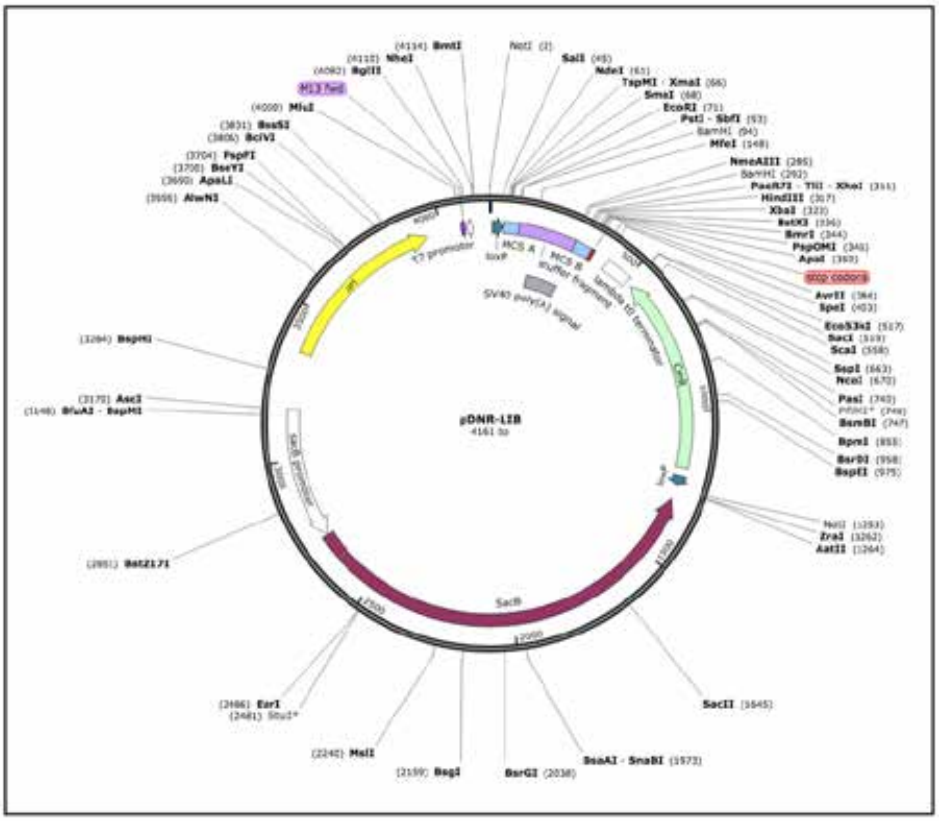

Figure 6. The pDNR-LIB plasmid featuring single Xba1 and Pst1 sites. Image source: SnapGene

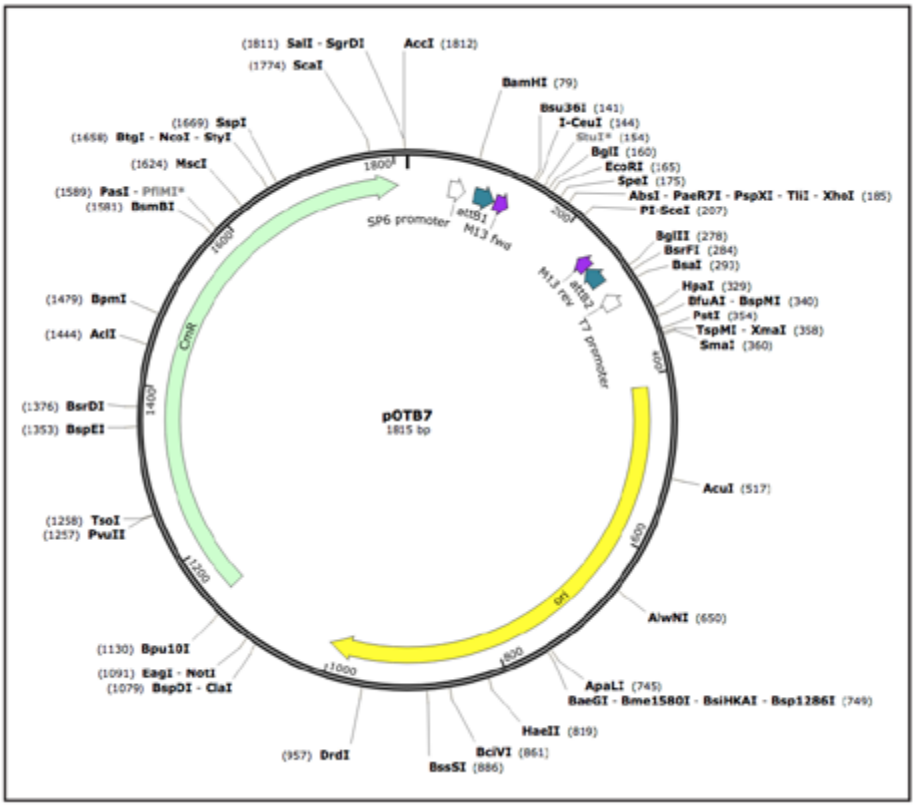

Figure 7. The pOTB7 plasmid featuring single Xba1 and Pst1 sites. Image source: SnapGene

Ligation of Hig1-1A/2A into Yip351-GAL10/LEU2 expression vector

The purified DNA fragments were ligated into Yip351/LEU2 plasmid downstream of the GAL10 promoter for expression of the human Hig1 proteins (Figure 5). The Yip351/LEU2 plasmid was pre-cut with Xba/Pst1 and treated with calf intestinal phosphatase (CIP) in preparation for the ligation reaction. The ligation reactions of purified Hig1-1A/2A DNA fragments into the Yip351 vector were performed overnight at 16°C using a 1:1 (vector:insert) ratio and 1 unit of T4 DNA ligase in appropriate buffer supplied by the manufacturer (New England Biolabs).

Transformation into E. Coli, colony PCR, analytical digestion and Yeast transformation

Ligated Yip351-Hig1-1A/2A plasmids were transformed into MH1 *E. coli* as described above in section (2.1.2), and grown overnight on plates containing selection medium (LB-Amp). Ampicillin-positive colonies were isolated by gentle removal from the plate using a sterile pipet tip, and colony PCR was performed to identify bacterial transformants that contained Yip351-Hig1-1A/2A plasmids. The reaction mixture for the PCR was prepared according to standard protocols and contained; template DNA, forward (Yip351) and reverse (Hig1-1A or Hig1-1A) primers [0.4 μM], 1x *Pfu* Buffer, dNTP mix [200 μM], *Pfu* DNA polymerase (1.25 units). The colony PCR products were run on a 1%agarose gel and successful transformants were selected for plasmid purification as described above. Analytical digestion was performed on the purified plasmid DNA in a reaction mixture containing 5 μl of purified plasmid DNA (approximately 2 μg of DNA), 1 unit of Xba1 and Pst1, and appropriate buffers provided

by the manufacturer (New England Biolabs). Following digestion at 37°C for 2 hours, the enzymes were heat inactivated by incubation at 80°C for 20 min. Successful transformants were verified by sequencing as described above, and following the linearization by BstEII, recombinant plasmid was transformed into the Δ*rcf1*;Δ*rcf2* yeast strain.

2.2.6 Isolation of mitochondria: Long, and Quick-Long, and Quick Preparation

Mitochondria were isolated from wild type and mutant strains to characterize the Rcf1 and Hig1 proteins by various biochemical and physiological analyses. Three different procedures were used to isolate mitochondria, with the specific method selected according to the level of mitochondrial function that is required for the biochemical analyses to be performed. The long preparation yields large quantities of intact mitochondria that are of sufficient quality for the majority of the biochemical and physiological analysis performed in our lab. The Quick-long and Quick preparations were adapted to expedite the isolation of mitochondria from yeast strains for routine analysis of protein content. While the Quick-long preparation yields large amounts of mitochondria, the use of glass beads to physically break the cell wall of the yeast can result in damage to the mitochondria, a hazard that is circumvented in the Long preparation by using zymolyase to digest the cell wall of yeast. The Quick preparation is primarily used as a rapid method of isolating mitochondria to test whether a protein of interest is expressed in the mitochondria in a stable manner.

Long Preparation Procedure.

Yeast strains were pre-inoculated at 30°C for 3 days prior to mitochondrial isolation in successively larger volumes (50-400 ml) of YP (yeast extract and peptone)-medium containing 0.5% lactate and 2% galactose. Mitochondria were isolated from a given yeast culture that was grown in 4L of medium, and harvested when the yeast were in mid-logarithmic phase. Mitochondria were isolated from yeast cells according to the method described in (Daum et al., 1982) with specific modifications (Herrmann et al., 1994). Following isolation, mitochondria were re-suspended in SEM buffer (250 mM sucrose, 2 mM EDTA, 10 mM MOPS-KOH pH7.2) and aliquoted at a protein concentration of 10 mg/ml into 25 µl aliquots, flash-frozen in liquid nitrogen and stored at -80°C.

Quick-long Preparation Procedure

Mitochondria were isolated according to the method described by (Arnold et al., 1998), and modified to isolate mitochondria from 500 ml cultures. Yeast strains were pre-inoculated at 30°C overnight in (50-100 ml) of YP (yeast extract and peptone)-Lactate containing 2% galactose, which was used to inoculate 500 ml of medium at an optical density (O.D.) of 0.2 A_{580nm}. Yeast cells were harvested by centrifugation at 4,000 rpm for 5 min when they reached an O.D. of 2.0 A_{580nm} and washed in H_2O. The weight of the cell pellet was measured and glass beads (0.5 mM) and SEM buffer were added accordingly (1g cells=1 ml SEM and 1ml glass beads). Yeast cells were vortexed at 30 s intervals for 10 min. Lysed cells were transferred to new tubes and centrifuged at 4,000 rpm for 5 min to separate mitochondria from the glass beads and cell debris. The supernatant, containing isolated mitochondria, was transferred to a new tube and centrifuged at 10,000 rpm for 12 min at 4°C. The pelleted mitochondria were re-

suspended in 10 ml of cold SEM buffer and centrifuged at 4,000 rpm for 5 min at 4°C to remove residual cell debris. The supernatant was transferred to a new tube and centrifuged at 12,000 rpm for 12 min at 4°C to pellet the isolated mitochondria. Protein concentration was determined and 10 mg/ml aliquots were flash-frozen in liquid nitrogen and stored at -80°C.

Quick Preparation Procedure

Mitochondria were isolated from 5 ml of yeast cells grown overnight in YP-lactate (2% galactose) at 30°C. Yeast cells were harvested by centrifugation at 2200 rpm for 3 min at room temperature (RT) and resuspended in 0.6 ml of cold SH (0.6 M sorbitiol, 20 mM -KOH pH 7.2) buffer containing 1mM PMSF. The cell suspension was divided equally between two microcentrifuge tubes and glass beads were added (approximately 100 µl). Cell suspension was vortexed 5-6 times for 30 s intervals and kept on ice for ≥ 30 s prior to next vortexing. Following centrifugation of the cell suspension at 3000 rpm for 3 min at 4°C, 500 ml of supernatant was removed and transferred to a new tube (supernatants were pooled from identical samples). Isolated mitochondria were pelleted by centrifugation at 12,000 rpm for 15 min at 4°C and resuspended in 20 µl of 1X Laemmli buffer containing β-mercaptoethanol (BME) prior to freezing at -80°C.

2.2.7 Serial Dilution Growth Analysis

Yeast strains to be tested were streaked from glycerol stocks onto a fresh YPAD plate and incubated at 30°C for 3 days prior to serial dilution. A small amount of yeast cells were extracted from the YPAD growth plate using a sterile pipet tip and transferred

to a microcentrifuge tube containing 900 µl of H_2O. The cell suspension was vortexed and 800 µl were transferred to a spectrophotometer cuvette prior to measurement of the O.D. at $A_{580\ nm}$. Based on the starting O.D., the remaining cell suspension (100 µl) was diluted to make a stock solution of O.D. 0.1 $A_{580\ nm}$. From the stock cell suspension, ten-fold dilutions were prepared in separate tubes. The serial dilutions were pipetted (4 µl) onto a new plate and incubated at 25°C, 30°C, or 37°C for 3-5 days. Images of the plate were scanned every 24 hours.

2.3 Protein Biochemistry and Physiology Methods

2.3.1 Protein determination (Bradford Method)

Mitochondrial protein concentration was determined using the Bradford method, a colorimetric-based detection assay for measuring the concentration of proteins in solution (Bradford, 1976). Bovine gamma globulin IgG (Bio-Rad) was used to generate protein standards for the assay by the resuspension of bovine gamma globulin IgG in 100 µl (total) H_2O in increasing concentrations (0, 0.04, 0.07, 0.15, 0.3, 0.6 mg/ml). Mitochondrial protein samples to be tested were diluted in H_2O (1:10) and 10 µl of the diluted sample was used for protein determination. Protein Assay Dye Reagent (Bio-Rad) was diluted (1:5) and 1 ml of reagent was added to samples and standards and mixed by inversion (6-10 times). The $A_{595\ nm}$ of each standard was measured using a spectrophotometer (Beckman Coulter) and plotted against the protein concentration. Mitochondrial samples were then measured and their protein concentration was calculated based on the standard curve.

2.3.2 SDS-PAGE

Sodium dodecyl sulfate polyacrylamide gel electrophoresis (SDS-PAGE) gels were prepared according to Laemmli (1970) as 9 cm x 15 cm separating layer and 1 cm x 15 cm stacking layer. For this study, 17.5% acrylamide, 0.2% bisacrylamide SDS-PAGE gels were used (Laemmli, 1970). Separation of proteins was performed by electrophoresis in 1X electrophoresis running buffer (2 M glycine, 0.1% SDS, 50 mM Tris-Cl pH 8.9). Samples were prepared with 1X Laemmli buffer and loaded into gel lanes using a Hamilton 50 µl syringe. A molecular weight marker (Thermo) was loaded onto the SDS-PAGE gel for estimation of molecular weight. Electrophoresis was performed at a constant voltage (25 mA) for approximately 2 hours.

2.3.3 Western Blotting: Transfer of SDS-PAGE Gel to Nitrocellulose Membrane

Following electrophoresis, the SDS-PAGE gel was transferred onto a nitrocellulose membrane (Whatman) for immuno-decoration. In this dissertation study, the transferring of proteins on an SDS-PAGE gel to nitrocellulose and the subsequent analysis by immuno-decoration is collectively referred to as western blotting. The semi-dry blotting method described by Kyshe-Anderson (1984) was used to transfer proteins from the SDS-PAGE gel to nitrocellulose, with modifications. A layered preparation consisting of: 3 Whatman filter papers (3mm), a nitrocellulose membrane (0.2 µm), an SDS-PAGE gel, and 2 Whatman filter papers (3mm) was assembled on a western blot apparatus (SCIE-PLAS) (each component was pre-soaked in transfer buffer. The western blot layered preparation was subjected to electrophoresis (250 mA) for 1.5 hours. Following electrophoresis, the nitrocellulose membrane was washed in H2O and stained

with Ponceau S solution (Sigma) to visualize proteins. The position of the molecular weight marker was recorded on the nitrocellulose membrane using a permanent marker prior to removal of ponceau by washing the membrane in H_2O.

2.3.4 Western Blotting: Immuno-decoration of Nitrocellulose Membrane

The nitrocellulose membrane was prepared for immune-decoration by blocking in 5% non-fat milk powder solution prepared in 1X TBS (10 mM Tris-Cl pH7.5, 150 mM NaCl) for 1 hour at RT. Primary antibody solution was prepared in 5% non-fat milk powder solution at a dilution recommended by the producer (typically 1:1,000). The membrane was incubated in primary antibody solution for 1 hour at RT or overnight at 4°C with continuous rocking. Following primary antibody incubation, the membrane was washed in 3 consecutive 10-15 minute steps: 1X TBS, 1X TBS with 0.05% (w/v) Triton X-100, and 1X TBS. The membrane was incubated in appropriate horseradish peroxidase –conjugated secondary antibody that was prepared in milk powder solution (1:5000 dilution) for 1 hour at RT.

Following secondary antibody incubation, the membrane was washed according to the 3-step procedure described above. The horseradish-peroxidase signal was detected by enzymatic chemiluminescence (ECL) (Roswell and White, 1978). Two separate ECL solutions were prepared accordingly: solution I (9.2 ml H_2O, 530 µl 1.875 M Tris-Cl pH 8.8, and 6 µl H_2O_2) and solution II (9.2 ml H_2O, 530 µl 1.875 M Tris-Cl pH 8.8, 44 µl Coumeric acid (15 mg/ml in DMSO), and 100 µl Luminol (44 mg/ml in DMSO)). The two solutions were mixed (1:1) in the dark room and the membrane was incubated for 1 min at RT in the ECL solution mixture with gentle rocking. The membrane was exposed

to X-ray film for appropriate time intervals and films were developed using an AGFA CP1000 automated developer.

2.3.5 BN-PAGE and 1D BN-PAGE/2D SDS-PAGE

For the resolution of protein complexes, Blue Native-PAGE was performed using the Novex® NativePAGE™ Bis-Tris gel system (Invitrogen/Thermo Fisher Scientific). For this study, pre-cast polyacrylamide 3-12% Bis-Tris mini-gels (8 cm x 8 cm, 1.0 mm thickness) were used. Separation of protein complexes was performed by electrophoresis at 150 V for 4.5-5.5 hours using a Novex® NativePAGE™ electrophoresis apparatus containing cold anode buffer (1X NativePAGE electrophoresis running buffer (50 mM Bis-Tris, 50 mM tricine pH 6.8)) in the outer chamber, and cold 1X blue cathode buffer (1X NativePAGE electrophoresis running buffer, 0.02-0.002% G250 Coomassie) in the inner chamber. Electrophoresis was performed first with 1X dark blue cathode buffer (0.02 % G250 Coomassie) in the inner chamber for 45 minutes, at which time the current was stopped and dark blue cathode buffer was replaced with light blue cathode buffer (0.002 % G250 Coomassie) in the inner chamber prior to resuming electrophoresis.

Preparation of Samples

Mitochondria (30 μg) were thawed on ice and pelleted by centrifugation at 13,000 rpm for 10 min at 4°C. Pelleted mitochondria were solubilized in buffer containing 1% digitonin or 0.6% n-Dodecyl-β-D-Maltoside (DDM) and Invitrogen pink sample buffer (50 mM Bis-Tris, 6 N HCl, 50 mM NaCl, 10% w/v glycerol, 0.001% Ponceau S, pH 7.2) for 20 min on ice. Following solubilization of the mitochondria, a clarifying spin was performed on the mitochondrial lysate by centrifugation at 15,000 rpm for 10 min at 4°C.

The supernatant was transferred to a new microcentrifuge tube and 0.35 µl of 5% G250 Coomassie was added and mixed with the supernatant by gently flicking the tube. Samples were loaded onto the BN-PAGE gel using a Hamilton syringe, and a NativeMARK™ unstained protein standard (Invitrogen/Thermo Fischer) was loaded onto the BN-PAGE gel for the estimation of molecular weight.

2nd Dimension SDS-PAGE

After the separation of protein complexes by BN-PAGE, individual lanes of the native gel were excised as a 60 mm rectangle for separation on a denaturing NuPAGE™ 4-12% Bis-Tris Gel. Selected lanes were excised using a razorblade and carefully transferred by spatula to a 15 ml conical tube. Gel strips were prepared for 2D SDS-PAGE by a series of 3 incubations in LDS (lithium dodecyl sulfate) solutions (4X LDS: 106 mM Tris HCl, 141 mM Tris Base, 2% LDS, 10% glycerol, 0.51 mM EDTA, 0.22 mM G250 Coomassie, 0.175 phenol red, pH 8.5): LDS-DTT (dithiothreitol) reducing solution (50 mM DTT, 1X LDS) for 30 min at RT, LDS-DMA (N,N-dimethylacrylamide) alkylating solution (50 mM DMA in 1X LDS) for 30 min at RT, and LDS-Ethanol-DTT quenching solution (5 mM DTT, 20% ethanol, 1X LDS) for 15 min at RT. Following incubations, gel strips were transferred to the 2nd dimension SDS-PAGE gel using a spatula, and the low molecular weight end of the gel strip was positioned directly adjacent to the 2nd dimension SDS-PAGE gel lane containing the molecular weight marker. Electrophoresis was performed at 100 V for 1.5-2 hours.

Semi-dry Transfer of 1D BN-PAGE and 1D BN-PAGE / 2D SDS-PAGE

BN-PAGE and 2nd dimension SDS-PAGE gels were transferred to a nitrocellulose as previously described (section 2.2.3), with the modification of a 1 hour transfer time.

2.3.6 Steady state analysis of mitochondrial proteins

Mitochondria were prepared for steady state analysis by resuspending 100-200 μg of mitochondria (10 mg/ml in SEM buffer pH 7.2) in an equal volume of 2X Laemmli buffer (4% SDS, 20% glycerol, 20 mM Tris, 0.02% bromophenol blue, 5% β-mercaptoethanol) followed by further dilution in 1X Laemmli buffer (final concentration of 2.5 mg/ml). Samples were mixed by pipetting up and down and stored at -20°C prior to analysis by SDS-PAGE, western blotting and immune-decoration with appropriate anti-serum.

2.3.7 Ni-NTA Affinity purification of His-tagged proteins.

The affinity purification of His-tagged proteins was performed using Ni-NTA agarose beads (Qiagen), as previously described (Jia et al., 2007).

Preparation of beads

The Ni-NTA agarose beads were equilibrated prior to the addition of mitochondrial lysate. Microcentrifuge tubes containing 30 μl of beads were prepared for each sample of mitochondria. Following a brief spin at 13,000 rpm for 2 min at RT, the beads were equilibrated by 3 iterations of addition of buffer (0.1 M KCl, 0.02 M Hepes-KOH pH 7.2, 0.001 M PMSF, 0.03 M imidazole 0.1% detergent, as indicated), followed by centrifugation at 13,000 rpm for 2 min at RT. After the last centrifugation and removal of supernatant, 9 μl of 1 M imidazole was added and the beads were stored on ice.

Affinity Purification of His-tagged protein on Ni-NTA beads

Mitochondria (200 µg) were solubilized in lysis buffer (100 mM KCl, 20 mM HEPES-KOH, 10 mM $MgCl_2$, 0.5 mM pheylmethylsulfonyl fluoride (PMSF), pH 7.4), containing either 0.25% Triton X-100, 0.6% n-Dodecyl-β-D-Maltoside (DDM) or 1% digitonin for 30 minutes on ice. Mitochondrial lysate was centrifuged at 10,000 rpm for 10 minutes at 4°C. Following centrifugation of the mitochondrial lysate, an aliquot (5% of total supernatant) of the supernatant was transferred to a separate tube and prepared for gel electrophoresis by the addition of 2X Laemmli buffer containing βME, and stored at -20°C. The remaining supernatant was added to the equilibrated beads, and after a quick vortex, the mixture was incubated with continuous agitation for 1 hour at 4°C. Following incubation, the Ni-NTA beads containing bound His-tagged protein were pelleted by centrifugation at 13,000 rpm for 2 minutes at 4°C. The beads were washed 3 times with buffer, as described in the *Preparation of the Beads*. After the final centrifugation the supernatant was removed completely using a syringe and 1X Laemmli buffer containing βME and 500 mM imidazole was added and vortexed hard for 1 min. Samples were stored at -20°C.

2.3.8 Chemical cross-linking

Chemical cross-linking was performed to identify proteins within the molecular environment of Rcf1 in the mitochondria and was performed as previously described by Jia, et al. ((Jia et al., 2009) with modifications. Cross-linking was carried out *in vivo*, and thus, provides the advantage of studying the native molecular environment of Rcf1 in the absence of solubilizing the outer mitochondrial membrane. Mitochondria (100 µg) were

resuspended in SH buffer pH7.2 (0.6 M sorbitol, 20 mM Hepes) at a final concentration of 0.5 mg/ml, and cross-linking was performed on ice for 30 min in the presence of cross-linker or DMSO control (all cross-linkers were dissolved in DMSO, and thus, DMSO served as the control condition). Cross-linking reactions were quenched with 10 mM glycine (for amino-based cross-linking) or *N*-ethylmaleimide (for sulfhydryl-based cross-linking) for 15 min on ice, followed by a clarifying centrifugation at 15,000 rpm for 15 min at 4°C. Pelleted mitochondria were then washed in SH Buffer and centrifuged again at 15,000 rpm for 15 min at 4°C. Mitochondria were resuspended in 1X Laemmli buffer containing βME and were stored at -20°C for analysis by SDS-PAGE and western blotting.

Chemical cross-linking under various mitochondrial bio-energetic states

Chemical cross-linking was performed under a number of mitochondrial bio-energetic states to determine whether the molecular environment of Rcf1 and partner proteins is influenced by the mitochondrial bio-energetic status. For bio-energetic cross-linking experiments, mitochondria were resuspended in isosmotic buffer (10 mM KPi, 20 mM Hepes-KOH, 2 mM $MgCl_2$, 1 mM EDTA, 1 mg/ml BSA, 0.6 M Mannitol; pH 7.2) in place of SH-buffer. State 4 respiration was achieved by the addition of the substrate NADH (0.5 mM final concentration) and proceeded for a duration of 2 min prior to the addition of cross-linking reagent (for state 4 cross-linking) or the subsequent addition of ADP (0.2 mM) to achieve state 3 respiration. State 3 respiration proceeded for 2 min, at which point cross-linking reagent was added (for state 3 cross-linking) or the protonophore CCCP (20 mM) was added to achieve an elevated level of respiration

where the translocation of protons is uncoupled from the phosphorylation of ADP. The uncoupled respiration induced by the addition of CCCP proceeded for 1 min, at which point cross-linking reagent was added. Following the pre-conditioning of mitochondria to achieve a specific bio-energetic status, cross-linking reactions proceeded as described above.

Chemical cross-linking in the presence of inhibitors

Chemical cross-linking was performed in the presence of specific inhibitors of AAC (atractyloside/AT, bongkrekic acid/B.A.) to determine whether the conformation of AAC influences the formation of the Rcf1-AAC cross-link adduct. Prior to the addition of cross-linking reagent, inhibitor was added to the resuspended mitochondria at a final concentration of 10 μM. The addition of inhibitor to the resuspended mitochondria was followed immediately by the addition of cross-linking reagent and the reaction proceeded as described above.

2.3.9 Mitochondrial *In organello* labeling of mitochondrial translation products

In organello [^{35}S] methionine labeling of mitochondrial translation products was performed according to Hell et al., ((Hell et al., 2001). Isolated mitochondria (200 μg) were incubated in translation buffer (0.6 M sorbitol, 150 mM KCl 15 mMKH_2PO_4, 13 mM $MgSO_4$, 0.15 mg/ml all amino acids (minus methionine), 3 mg/ml fatty-acid free bovine serum albumin, 4 mM ATP, 0.5 mM GTP, 5 mM α-ketoglutarate, 5 mM phosphoenolpyruvate, and 20 mM Tris-Cl, pH7.4) containing 0.6 units of pyruvate kinase and 2 mM NADH prior to the addition of 1 μl (10-15 μCi) of [^{35}S] methionine. Samples were incubated in buffer containing [^{35}S] methionine for 20 min at 30°C before being

stopped by the addition of puromycin (42 μg/ μL) and 10 mM unlabeled methionine. The samples were incubated an additional 5 min at 30°C to completely stop synthesis, and isolated by centrifugation at 10,000 rpm for 10 min at 4°C. Pelleted mitochondria were washed once in SH-buffer, pelleted again by centrifugation at 10,000 rpm for 10 min at 4°C. Following further analysis (i.e. Ni-NTA affinity chromatography, SDS-PAGE (or 1D BN-PAGE/2D SDS-PAGE) and western blotting, radiolabeled translation products were visualized by autoradiography for various time intervals.

2.3.10 Silver staining of SDS-PAGE Gels

SDS-PAGE gels were silver stained to visualize mitochondrial proteins for further analysis (i.e. extraction for LC-MS/MS or to directly compare protein composition and abundance between samples). Immediately following SDS-PAGE, the gel was washed briefly in H_2O, and fixed by incubation for 30 min at RT in a methanol (45% final concentration)- acetic acid (7% final concentration) solution. The gel was washed 3 X 5 min in H_2O prior to incubation in 1mM sodium thiosulfate penthydrate (Sigma) solution for 1.5 min. Following incubation, the gel was washed 3 X 0.5 min and stained in 10 mM silver nitrate (Sigma) solution for 25 min at RT. The silver stained gel was then washed 3 X 1 min in H_2O prior to incubation in developing solution (0.6 M sodium carbonate (Sigma), 0.02 mM sodium thiosulfate penthydrate, and 0.02% formaldehyde) for 5-10 min. Developing was stopped by incubating the gel in methanol - acetic acid solution for 10 min.

2.3.11 Cytochrome *c* oxidase 'In Gel' activity assay

The specific activity of complex IV was determined by performing an 'in-gel' activity assay following the separation of protein complexes by BN-PAGE (0.6% DDM). BN-PAGE was performed as described above with the following modifications. Mitochondrial protein (200 μg) was solubilized in buffer (80 μl) containing 0.6% DDM for 30 minutes at 4°C. Solubilized mitochondria were subjected to clarifying centrifugation for 10 minutes at 15,000 rpm at 4°C. Following centrifugation, the supernatant was removed and split between 2 microcentrifuge tubes. 0.7 μl of G250 coomassie was added to each sample and samples (duplicates) were loaded into one 3-12% BIS-TRIS Invitrogen NuPAGE 10-well gel. Electrophoresis was performed at 150 V for 5 hours and 30 min, and the gel was cut in two; one half of the gel (containing one set of samples) was prepared for western blotting and the second half of the gel (containing a set of identical samples) was used for the cytochrome *c* oxidase in gel activity assay detailed below.

Prior to incubation in *Activity Assay Buffer*, the gel was placed on a glass plate and scanned (SCAN1). The gel was then incubated for 90 minutes at room temperature in *Activity Assay Buffer* (50 mM phosphate buffer pH 7.4, 1 mg/ml 3,3' diaminobenzidine (DAB), 1 nM catalase, 1mg/ml cytochrome *c*, 75 mg/ml sucrose). Immediately following the incubation, the gel was washed well for 1 min in several washes of distilled water to remove excess DAB and then scanned (SCAN2). The reaction was stopped by fixing the gel in 45% Methanol / 10% Acetic acid solution for 1 hour at RT. Following the methanol/acetic acid fixation, the gel was again scanned (SCAN3), and then de-stained in 10% Methanol / 10% Acetic acid solution overnight to remove residual coomassie from

the BN-PAGE gel. Following overnight de-staining the gel was scanned (SCAN4) one last time.

2.3.12 Oxygen consumption rates (OCR)

The oxygen consumption rate (OCR) of isolated mitochondria was calculated from the decrease in oxygenation of media within the chamber of a Clark-type oxygen electrode (Rank Brothers, Digital Model 10) using isolated mitochondria (80 μg) in an isosmotic buffer (10 mM KPi, 20 mM Hepes-KOH, 2 mM $MgCl_2$, 1 mM EDTA, 1 mg/ml BSA, 0.6 M Mannitol; pH 7.2) at room temperature. State 4 respiration was achieved by the addition of substrate, NADH (0.5 mM), and measured for 3 min. State 3 was achieved by the subsequent addition of ADP (0.2 mM) and the measurement of O_2 consumption for an additional 5 min. Bioenergetically isolated complex IV OCR was attained by the addition of TMPD/ascorbate (0.4 mM/1.6 mM) to directly reduce cytochrome *c*. Maximal bioenergetically isolated complex IV activity was achieved by the subsequent addition of a protonophore (CCCP, 0.2 mM). The DCCD inhibition of bioenergetically isolated complex IV was measured as described above following a 90-minute, 25°C incubation of mitochondria in MES-TRIS buffer pH 7.3, containing 0.2% DDM and 0.6 or 1.2 mM DCCD (in methanol) or control (methanol alone).

2.4 Miscellaneous

2.4.1 Yeast strains and growth conditions.

The *S. cerevisiae* strains used in this study are the wild type (WT; W303-1A *mat*a *leu2 trp1 ura3 his3 ade2*), an *RCF1::HIS3 RCF2::KAN* (Δ*rcf1* Δ*rcf2*) strain (W303-1A *mat*a *leu2 trp1 ura3 ade2*), the *AAC2::KAN* (Δ*aac2*) strain (Chen, 2004)., an

MMP37::KANMX (Δ*tam41, aka* Δ*mmp37)* strain (Gallas et al., 2006), and the (Δ*crd1)* strain, constructed in our lab by disruption of the CRD1 gene using a KAN marker. The creation of the Δ*rcf1*;Δ*rcf2* double mutant, the Δ*aac2* mutant, and the Δ*tam41* mutant have been previously described in (Strogolova et al., 2012), (Chen, 2004) and (Gallas et al., 2006), respectively. Yeast strains were maintained and cultured at 30°C on YP medium supplemented with 2% glucose and 20 mg/liter adenine hemisulfate (YPAD) under standard protocols. Mitochondria were harvested from cultures grown in YP medium containing 0.5% lactate and supplemented with 2% galactose. A complete list of the yeast strains that were used in this study is provided (Table 2).

TABLE 2
Yeast Strains Used in This Study

Yeast Strain	Genotype	Source
WT W303-1A	*mat***a**, *leu*2, *trp*1, *ura*3, *his*3, *ade*2	Tzagoloff A.
WT+Rcf1$_{His}$	W303-1A, Plasmid YIP351GAL$_{10}$-Rcf1His/LEU2	Strogolova et al. 2012
WT+Rcf1$_{His}$ ρ^0	W303-1A ρ^0, Plasmid YIP351GAL$_{10}$-Rcf1His/LEU2	Strogolova et al. 2012
Δ*rcf1*	W303-1A, *mat***a**,*leu*2,*trp*1,*ura*3, *ade*2, *RCF1::HIS3*	Strogolova et al. 2012
Δ*rcf2*	W303-1B, *mat***α**,*leu*2,*trp*1,*ura*3, *his*3, *ade*2, *RCF2::KAN*	Strogolova et al. 2012
Δ*rcf1*;Δ*rcf2*	W303-1A, *mat***a**,*leu*2,*trp*1,*ura*3,*ade*2 *RCF1::HIS3,RCF2::KAN*	Strogolova et al. 2012
Rcf1$_{His}$	Δ*rcf1*;Δ*rcf2,* Plasmid YIP351GAL$_{10}$- Rcf1$_{His}$/LEU2	Strogolova et al. 2012
rcf1$_{His}^{C28A,C38A}$	Δ*rcf1*;Δ*rcf2,* Plasmid YIP351GAL$_{10}$- *rcf1*$_{His}^{C28A,C38A}$ /LEU2	This study
rcf1$_{His}^{P32A}$	Δ*rcf1*;Δ*rcf2,* Plasmid YIP351GAL$_{10}$- *rcf1*$_{His}^{P32A}$ /LEU2	This study
rcf1$_{His}^{P35A}$	Δ*rcf1*;Δ*rcf2,* Plasmid YIP351GAL$_{10}$- *rcf1*$_{His}^{P35A}$ /LEU2	This study
rcf1$_{His}^{W58C}$	Δ*rcf1*;Δ*rcf2,* Plasmid YIP351GAL$_{10}$- *rcf1*$_{His}^{W58C}$ /LEU2	This study
rcf1$_{His}^{A60C}$	Δ*rcf1*;Δ*rcf2,* Plasmid YIP351GAL$_{10}$- *rcf1*$_{His}^{A60C}$ /LEU2	This study
rcf1$_{His}^{Q61A,Q71A}$	Δ*rcf1*;Δ*rcf2,* Plasmid YIP351GAL$_{10}$- *rcf1*$_{His}^{Q61A,Q71A}$ /LEU2	This study
rcf1$_{His}^{Q61A,R65A}$	Δ*rcf1*;Δ*rcf2,* Plasmid YIP351GAL$_{10}$- *rcf1*$_{His}^{Q61A,R65A}$ /LEU2	This study
rcf1$_{His}^{R65A}$	Δ*rcf1*;Δ*rcf2,* Plasmid YIP351GAL$_{10}$- *rcf1*$_{His}^{R65A}$ /LEU2	This study
rcf1$_{His}^{R67A}$	Δ*rcf1*;Δ*rcf2,* Plasmid YIP351GAL$_{10}$- *rcf1*$_{His}^{R67A}$ /LEU2	This study
rcf1$_{His}^{R67Q}$	Δ*rcf1*;Δ*rcf2,* Plasmid YIP351GAL$_{10}$- *rcf1*$_{His}^{R67Q}$ /LEU2	This study

rcf1$_{His}^{R67E}$	Δ*rcf1*;Δ*rcf2,* Plasmid YIP351GAL$_{10}$- *rcf1*$_{His}^{R67E}$ /LEU2	This study
rcf1$_{His}^{R67K}$	Δ*rcf1*;Δ*rcf2,* Plasmid YIP351GAL$_{10}$- *rcf1*$_{His}^{R67K}$ /LEU2	This study
rcf1$_{His}^{R67H}$	Δ*rcf1*;Δ*rcf2,* Plasmid YIP351GAL$_{10}$- *rcf1*$_{His}^{R67H}$ /LEU2	This study
rcf1$_{His}^{R67A,Q71A}$	Δ*rcf1*;Δ*rcf2,* Plasmid YIP351GAL$_{10}$- *rcf1*$_{His}^{Q61A,R65A}$ /LEU2	This study
rcf1$_{His}^{V68C}$	Δ*rcf1*;Δ*rcf2,* Plasmid YIP351GAL$_{10}$- *rcf1*$_{His}^{V68C}$ /LEU2	This study
rcf1$_{His}^{G69C}$	Δ*rcf1*;Δ*rcf2,* Plasmid YIP351GAL$_{10}$- *rcf1*$_{His}^{G69C}$ /LEU2	This study
HsHig1-1A$_{His}$	Δ*rcf1*;Δ*rcf2,* Plasmid YIP351GAL$_{10}$- HsHig1-1A$_{His}$ /LEU2	This study
HsHig1-2A$_{His}$	Δ*rcf1*;Δ*rcf2,* Plasmid YIP351GAL$_{10}$- HsHig1-2A$_{His}$ /LEU2	This study
Δ*aac2/ CS282/1*	W303-1B, *mat***a**, *leu2-3, 112 his3-11- 15 ura3-1 ade2-1 trp1-1 can1-100 SAL1, AAC2::KAN*	Chen X.J.
Δ*tam41/* YLM2814[b]	W303-1A, *mat**a**, ura3, leu2-3,112, his3-11, trp1-1, ade2-1, ho, can1-100, mmp37*Δ*::KAN*	Gallas M.R.
Δ*crd1*	W303-1A,*CRD1::KAN*	Stuart R.A.

2.4.2 Preparation of yeast and bacterial competent cells

The MH1 *E coli*. bacterial strain was inoculated in 5 ml of medium (LB-Amp) and grown at 37°C overnight. From this culture, 500 ml of fresh LB-Amp was inoculated and grown at 37°C until an O.D. at $A_{580\ nm}$ of 0.5 was reached. The bacterial cells were then harvested by centrifugation at 5,000 rpm for 15 min at 4°C and resuspended in cold, sterile 10% (w/v) glycerol and washed 3 X with progressively lower volumes of glycerol (500 ml, 250 ml, and lastly 50 ml). Following the final wash, the cells were resuspended in 500 µl of cold, sterile 10% (w/v) glycerol, and frozen at -80°C as 50 µl aliquots.

Yeast cells (wild type and mutant strains) were inoculated in 10 ml of YPAD and grown at 30°C with overnight with constant agitation (200 rpm). Following overnight incubation, 100 ml of fresh media was inoculated from overnight cultures at a final concentration $A_{580\ nm}$ of 0.2 and harvested by centrifugation at 500 x g for 5 min at RT when cultures reached an $A_{580\ nm}$ of 0.5-0.7. Pelleted yeast cells were washed once with sterile H_2O (12.5 ml), and then with 10 ml SORB buffer (1 M sorbitol, 100 mM LiOAc,

10 mM Tris-Cl pH 8.0, and 1 mM EDTA pH 8.0). Following washes, yeast cells were resuspended in 720 µl SORB buffer and treated with 80 µl salmon sperm DNA (10 mg/ml, prepared by heating at 95°C for 10 min and cooled on ice) (Knop et al., 1999). Competent yeast cells were stored at -80°C as 50 µl aliquots.

2.4.3 Maintenance of yeast and bacterial strains

Bacterial stocks were prepared by mixing 500 µl of bacterial culture grown in LB-Amp medium overnight at 37°C with approximately 500 µl of 100% (w/v) glycerol sterilized in 2 ml cryogenic tubes and stored at -80°C. Yeast stocks were prepared by isolating a fresh yeast culture from a plate of appropriate medium (YPAD, YPG or selective media) by scraping, and resuspending yeast cells in 1 ml of 15% (w/v) glycerol sterilized in 2 ml cryogenic tubes. Following mixing of the cell suspension by vortexing, yeast stocks were stored at -80°C.

2.4.4 Primer design and Sequence analysis

Oligonucleotide primers for PCR mutagenesis were designed manually using Vector NTI (Thermo-Fisher Scientific) and ApE Plasmid Editor v2.0.45 (M. Wayne Davis) software, and manufactured by Eurofins. The GC content and melting temperature of the primers was calculated using OligoEvaluator™ (Sigma-Aldrich). DNA sequencing reactions (Sanger method) were performed by Functional Biosciences (Madison, WI) using Big Dye V3.1 and run on ABI 3730xl instruments. Verification of mutations was performed using Vector NTI and the ApE Plasmid Editor software.

2.4.5 Sequence Alignment

Rcf1 homologs were identified by performing a BLASTp (protein-protein BLAST) search using the NCBI protein database. Sequences were aligned using the Clustal Omega Multiple Sequence Alignment method.

2.4.6 Structure Modeling

Saccharomyces cerevisiae Rcf1 was modeled by protein structure homology modeling using SWISS-MODEL (Arnold et al., 2006; Bordoli et al., 2009). Structural representation of complex IV was created in The PyMOL Molecular Graphics System, Version 1.8 (Schrödinger, LLC) using the X-ray structure of bovine cytochrome *c* oxidase (PDB 2DYR).

CHAPTER 3: MUTATIONAL ANALYSIS OF THE HIG1-TYPE 2 QRRQ MOTIF IN *S. CEREVISIAE* RCF1

3.1 Introduction

The Hig1 protein family is conserved throughout evolution, with members found in α-proteobacteria and a wide variety of diverse eukaryotic taxa, including plants, fungi and mammals. Hig1 proteins can be divided into two similar, but distinct groups, type 1 and type 2, based on their sequences. Hig1 proteins, including yeast Rcf1, contain a highly conserved sequence motif that is located adjacent to TM2, and is referred to herein as the QRRQ motif. The QRRQ motif in Rcf1 corresponds to (yeast Rcf1 numbering) $[Q^{61}]$-$(X)_3$-$[R^{65}]$-(X)-$[R^{67}]$-$(X)_3$-$[Q^{71}]$. Sequence alignments indicate that the residues that correspond to R^{67} and Q^{71} are absolutely conserved throughout Hig1 proteins (FIGURE 8A). However, residues that correspond to Q^{61} and R^{65} represent a point of sequence divergence between Hig1-type1 and type2 proteins, where the QRRQ motif is a conserved feature among bacterial and mitochondrial type 2 proteins, and type 1 proteins contain a modified QRRQ motif sequence, [I/V]-HLIHM-R-$(X)_3$-[Q], that differentiates them from type 2 proteins. Sequence alignment of the *S. cerevisiae* Hig1 homologs Rcf1 and Rcf2 indicates that their similarity is mostly limited to the QRRQ motif, thereby raising the possibility that the QRRQ motif might represent a critical region for the interaction between Hig1 proteins, including Rcf1 and Rcf2, and the III-IV supercomplex/complex IV and underlie their overlapping function in supporting respiratory growth.

Hig1 proteins have been shown to be important for the correct assembly of complex IV and for respiration-based growth in yeast, and a close physical relationship

has been established between Hig1 family members, including Rcf1, and the complex IV subunits Cox3 and Cox12 (Strogolova et al., 2012). However, the functional significance of the relationship between Rcf1 and Cox3/complex IV, and the molecular basis of the respiratory growth defect in the absence of yeast Hig1 proteins Rcf1 and Rcf2, remains unknown.

Rcf1 physically associates with newly-synthesized Cox3 prior to its assembly into complex IV and, together with Rcf2, influences the assembly of the peripheral complex IV subunits Cox12 and Cox13 (Strogolova et al., 2012). The relationship with Cox12 appears to be a conserved feature among Hig1 proteins. When expressed in Hig1-deficient yeast (Δ*rcf1;*Δ*rcf2*) the *C. elegans* Hig1-type2 homolog (M05D6.5$_{His}$) co-purifies a greater amount of Cox12, relative to other complex IV subunits, than the authentic yeast Hig1 homolog Rcf1$_{His}$ (Strogolova et al., 2012). These results suggest that in addition to (or possibly via) Cox3, a close relationship may exist between Hig1 proteins and Cox12, whereby the interaction between Rcf1 and Cox12 might be flexible, and the *C.* M05D6.5$_{His}$ interaction with Cox12 is less dynamic, or possibly "locked in". Thus, the respiratory growth deficiency and reduced complex IV activity observed in the absence of Hig1 proteins in *S. cerevisiae* might be attributed to changes in the Cox3 protein, or the relationship between Cox3 and its associated protein partners within complex IV, including Cox12 and Cox4. Interestingly, Cox12, Cox4 and Hig1 proteins each interact with Cox3, and also represent the only nuclear-encoded complex IV subunits that are shared between diverse eukaryotic taxa, suggesting that a potential shared function may underlie their co-evolution.

The Cox3 protein is one of three mitochondrial-encoded protein subunits (Cox1, Cox2 and Cox3) that form the central core of the enzyme, with the heme- and Cu-containing Cox1 and Cox2 protein subunits forming the catalytically active core. While the Cox3 subunit does not directly contribute to electron transfer and O_2 reduction, it represents an evolutionarily conserved component of prokaryotic and eukaryotic forms of the enzyme and has been proposed to play a regulatory role in enzyme function.

Cox3, through its position within the enzyme, maintains the potential to exert regulatory control over complex IV activity through a number of possible mechanisms. Cox3 interacts with Cox13, a non-essential subunit that has been shown to allosterically regulate the activity of complex IV through the binding of ATP. Together with Cox2 and Cox12, Cox3 forms the complex IV cytochrome *c* binding site. Additionally, Cox12 is a peripheral (IMS)-located complex IV subunit that, while not essential, supports complex IV activity. The presence of mammalian Cox12 (mCox6b) is required for optimal complex IV activity, and a mutation in the mCox6b1 isoform causes complex IV deficiency and is the underlying cause of a mitochondrial encephalomyopathy. Cox3 has also been postulated to play an important role in modulating the access of O_2 to the active site of the enzyme. According to the crystal structure of bovine complex IV, Cox3 interacts with 2 phosphatidylglycerol (PG1 and PG2) lipids that, together with Cox3, form a regulatory feature of the O_2 uptake pathway. The F_1F_O ATP synthase inhibitor DCCD has been shown to inhibit complex IV through binding to the Cox3 subunit. The binding of DCCD to a highly conserved residue of Cox3 (bovine Glu90, yeast Glu98) leads to the formation of a DCU derivative that causes the subsequent migration of palmitate tails from the two proximal Cox3-associated PG molecules, inhibiting the O_2

uptake pathway of complex IV (Shinzawa-Itoh et al., 2007). It has therefore been proposed that Cox3 regulates the enzymatic activity of complex IV through conformational changes that affect the position of associated PG lipid molecules, thereby modulating the access of O_2 to the active site. Thus, Cox3 is positioned to exert significant regulatory control over complex IV enzyme activity; either through its modulation of peripherally bound complex IV subunits Cox12, Cox13 and Cox4, or through the modulation of the O_2 uptake pathway via associated PG lipid molecules.

The primary focus of this chapter is to characterize the role of the Hig1/Rcf1 QRRQ motif in the interaction between Rcf1 and Cox3/complex IV, and the importance of this motif in Rcf1's role in supporting complex IV assembly and III-IV supercomplex organization. Preliminary characterization of the ability of Rcf1 and Rcf2 to cooperatively support the correct assembly of complex IV and its optimal activity demonstrated that the expression of a his-tagged Rcf1 derivative ($Rcf1_{His}$) in Δ*rcf1*;Δ*rcf2* mitochondria restores the steady state protein levels of complex IV protein subunits (reduced in Δ*rcf1*;Δ*rcf2* mutant mitochondria) to those of wild type mitochondria. The expression of $Rcf1_{His}$ in the Δ*rcf1*;Δ*rcf2* mutant was also shown to restore the levels of assembled complex IV to those of wild type mitochondria, determined by blue native gel analysis. Furthermore, Δ*rcf1*;Δ*rcf2* mutant mitochondria display a decrease in complex IV O_2 consumption activity that is rescued by the expression of $Rcf1_{His}$. The ability of the his-tagged Rcf1 derivative to complement the reduced complex IV levels and activity of the Δ*rcf1*;Δ*rcf2* double mutant, provides a model by which the importance of the QRRQ motif for Rcf1 function can be characterized. Therefore, Rcf1 mutant derivatives harboring mutations in conserved residues in the QRRQ motif were created and

expressed in Δ*rcf1*;Δ*rcf2* mutant mitochondria, and the ability of these mutants to complement the defects of the Δ*rcf1*;Δ*rcf2* double mutant were directly compared to the double mutant harboring wild type $Rcf1_{His}$.

A secondary aim of this chapter is to investigate potential functional differences between Hig1-type1 and Hig1-type2 proteins. While Hig1-type2 proteins are found in α-protoeobactria, plants, fungi and animals, Hig1-type1 proteins are found exclusively in higher eukaryotes, and represent the predominant Hig1 type that have been detected in screens designed to identify genes that are expressed in response to hypoxic and oxidative stress. However, it remains unknown whether there exist functional differences between the two sub-types of Hig1 proteins. Initial experiments using the *C. elegans* Hig1-type2 isoform, suggested that homologous Hig1 proteins expressed in yeast maintain the capacity to interact with complex IV and can support respiratory growth. Therefore, human type1 and type2 Hig1 proteins expressed in the yeast Hig1-deficient strain (Δ*rcf1*;Δ*rcf2*) will be comparatively analyzed in their ability to complement the respiratory growth deficiency of Δ*rcf1*;Δ*rcf2* mitochondria and interact with complex IV.

Finally, the molecular environment of the Rcf1 QRRQ motif was analyzed by using a cysteine (Cys)-based scanning strategy to identify Rcf1 partner proteins that may interact with the QRRQ motif, thereby providing further insight into the molecular interaction of Rcf1.

3.2 Chapter 3 Results

3.2.1 Expression of Rcf1 QRRQ mutant derivatives

The functional significance of the conserved QRRQ motif in the yeast Rcf1 protein was investigated by adopting a strategy of alanine site-directed mutagenesis. Three distinct Rcf1 mutant derivatives were initially created. In the first mutant, glutamines (Gln, Q) 61 and 71 were simultaneously mutated to alanine (Ala, A), to create the *rcf1*^{Q61A,Q71A} derivative. In the second and third mutant derivatives arginines (Arg, R) 65 and 67 were individually mutated to Ala, to create *rcf1*^{R65A} and *rcf1*^{R67A}, respectively. The mutated residues are predicted to reside within, or directly adjacent to the matrix loop of Rcf1, with residue R67 predicted to be near the matrix interface (FIGURE 8B). Rcf1 mutant derivatives were expressed as C-terminal His-tagged derivatives in the Δ*rcf1*;Δ*rcf2* double null yeast strain. Expression was verified by western blot analysis of purified mitochondria fractions isolated from wild type and mutant derivative strains (FIGURE 8C). The steady state levels of the *rcf1*$_{His}^{Q61A,Q71A}$ and *rcf1*$_{His}^{R67A}$ derivatives appeared to be similar to that of wild-type Rcf1$_{His}$ control, indicating that mutation of the QRRQ motif in this manner did not appear to adversely affect the stability of the Rcf1 protein. The expression of *rcf1*$_{His}^{Q61A,Q71A}$ and *rcf1*$_{His}^{R67A}$ derivatives appeared to complement the Δ*rcf1*;Δ*rcf2* respiratory growth defect (growth on the non-fermentable carbon source, glycerol) to a similar extent as the wild type Rcf1$_{His}$ derivative (FIGURE 8D). This finding indicates that an intact QRRQ motif is not essential for Rcf1's ability to support OXPHOS-based yeast growth.

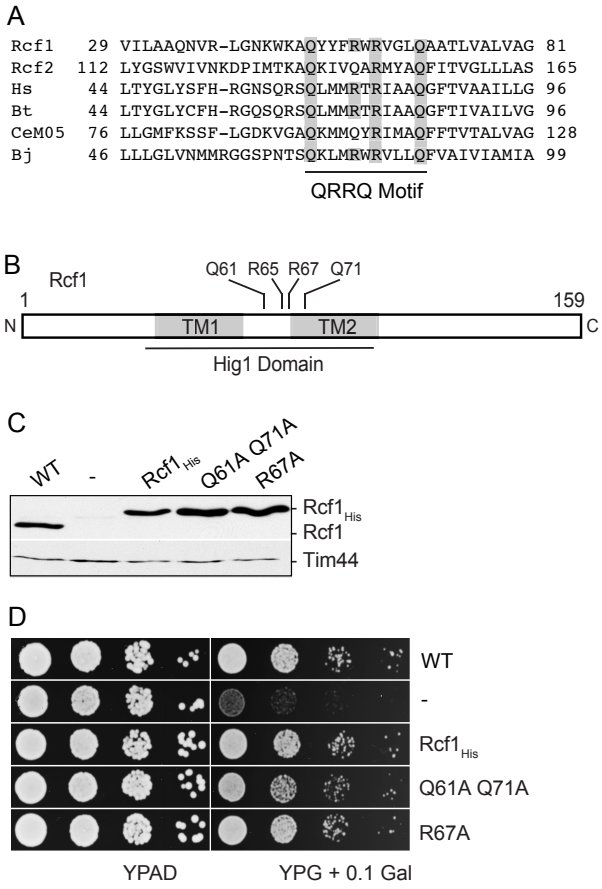

Figure 8. Rcf1 is an inner mitochondrial membrane protein and a member of the Hig1-type 2 protein family that contain a conserved QRRQ motif. (A) Limited sequence alignment (amino acid residue numbers indicated) of the QRRQ motif region from a selection of Hig1-type 2 family members. Hs, Homo sapiens (NP_620175); Bt, Bos taurus (NP_001071329); Ce, Caenorhabditis elegans (NP_001254152) and Bj, Bradyrhizobium japonicum (WP_014491643). **(B)** Depiction of the predicted orientation of Rcf1 within the inner mitochondrial membrane, where N- and C-tails are predicted to be exposed to the intermembrane space. The location of the QRRQ (Q61, R65, R67, Q71) motif relative to the two predicted transmembrane segments (TM1 and TM2 respectively) is indicated. **(C)** Mitochondria were isolated from the wild type or the Δ*rcf1*;Δ*rcf2* controls (-) and the Δ*rcf*1;Δ*rcf2* strain harboring either His-tagged Rcf1 ($Rcf1_{His}$), $rcf1_{His}^{Q61A,Q71A}$ (Q61,Q71) or $rcf1_{His}^{R67A}$ (R67A) derivatives. Rcf1 and Tim44 (control) levels were analyzed by Western blotting. **(D)** Serial 10-fold dilutions of wild type (WT), and Δ*rcf1*;Δ*rcf2* strains expressing $Rcf1_{His}$, $rcf1_{His}^{Q61A,Q71A}$ (Q61,Q71), $rcf1_{His}^{R67A}$ (R67A) derivatives or not (-), as indicated, were spotted on YP plates containing glucose (YPAD) or glycerol supplemented with 0.1 % galactose (YPG+0.1% Gal) and grown at 30°C.

3.2.2 Expression of *rcf1*$_{His}^{R67A}$ alters the complex IV assembly state

To gain more insight into the extent to which the mutated QRRQ derivatives can support the functions of Rcf1, mitochondria were isolated from the strains harboring the *rcf1*$_{His}^{Q61A,Q71A}$ and *rcf1*$_{His}^{R67A}$ derivatives and a more in-depth biochemical analysis was performed.

The steady state levels of individual complex IV subunits were analyzed in mitochondria harboring the mutant Rcf1 derivatives. As previously reported the Δ*rcf1;*Δ*rcf2* mutant mitochondria contained reduced levels of complex IV subunits (FIGURE 9A) (Strogolova et al., 2012). In contrast, the mitochondria harboring his-tagged wild type Rcf1 or the *rcf1*$_{His}^{Q61A\ Q71A}$ or *rcf1*$_{His}^{R67A}$ derivatives, appeared to have normal levels of the complex IV subunits examined (FIGURE 9A). It can therefore be concluded that an intact QRRQ motif does not appear to be required by Rcf1 to support the stable accumulation complex IV subunits.

The assembly of complex IV and its association with complex III into the III-IV supercomplex is altered in the absence of Rcf1 and Rcf2 (Strogolova et al., 2012). Therefore, the ability of the QRRQ mutated derivatives of Rcf1 to support the assembly of complex IV and the III-IV supercomplex was analyzed. Mitochondria harboring the *rcf1*$_{His}^{Q61A,Q71A}$ or *rcf1*$_{His}^{R67A}$ derivatives were solubilized with the mild detergent digitonin, which preserves the III-IV assembly state, and the protein complexes were analyzed by blue native gel electrophoresis (BN-PAGE), followed by western blotting and immunedecoration, with antisera against a complex III subunit, cytochrome c_1 (FIGURE 9B). As previously reported, in the Δ*rcf1;*Δ*rcf2* mitochondria there is a pronounced shift from the III_2-IV_2 form (observed in the wild type control mitochondria)

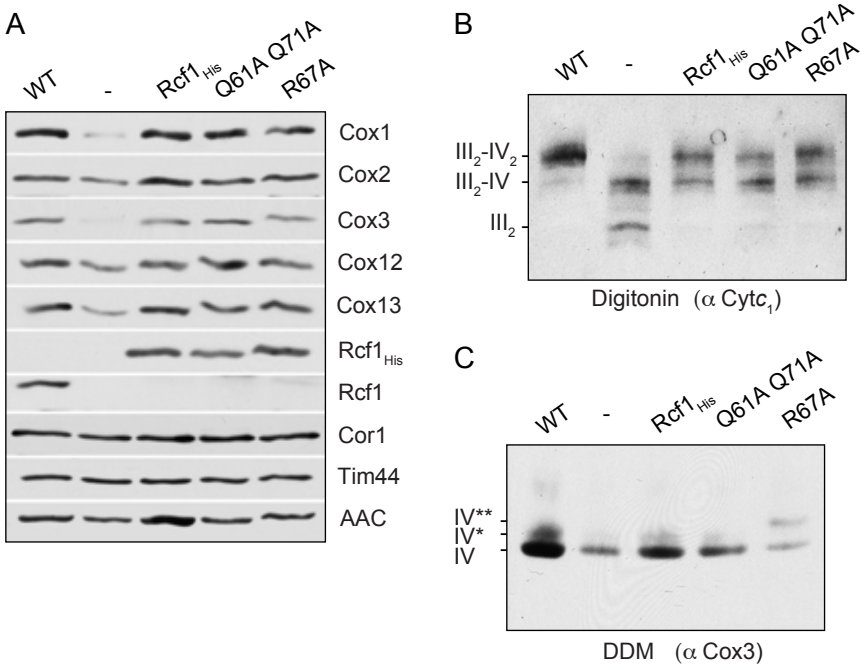

Figure 9. Mutation of the Rcf1 QRRQ motif affects the stability but not the assembly of complex IV. (A) Steady state protein levels of the OXPHOS subunits in mitochondria (50 µg) isolated from indicated strains and as detailed in Fig. 3.1C. Tim44 was used as a loading control. **(B)** Mitochondria isolated from WT and indicated Δ*rcf1*;Δ*rcf2* strains were solubilized in digitonin (1%) and subjected to BN-PAGE analysis, Western blotting and immunedecoration with antibodies against complex III subunit, cytochrome c_1 (α Cytc1). **(C)**, same as in (B), with the exception that mitochondria were solubilized with DDM (0.6%) prior to BN-PAGE and decoration was performed with antibodies against the complex IV subunit Cox3 (α Cox3).

to a predominately III_2-IV form and also to free III_2 complexes (Fig. 9B) (Strogolova et al., 2012). Normal III_2-$IV_{(1-2)}$ supercomplex organizational state was largely restored in the Δ*rcf1;*Δ*rcf2* mitochondria harboring the wild type $Rcf1_{His}$. The *rcf1*$_{His}^{Q61A,Q71A}$ or *rcf1*$_{His}^{R67A}$ mutants, analyzed in parallel, appeared to display a similar capacity as the wild type $Rcf1_{His}$ derivative to support the organization of the III-IV supercomplex in the Δ*rcf1;*Δ*rcf2* mitochondria.

These results would indicate that an intact QRRQ motif is not required for the ability of Rcf1 to support the assembly of complex IV and its ability to co-assemble with complex III. While this conclusion is consistent with the observed steady state levels of complex IV subunits, which appeared normal in the *rcf1* mutant mitochondria, a noticeable difference was observed in the behavior of the complex IV from the *rcf1*$_{His}^{R67A}$ mitochondria when solubilized with the detergent, dodecylmaltoside (DDM), prior to the BN-PAGE analysis (Fig 9C). Solubilization of wild type mitochondria with DDM causes complex IV to become physically separated from the supercomplex assembly state with complex III and complex IV migrates on the BN-PAGE with an apparent mass that is consistent with the complex IV monomer (Strecker et al., 2016; Vukotic et al., 2012). A small fraction of a slightly larger form of complex IV, termed IV* was also detected, as previously reported and may represent the population of complex IV where peripheral subunits Cox12 and Cox13 remain associated under the DDM conditions (FIGURE C) (Vukotic et al., 2012). The level of the DDM solubilized complex IV from the wild type or Δ*rcf1;*Δ*rcf2*+$Rcf1_{His}$ mitochondria (and also from the *rcf1*$_{His}^{Q61A\ Q71A}$) were similar to each other, and all were significantly greater than that observed from the Δ*rcf1;*Δ*rcf2* mitochondria, where complex IV levels were reduced by approximately 50% as

previously reported (Strogolova et al., 2012). In contrast however, the *rcf1*$_{His}^{R67A}$ containing mitochondria analyzed in parallel, displayed strongly reduced levels of assembled complex IV following DDM solubilization (FIGURE 9C). Furthermore, in addition to the monomeric complex IV population, the *rcf1*$_{His}^{R67A}$ mitochondria contained a novel complex IV sub-population, termed IV**, that migrated slower on the BN-PAGE gel. The sum of the levels of both complex IV populations observed in the *rcf1*$_{His}^{R67A}$ mutant mitochondria following DDM solubilization was approximately equal to the complex IV levels in the Δ*rcf1;*Δ*rcf2* mutant, and thus were significantly lower than those from the mitochondria harboring the Rcf1$_{His}$ or *rcf1*$_{His}^{Q61A,Q71A}$ derivatives.

The reduced levels of the complex IV species observed in the DDM extracts of the *rcf1*$_{His}^{R67A}$ is inconsistent with the apparently normal steady state levels of complex IV subunits and the regular appearance of the digitonin-solubilized III-IV supercomplex in these mitochondria. Together with the observed presence of the novel complex IV** species, these results suggest that the assembly state of the complex IV is somewhat altered and more DDM detergent labile in the *rcf1*$_{His}^{R67A}$ mitochondria, as compared to the wild type control.

The appearance of a novel, larger IV** species in the Δ*rcf1;*Δ*rcf2* mutant harboring the *rcf1*$_{His}^{R67A}$ mutant derivative was unexpected. To directly compare the composition of the complex IV (IV and IV**) species from *rcf1*$_{His}^{R67A}$ mitochondria to that of complex IV from the Δ*rcf1;*Δ*rcf2* mutant in the presence or absence of the his-tagged wild type Rcf1, mass spectrometry analysis was performed by a collaborator, Dr. Ilka Wittig (Goethe-Universität Frankfurt, Germany). Mitochondria were initially solubilized in DDM-containing buffer and complexes were separated by first-dimension

(1-D) BN-PAGE. Following 1-D BN-PAGE, lanes of the Δ*rcf1;*Δ*rcf2* mutant and Δ*rcf1;*Δ*rcf2* harboring his-tagged wild-type or *rcf1*$_{His}^{R67A}$ derivatives were analyzed by mass spectrometry (FIGURE 10). The protein abundance profiles of subunits showed that in the Δ*rcf;*Δ*rcf2* mutant mitochondria, the complex IV subunits largely co-migrated together in the region that corresponded to the monomeric IV complex. In the presence of Rcf1$_{His}$ the majority of the complex IV subunits detected were also present as IV/IV* species, however, the presence of a low level of complex IV subunits was also co-detected in a larger molecular weight complex, whose migration corresponded to that of the IV** form in the *rcf1*$_{His}^{R67A}$ mitochondria and where a low level of Rcf1$_{His}$ protein co-migrated too. This finding indicates that the majority of the complex IV was not associated with Rcf1 and the minor subpopulation of complex IV+Rcf1 co-migrated as a larger IV** species. Consistent with the 1D-BN-PAGE (FIGURE 9C), the ratio of the IV** to the IV subpopulations was significantly increased in the *rcf1*$_{His}^{R67A}$ sample, with comparable levels of IV** and IV populations detected and, with the exception of the *rcf1*$_{His}^{R67A}$ protein, exhibited similar subunit profiles and abundance distributions. The *rcf1*$_{His}^{R67A}$ protein was detected co-migrating with the IV** species (and also in fractions larger than the IV** complex) and the total amount of *rcf1*$_{His}^{R67A}$ present in these fractions was significantly higher than that observed for corresponding fractions with the mitochondria harboring wild type Rcf1$_{His}$ (FIGURE 10).

Since the relative stoichiometric abundance of the complex IV subunits in the complex IV** species appeared to be relatively similar to that in the IV subpopulation, it can be concluded that the novel complex IV** subpopulation is, at least in part, characterized by the stable association of the Rcf1 protein. This association is more

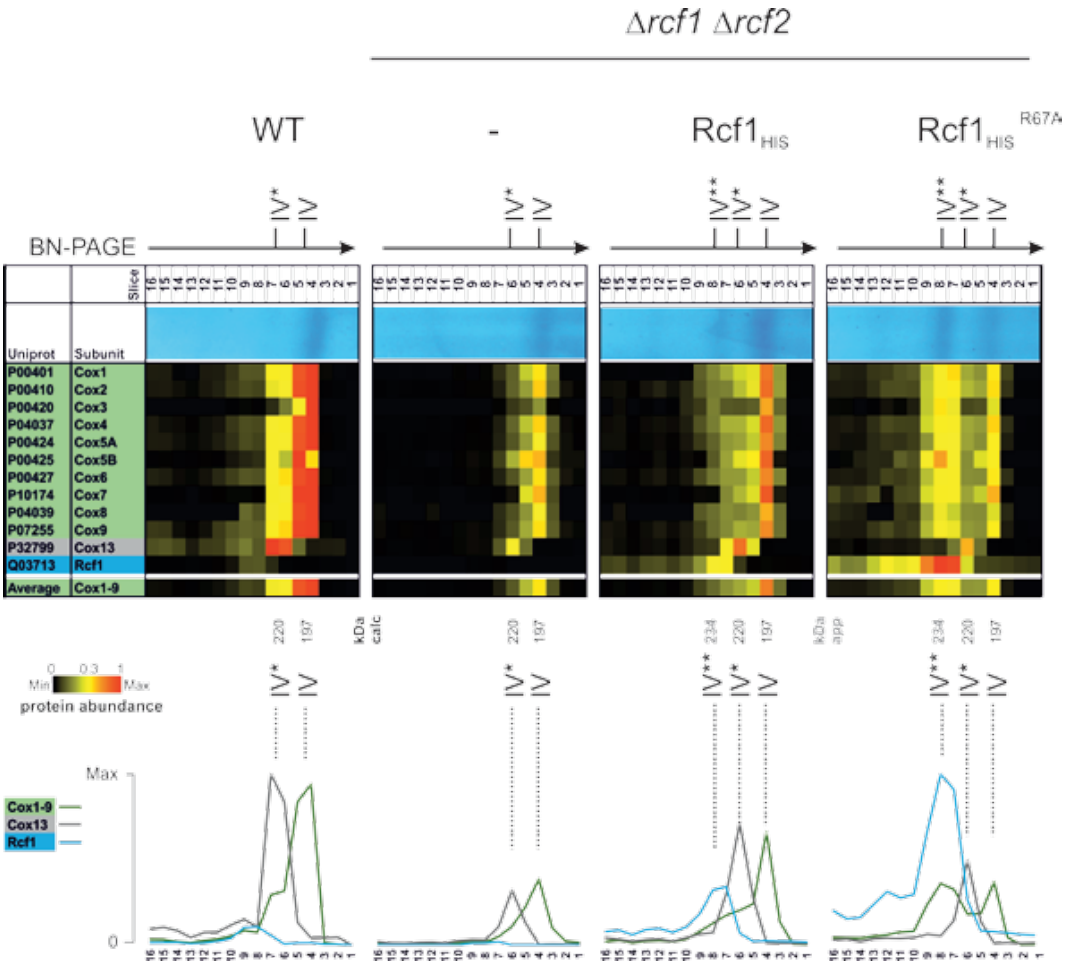

Figure 10. Compositional analysis of the complex IV subpopulation.** 1-D BN-PAGE analysis of protein complexes in wild type, Δ*rcf1*;Δ*rcf2* mitochondria and those harboring $Rcf1_{His}$ or $rcf1_{His}^{R67A}$ following solubilization with DDM (0.6%) was performed. The areas of the gel encompassing the complex IV and IV** species (as shown) were fractionated and proteins were identified and quantified by mass spectrometry. The abundance of identified proteins was quantified using intensity-based absolute quantification value (IBAQ), as described in Chapter 2. Heat maps and graphs show protein profiles normalized to the maximum abundance of a protein within BN lanes of the wild type and Δ*rcf1*;Δ*rcf2* mutants.

pronounced in the case of *rcf1*$_{His}^{R67A}$ mutant derivative and thus most likely accounts for the higher content of this subpopulation in the *rcf1*$_{His}^{R67A}$ mitochondria (relative to the null mutant or null mutant plus wild type Rcf1$_{His}$ controls). Therefore, the size difference between the IV** and the IV species, may solely be attributed the presence of the Rcf1 protein.

When a second dimension SDS-PAGE (2D-SDS-PAGE) was performed following the 1D-BN-PAGE, the presence of *rcf1*$_{His}^{R67A}$ with the complex IV** species was confirmed by Western blotting followed by immunedecoration (FIGURE 11), where *rcf1*$_{His}^{R67A}$ was detected co-migrating with Cox2 and Cox3 proteins in the IV** subpopulation. In addition, a fraction of the *rcf1*$_{His}^{R67A}$ was also observed to be present in a higher molecular mass range, which also contained some Cox2 species (but not Cox3), which may represent a Cox2-containing assembly intermediate of complex IV. The level of Rcf1 co-migrating with complex IV species/subpopulations was significantly greater in the case of the *rcf1*$_{His}^{R67A}$ mitochondria, when compared to the wild type Rcf1$_{His}$-containing control, and indicates that the majority of complex IV is not normally present in association with Rcf1 (FIGURE 11). These results are consistent with the mass spectrometry analysis and suggest that the *rcf1*$_{His}^{R67A}$ may have a tighter association (possibly a higher affinity or less dynamic of an interaction) with complex IV than its wild type Rcf1 counterpart.

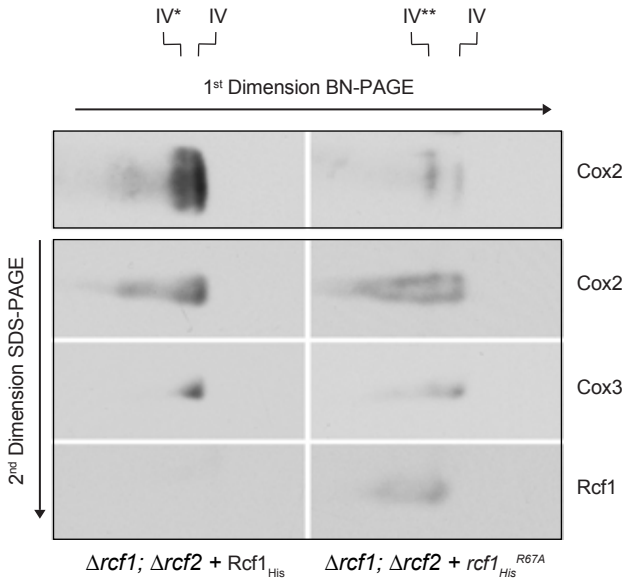

Figure 11. 2 Dimension (1D BN-PAGE/2D SDS-PAGE) analysis of the complex IV subpopulation.** Mitochondria isolated from the Δ*rcf1*;Δ*rcf2* mutant strain harboring $Rcf1_{His}$ or $rcf1_{His}^{R67A}$ were solubilized in digitonin (1%) and subjected to BN-PAGE analysis, 1D gel fragments from indicated mitochondria were subjected to SDS-PAGE analysis (2D), Western blotting and immunedecoration with antibodies against complex IV subunits and the Rcf1 protein.

3.2.3 The QRRQ motif influences the association of Rcf1 with complex IV, in particular with the Cox12 and Cox3 subunits

The levels of complex IV associated with the His-tagged Rcf1 derivatives was also investigated through affinity purification via Ni-NTA chromatography, following solubilization from mitochondria with Triton X-100 (FIGURE 12A). A significantly higher level of complex IV subunits co-purified with the *rcf1*$_{His}^{R67A}$ derivative, as compared to the control Rcf1$_{His}$ protein, which was analyzed in parallel (FIGURE 12A). Consistent with the Triton X-100 lysis/purification results, an enhanced association of complex IV subunits with the *rcf1*$_{His}^{R67A}$ derivative, relative to the wild type Rcf1$_{His}$ control, was also observed under the digitonin conditions (where the III-IV association is preserved). Of particular note was the Cox12 subunit, which was found to co-purify with *rcf1*$_{His}^{R67A}$, but not with the Rcf1$_{His}$ (or *rcf1*$_{His}^{Q61A,Q71A}$) derivative (FIGURE 12A). Cox12 is a non-essential subunit of complex IV, which is peripherally associated with the complex on the intermembrane space-side of the inner membrane and Rcf1 has been previously proposed to modulate its association with the complex IV. The co-purification of Cox12 with *rcf1*$_{His}^{R67A}$ may indicate that mutation of R67 residue in this manner may enhance the complex IV-Cox12 association.

Complex IV subunits did not co-purify with the *rcf1*$_{His}^{Q61A,Q71A}$ derivative under the Triton X-100 solubilization conditions, suggesting that mutation of the Q61/Q71 residue pair in the QRRQ motif disturbs the integrity of the Rcf1-complex IV interaction (FIGURE 12A). However, when affinity purification of the his-tagged Rcf1 derivatives was performed under milder digitonin solubilization conditions, co-purification of the complex IV (and complex III) subunits with *rcf1*$_{His}^{Q61A,Q71A}$ was observed, and the

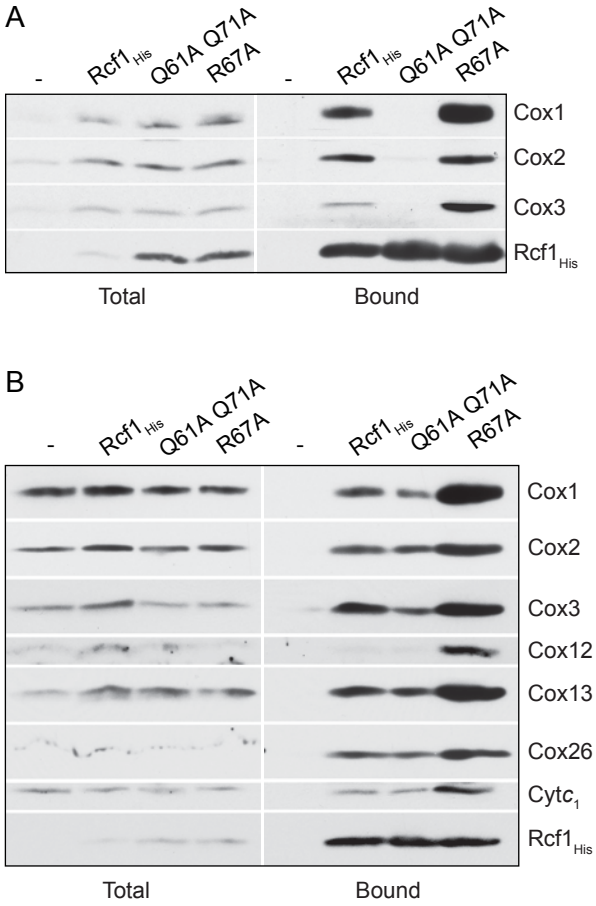

Figure 12. Mutation of the QRRQ motif affects the association of Rcf1 with Cox3 and complex IV. (A) Affinity purification of $Rcf1_{His}$, $rcf1_{His}^{Q61A,Q71A}$, $rcf1_{His}^{R67A}$ derivatives following solubilization with Triton X-100 detergent was performed, followed by SDS-PAGE, Western blotting and immunedecoration, as indicated. Total, 5% of solubilized material; Bound, affinity purified material on the Ni-NTA beads. **(B)** Same as (A), except solubilization was performed with 1 % digitonin.

amounts of associated complex III and IV subunits were similar to the wild type $Rcf1_{His}$ control (FIGURE 12B). Together, these observations would suggest that mutation of the Q61/Q71 pair within the QRRQ motif compromises the association of Rcf1 with the complex IV, such that it does not remain stable in the presence of Triton X-100, but can be preserved when the milder detergent (digitonin) solubilization conditions are applied.

Association of the Rcf1 protein with the complex IV, at least in part, involves the mitochondrially-encoded subunit 3, Cox3, of complex IV, which can physically associate with Rcf1 prior to its assembly into the complex IV. Therefore, the consequence of mutation of the QRRQ motif on its ability to interact with newly synthesized Cox3 was analyzed (FIGURE 13A). *In organello* translation in the presence of [^{35}S]methionine was performed in isolated mitochondria and the His-tagged Rcf1 derivatives were purified by Ni-NTA chromatography following detergent solubilization with Triton X-100. Radiolabeled Cox3 co-purified with both the wild type $Rcf1_{His}$ and the $rcf1_{His}^{R67A}$ derivatives. Association of radiolabeled Cox3 with the $rcf1_{His}^{Q61A,Q71A}$ derivative under these detergent conditions was, however, not observed (FIGURE 13A). Furthermore, a pulse-chase kinetic analysis indicated that the association of radiolabeled Cox3 with the $rcf1_{His}^{R67A}$ derivative appeared to be more stable/prolonged than with the wild type $Rcf1_{His}$ control, suggesting that mutation of the R67 residue to alanine causes an enhanced association with Cox3, which may protect Cox3 from subsequent proteolytic turnover (FIGURE 13B).

Taken together these results indicate that mutation of the QRRQ motif has the potential to impact the nature of the Rcf1-complex IV interaction, through an altered interaction with the Cox3 and Cox12 subunits. Mutation of R67 to alanine, causes an

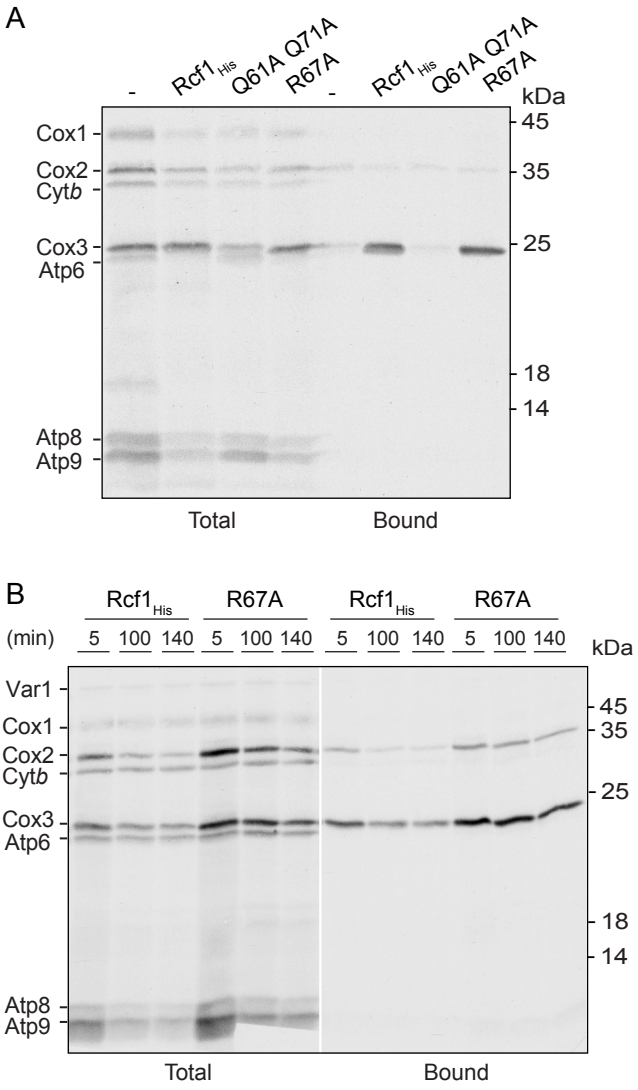

Figure 13. Mutation of the QRRQ motif affects the association of Rcf1 with Newly-synthesized Cox3 . (A) In organello labeling in the presence of [^{35}S]methionine was performed for 20 min in the isolated mitochondria, prior to solubilization with Triton X-100. Affinity purification of the his-tagged Rcf1 derivatives was performed as described in (Figure 3.5), except following SDS-PAGE, the gels were subjected to autoradiography. **(B)** As described in (A), except, following the pulse of translation (20 min), translation was stopped through the addition of puromycin and cold methionine and further chased for the time periods indicated, prior to solubilization of the mitochondria with Triton X-100 and affinity purification of the Rcf1-deriviatives.

enhanced complex IV interaction, as evidenced by the presence of the complex IV** species, and the increased association of complex IV subunits, Cox12 and radiolabeled Cox3 with the *rcf1*$_{His}^{R67A}$ derivative. On the other hand, mutation of the Q61/Q71 pair compromises the interaction of Rcf1 with Cox3 and thus with the complex IV, as it was not observed under Triton X-100 purification conditions, and could only be observed under milder detergent conditions, digitonin.

3.2.4 The complex IV in mitochondria harboring the *rcf1*$_{His}^{R67A}$ derivative displays altered enzymatic properties.

To further explore the properties of the complex IV in the *rcf1*$_{His}^{R67A}$ mitochondria, experiments were performed to assess its enzymatic activity properties. The complex IV enzyme solubilized in DDM retains its enzymatic activity, as evidenced by 'in-gel' activity assays performed following BN-PAGE analysis (FIGURE 14A). The level of complex IV activity was strongly reduced in the Δ*rcf1;*Δ*rcf2* mutant compared both to the wild type control and the null mutant harboring the Rcf1$_{His}$ protein. This reduced complex IV enzyme activity can be attributed to the strong reduction in complex IV protein levels in the Δ*rcf1;*Δ*rcf2* mutant (FIGURE 9A). Despite also being so reduced in protein content, the levels of DDM solubilized complex IV activity in both the IV and IV** subpopulations in the *rcf1*$_{His}^{R67A}$ sample appeared similar to, or even higher than, those obtained for the IV population in the Δ*rcf1;*Δ*rcf2* +Rcf1$_{His}$ or the *rcf1*$_{His}^{Q61A,Q71A}$ mitochondria. These results suggest that the complex IV and complex IV** enzyme subpopulations solubilized from the *rcf1*$_{His}^{R67A}$ exhibit an increased level of enzyme specific activity, relative to those in the mitochondria harboring the wild type Rcf1$_{His}$

control under these analysis conditions.

The O_2-consuming capacity of the mitochondria harboring the *rcf1*$_{His}^{R67A}$ derivative was analyzed directly and under different bioenergetic states. Initially, the rate of O_2 consumption was measured following the addition of substrate NADH, i.e. basal respiration, and known as "state 4" respiration (FIGURE 14 B). The state 4 O_2 consumption rates (OCR) in the Δ*rcf1;*Δ*rcf2* mitochondria were approximately half of those in the mitochondria harboring the Rcf1$_{His}$ or *rcf1*$_{His}^{Q61A,Q71A}$ proteins. The mitochondria harboring the *rcf1*$_{His}^{R67A}$ derivative on the other hand contained slightly higher levels of state 4 respiration, relative to the Rcf1$_{His}$ control. The increase in state 4 OCR in the *rcf1*$_{His}^{R67A}$ mitochondria did not appear to be due to an elevated basal OCR activity caused by a H^+ leaky membrane. The respiratory control rate (state 3 respiration [NADH+ADP]/state 4) in the *rcf1*$_{His}^{R67A}$ mitochondria was similar to the other mitochondria measured, indicating the coupled state of these mitochondria (FIGURE 14C).

The maximum oxygen consumption capacity of the complex IV was measured directly in the presence of ascorbate/TMPD and CCCP (FIGURE 14D). Compared to the double mutant harboring Rcf1$_{His}$, the Δ*rcf1;*Δ*rcf2* mutant contained approximately a 50% reduction in the maximal complex IV capacity (FIGURE 14D). The maximal complex IV OCR of mitochondria harboring the *rcf1*$_{His}^{Q61A,Q71A}$ or *rcf1*$_{His}^{R67A}$ mutant derivatives were similar or slightly higher than that of Δ*rcf1;*Δ*rcf2*+Rcf1$_{His}$ mitochondria. From these results it was concluded that both the *rcf1*$_{His}^{Q61A,Q71A}$ or *rcf1*$_{His}^{R67A}$ mutant derivatives displayed the capacity to fully support maximal complex IV activity when expressed in Δ*rcf1;*Δ*rcf2* strain and when the complex IV is working to its maximum capacity.

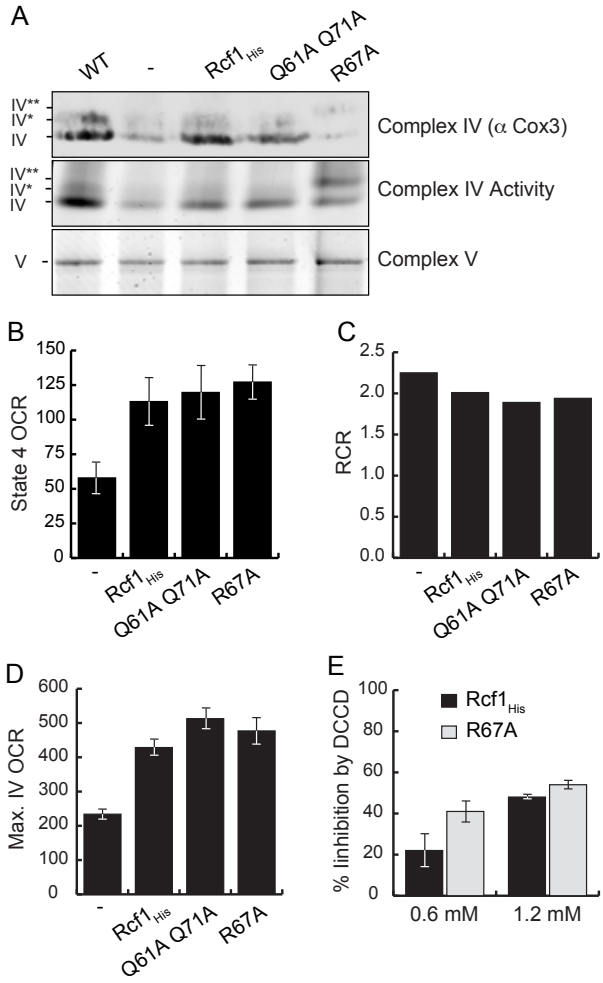

Figure 14. Complex IV in *rcf1*$_{His}^{R67A}$ mitochondria displays altered catalytic properties. (A) Mitochondria isolated from wild type (WT) or the Δ*rcf1*;Δ*rcf2* strain harboring the Rcf1$_{His}$, *rcf1*$_{His}^{Q61A,Q71A}$, *rcf1*$_{His}^{R67A}$ derivatives, as indicated, were solubilized with DDM (0.6%) and subjected to duplicate BN-PAGE analysis. The complex IV enzyme activity levels were analyzed in one set of samples by performing an in gel enzyme assay (middle panel) and in a parallel sample the complex IV protein levels were determining following Western blotting and decoration with Cox3 antibody (upper panel), as indicated. The levels of the Coomassie stained complex V (F_1F_o-ATP synthase) are shown in lower panel, as a loading control. (B and C) The oxygen consumption rates (OCR) of the NADH driven state 4 and respiratory control ratio (RCR) - the ratio of state 3 (NADH/ADP) to state 4 (NADH) OCR's - were measured in the indicated isolated mitochondria, n = 3. **(D)** The maximal capacity of complex IV was determined by measuring the OCR driven by ascorbate/TMPD in the presence of CCCP to dissipate the membrane potential, n= 6. **(E)** Isolated Δ*rcf1*;Δ*rcf2* mitochondria harboring the Rcf1$_{His}$ or *rcf1*$_{His}^{R67A}$ derivatives were incubated with DCCD at concentrations indicated for 30 min at room temperature, prior to measuring the maximal complex IV OCR in the presence of ascorbate/TMPD and CCCP. The percent inhibition caused by the DCCD treatment, relative to the control (no DCCD) is indicated, n =3

Finally, the 'in gel' enzyme activity assay and the measurement of state 4 OCR's would suggest that the complex IV enzyme in the *rcf1*$_{His}^{R67A}$ mitochondria may display differential enzymatic properties than when the wild type Rcf1 control protein is present. In support of this, it was observed that the complex IV enzyme displayed an increased sensitivity to DCCD (FIGURE 14E). DCCD binds to Cox3 (Glu90 residue in bovine Cox3, equivalent to Glu98 in yeast) and in doing so interferes with the oxygen uptake pathway of complex IV, which involves associated lipids (phosphatidylglycerol and cardiolipin molecules) with the enzyme (Ogunjimi et al., 2000; Shinzawa-Itoh et al., 2007). The changes observed in complex IV caused by the enhanced association of *rcf1*$_{His}^{R67A}$, potentially alter the accessibility of DCCD to its target, possibly due to altered lipid association/arrangements and support the findings of altered structure and enzymatic function of the complex in the *rcf1*$_{His}^{R67A}$ mitochondria.

To further explore the possible role of the Rcf1 protein in the insertion/remodeling of cardiolipin associated with complex IV, the ability of Rcf1$_{His}$ and mutant derivatives to associate with Taz1, an enzyme involved in the remodeling of cardiolipin, was determined by Ni-NTA purification. While association between Taz1 and wild type Rcf1$_{His}$ or the *rcf1*$_{His}^{Q61A,Q71A}$ derivative was not observed, the *rcf1*$_{His}^{R67A}$ derivative co-purified a low level of Taz1, suggesting that the Rcf1 protein might be involved in the insertion or remodeling of cardiolipin (FIGURE 15). The inability of wild type Rcf1$_{His}$ (and the *rcf1*$_{His}^{Q61A,Q71A}$ derivative) to co-purify Taz1, together with the altered interaction kinetics observed between newly synthesized Cox3 and the *rcf1*$_{His}^{R67A}$ derivative (FIGURE 13B), suggests that the mutation of the R67 residue in Rcf1 may affect an otherwise dynamic association of Taz1 with Rcf1-containing populations.

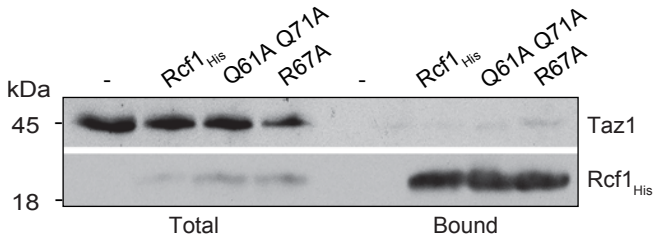

Figure 15. The *rcf1*$_{His}^{R67A}$ mutant derivative associates with the cardiolipin remodeling enzyme, Taz1. Affinity purification of Rcf1$_{His}$, *rcf1*$_{His\text{-}Q61A,Q71A}$, *rcf1*$_{His}^{R67A}$ derivatives following solubilization with Triton X-100 detergent was performed, followed by SDS-PAGE, Western blotting and immunedecoration, as indicated. Total, 5% of solubilized material; Bound, affinity purified material on the Ni-NTA beads.

3.2.5 Rcf1 may be involved in post-translational modification of complex IV

Analysis of the amino acid sequence region encompassing the QRRQ motif in an alpha-helical plot indicated that the R67 residue co-aligned with the Q71 residue, where the Q61 residue neighbored the R65 residue, suggesting they may form Q/R pairs (FIGURE 16A). The QRRQ motif in the Rcf1 protein was further explored by making double mutants of the Q/R pairs independently, i.e. *rcf1*$_{His}^{Q61A,R65A}$ and *rcf1*$_{His}^{R67A,Q71A}$ and expressing them in the Δ*rcf1*;Δ*rcf2* null mutant. Steady state analysis of proteins isolated from the resulting strains indicated that the levels of both mutant Rcf1 derivatives were strongly reduced, in particular the *rcf1*$_{His}^{Q61A,R65A}$ derivative, as compared to the wild type Rcf1$_{His}$ control (FIGURE 16B). Therefore, mutation of either of the Q/R pairs strongly impacts the stability and thus the steady state levels of the Rcf1 protein.

Despite the strongly reduced levels of the *rcf1*$_{His}^{Q61A,R65A}$ protein, analysis of the complex IV subunit levels in the mutant mitochondria demonstrated that they were similar to that of the Rcf1$_{His}$ control and significantly higher than those observed in the Δ*rcf1*;Δ*rcf2* null mitochondria (FIGURE 16B). BN-PAGE analysis of the III-IV supercomplex demonstrated that the levels of III_2-$IV_{(1-2)}$ in Δ*rcf1*;Δ*rcf2* harboring the *rcf1*$_{His}^{Q61A,R65A}$ protein were similar to the wild type levels of III_2-$IV_{(1-2)}$ (FIGURE 16C, left panel). The levels of DDM-solubilized complex IV in the *rcf1*$_{His}^{Q61A,R65A}$ mitochondria were also similar to those of the wild type Rcf1$_{His}$ control (FIGURE 16C, right panel).

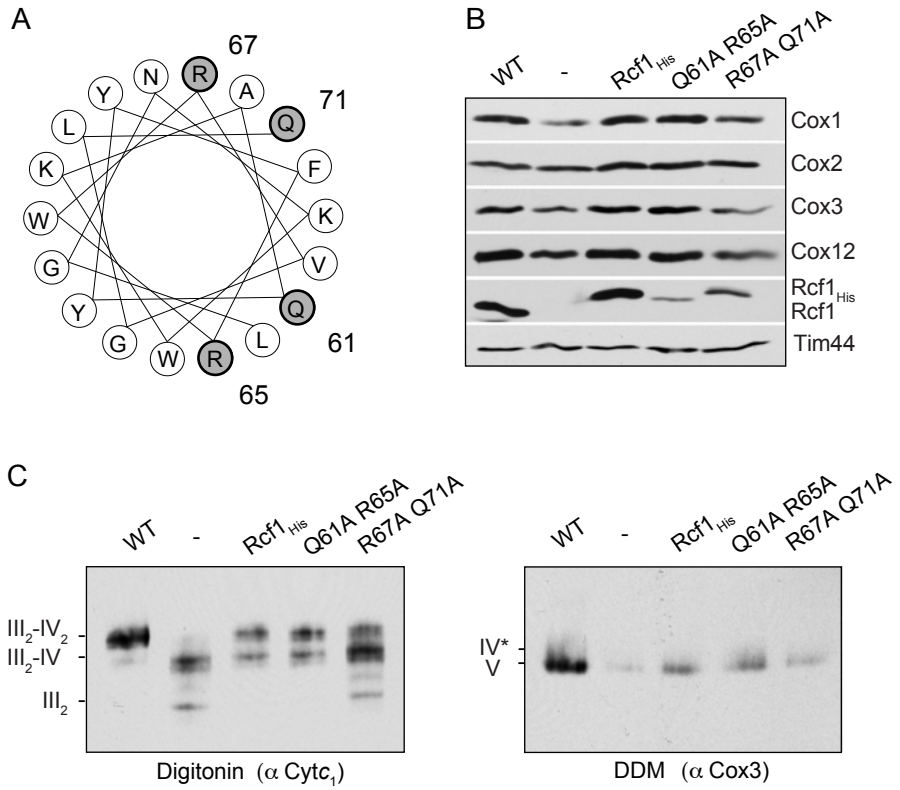

Figure 16. Mutation of the QR pairs in the QRRQ motif in Rcf1 affects the stability of Rcf1, but complex IV assembles. (A) An α-helical plot of residues Leu(L)54 through Gln(Q)71of Rcf1 depicting the co-localization of the Q61/R65 residue pair and the R67/Q71 residue pair on the helix. **(B)** Steady state protein levels of the OXPHOS subunits in the mitochondria (50 µg protein) isolated from indicated strains. Tim44 was used as a loading control. **(C)** Mitochondria isolated from WT and indicated Δ*rcf1*,Δ*rcf2* strains were solubilized in digitonin (1%) (left panel) or DDM (0.6 %) (right panel) and subjected to BN-PAGE analysis, Western blotting and immunedecoration with antibodies against complex III subunit, cytochrome c_1 (α Cytc1, left panel) and complex IV subunit, Cox3 (right panel).

Although the steady state levels of the *rcf1*$_{His}^{R67A,Q71A}$ derivative were marginally higher than that of *rcf1*$_{His}^{Q61A,R65A}$ protein, the presence of the *rcf1*$_{His}^{R67A,Q71A}$ protein only partially restored the complex IV subunits to wild type levels, indicating that mutation of the R67/Q71 pair compromised the ability of this Rcf1 derivative to support complex IV assembly (FIGURE 16B). Consistently, a partial restoration of the III_2-IV_{1-2} species was observed in the BN-PAGE analysis of the digitonin solubilized *rcf1*$_{His}^{R67A,Q71A}$ mitochondria, paralleling the observation that the levels of the complex IV subunits in the *rcf1*$_{His}^{R67A,Q71A}$ mitochondria are greater than those in the Δ*rcf1*;Δ*rcf2* control, but not equivalent to those of the wild type control (FIGURE 16C, left panel). However, when solubilized with DDM and analyzed by BN-PAGE, the levels of free complex IV from the *rcf1*$_{His}^{R67A,Q71A}$ mitochondria appeared similar to those of the Δ*rcf1*;Δ*rcf2* null mitochondria, and in contrast to those from the *rcf1*$_{His}^{Q61A,R65A}$ mitochondria, where the levels of complex IV were similar to the wild type Rcf1$_{His}$ control (FIGURE 16 C, right panel). These results together suggest that complex IV from the *rcf1*$_{His}^{R67A,Q71A}$ mitochondria may exhibit some detergent instability to DDM, in a similar manner as was previously observed in the *rcf1*$_{His}^{R67A}$ mitochondria (FIGURE 9C). In contrast to the *rcf1*$_{His}^{R67A}$ mitochondria, the presence of a complex IV** form was not detected in the *rcf1*$_{His}^{R67A,Q71A}$ mitochondrial sample. This may be attributed to the strongly reduced levels of *rcf1*$_{His}^{R67A,Q71A}$ derivative in these mitochondria and thus would be limiting to form detectable levels of the complex IV** species. Alternatively, (or additionally) the introduction of the additional Q71A mutation, may have compromised the stability of the Rcf1-complex IV association.

Measurement of the maximal O_2 consumption rates of complex IV in the

rcf1$_{His}^{Q61A,R65A}$ mitochondria demonstrated them to be fully restored to the levels in the wild type Rcf1$_{His}$ control mitochondria, whereas in the *rcf1*$_{His}^{R67A,Q71A}$ mitochondria, although they were significantly higher than those measured in the Δ*rcf1*;Δ*rcf2* null mitochondria, they were not equivalent to the *rcf1*$_{His}^{Q61A,R65A}$ or wild type Rcf1$_{His}$ mitochondria (FIGURE 17A). The increased level of complex IV activity in these mutants was sufficient to restore aerobic growth, as expression of both *rcf1*$_{His}^{Q61A,R65A}$ and *rcf1*$_{His}^{R67A,Q71A}$ derivatives, ensured complementation of the growth defect phenotype of the Δ*rcf1*;Δ*rcf2* strain (FIGURE 17B).

In summary, the Q61/R65 and R67/Q71 residue pairs within the QRRQ motif of Rcf1 are independently critical for the stability of the Rcf1 protein. However, despite being strongly reduced in levels, the Q/R pair mutated Rcf1 derivatives could support (fully for the Q61/R65 mutant and partially for the R67/Q71 mutant) the assembly and activity of complex IV. Importantly these findings indicate that Rcf1 does not need to be present at its wild type levels to support the activity of complex IV. Thus, these findings argue against Rcf1 exerting its influence on complex IV activity as a stoichiometrically equivalent component or subunit of the assembled complex IV enzyme.

3.2.6 Rcf1 associates with a cardiolipin binding protein of complex III

The altered complex IV enzymatic activity in *rcf1*$_{His}^{R67A}$ mitochondria, together with the interaction between *rcf1*$_{His}^{R67A}$ and the cardiolipin-remodeling enzyme Taz1, suggested that Rcf1 might be involved in the arrangement or modification of lipids (specifically cardiolipin) within complex IV. Initial analysis of the nature of Rcf1's interaction with the III-IV supercomplex revealed that Rcf1 could interact with complex

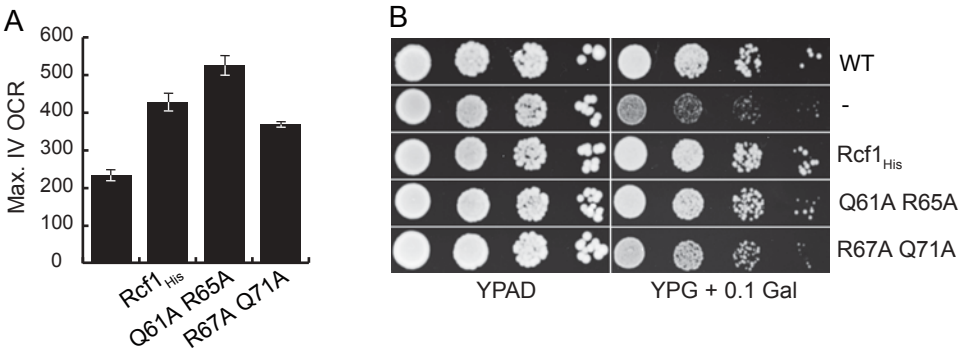

Figure 17. Mutation of the QR pairs in the QRRQ motif in Rcf1 does not negatively affect the catalytic activity of complex IV. (A) Maximal OCR of bioenergetically isolated complex IV was measured in mitochondria isolated from the Δ*rcf1*;Δ*rcf2* strain and the Δ*rcf1*;Δ*rcf2* strain harboring the $rcf1_{His}^{Q61A,R65A}$ or $rcf1_{His}^{R67A,Q71A}$ derivatives, following addition of ascorbate/TMPD and CCCP. **(B)** Serial 10-fold dilutions of wild type (WT), and Δ*rcf1*;Δ*rcf2* expressing $Rcf1_{His}$, $rcf1_{His}^{Q61A,R65A}$ or $rcf1_{His}^{R67A,Q71A}$ derivatives or not, as indicated, were spotted on YP plates containing glucose (YPAD) or glycerol supplemented with 0.1 % galactose (YPG+0.1% Gal) and grown at 30 oC.

III in the absence of a completely assembled complex IV (Strogolova et al., 2012). This finding raised the possibility that Rcf1 might independently bind to components of both complex III and complex IV through, or due to a functional relationship with, a feature common to both complexes (e.g. the modification of cardiolipin).

To determine the interaction partner(s) of Rcf1 within complex III, $Rcf1_{His}$ was purified from a mutant deficient in the assembly of both complex III and complex IV (e.g. a strain of yeast in which the mitochondrial DNA has been lost, i.e. ρ° yeast), and the association of specific complex III subunits was determined using antibodies directed against individual complex III subunits (FIGURE 18). In testing all but one of the complex III subunits (an effective Qcr8 antibody has yet to be acquired), only cytochrome c_1, and to a lesser extent Qcr6, co-purified with $Rcf1_{His}$. According to the crystal structure of the yeast complex III, Qcr6 interacts with cytochrome c_1 within the fully assembled complex III enzyme (Hunte et al., 2000). Similar to other proteins within the Rcf1 interactome (e.g. Cox3, Cox12) cytochrome c_1 interacts with cardiolipin (Lange et al., 2001). This result identifies cytochrome c_1 as an interaction partner of Rcf1, and further supports a role of Rcf1 in the arrangement or modification of cardiolipin within respiratory enzyme complexes.

3.2.7 Comparative analysis of Hig1-type1 and Hig1-type2 proteins and their association with complex IV

Characterization of the Rcf1/Hig1 QRRQ motif suggested that conserved residues of the QRRQ motif influence the dynamic interaction between Rcf1 and complex IV, and may potentially influence the lipid assembly or modification that ultimately affects

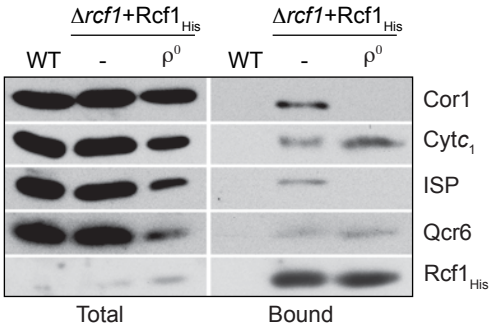

Figure 18. Rcf1 associates with the Complex III cardiolipin-associated subunit, cytochrome c_1. Affinity purification of $Rcf1_{His}$, from ρ^+ (-) and ρ^0 Δ*rcf1* mitochondria following solubilization with digitonin (1%) detergent was performed, followed by SDS-PAGE, Western blotting and immunedecoration, as indicated. Total, 5% of solubilized material; Bound, affinity purified material on the Ni-NTA beads

complex IV enzymatic activity. The QRRQ motif represents a differentiating feature between Hig1-type1 and -type2 proteins. However, it is unknown whether the altered [I/V]-HLIHM-R-$(X)_3$-[Q] motif of Hig1-type1 proteins affects the ability to support respiration-based growth or associate with complex IV.

To determine whether functional differences exist between Hig1-type 1 and type2 proteins, both human isoforms were expressed as C-terminal His-tagged derivatives in the Hig1-deficient yeast strain Δ*rcf1;*Δ*rcf2*. Expression was verified by western blot analysis of purified mitochondria fractions isolated from wild type and mutant derivative strains (FIGURE 19A). The steady state levels of the Hig1-$1A_{His}$ and Hig1-$2A_{His}$ derivatives appeared to be slightly reduced when compared to the wild-type $Rcf1_{His}$ control, and may suggest that heterologous human Hig1 proteins are not entirely stable when expressed in Hig1-deficient yeast.

The ability of human Hig1 proteins to support respiratory-based growth in yeast was tested by growth on the non-fermentable carbon source glycerol (FIGURE 19B). The expression of Hig1-2A partially complemented the respiration-based growth defect of the Δ*rcf1*;Δ*rcf2* yeast strain, while the expression of Hig1-1A did not restore growth. When the level of phenotype complementation was compared between human Hig1-$2A_{His}$ and the his-tagged *C. elegans* Hig1 derivative M05D6.5_{His} (a type 2 Hig1 derivative) expressed in the same background, respiration-based growth was similar between Δ*rcf1*;Δ*rcf2* yeast strains harboring the human (Hig1-$2A_{His}$) or nematode (M05D6.5_{His}) Hig1 proteins, where both partially restored the Δ*rcf1*;Δ*rcf2* growth deficiency (FIGURE 19B).

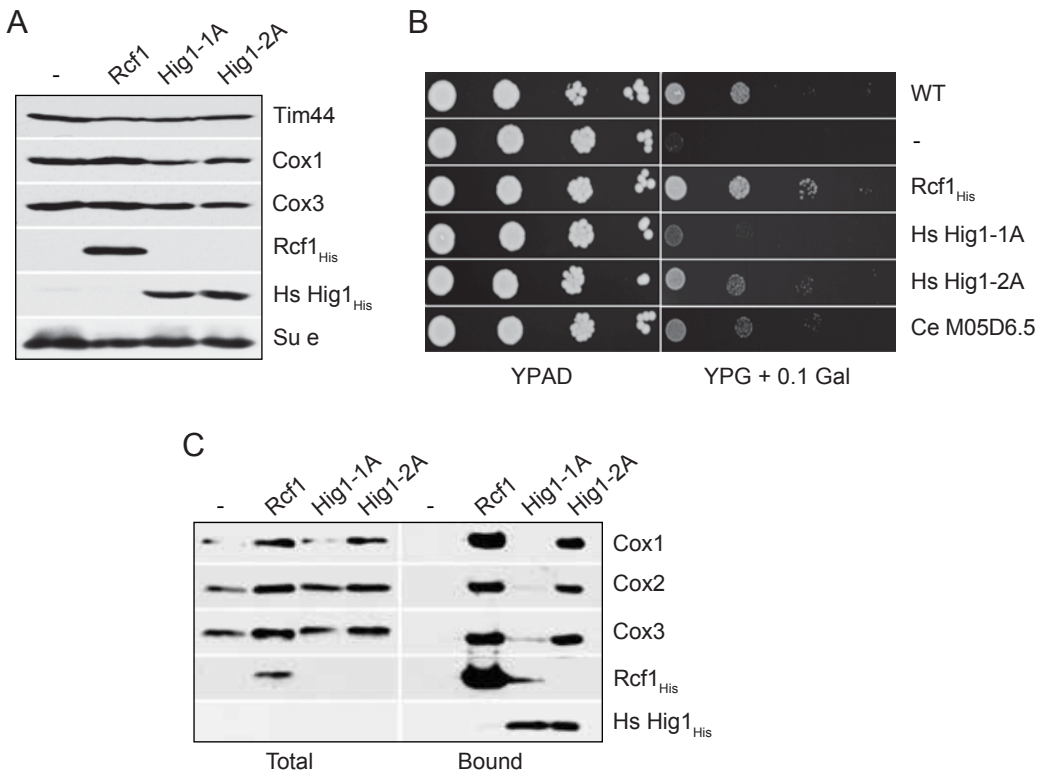

Figure 19. Hig1-type 1 and -type 2 proteins display contrasting levels of association with Complex IV. (A) Steady state protein levels of OXPHOS subunits in the mitochondria (50 µg protein) isolated from the Δ*rcf1*;Δ*rcf2* strain harboring his-tagged yeast Rcf1, or human Hig1-type1(Hig1-1A) or -type 2 (Hig1-2A) isoforms, or not (-). Mitochondria were analyzed by SDS-PAGE, Western blotting and immunedecoration with antibodies against complex IV subunits (Cox1 and Cox3), with Tim44 and the F_1F_O ATP-synthase subunit, Su e, levels as loading controls. (B) Serial 10-fold dilutions of wild type (WT), and Δ*rcf1*;Δ*rcf2* yeast strains expressing Rcf1His, human (Hs) Hig1-1A, Hs Hig1-2A, or C.elegans (Ce) M05D6.5 (Hig1-type 2 protein) derivatives or not, as indicated, were spotted on YP plates containing glucose (YPAD) or glycerol supplemented with 0.1 % galactose (YPG+0.1% Gal) and grown at 30 °C. (C) Affinity purification of Rcf1His (Rcf1), Hs Hig1-1A (Hig1-1A) or Hs Hig1-2A (Hig1-2A) derivatives following solubilization with Triton X-100 detergent was performed, followed by SDS-PAGE, Western blotting and immunedecoration, as indicated. Total, 5% of solubilized material; Bound, affinity purified material on the Ni-NTA beads.

The capacity of the his-tagged human Hig1 derivatives to associate with complex IV was investigated through affinity purification via Ni-NTA chromatography, following solubilization from mitochondria with Triton X-100 (FIGURE 19C). The relative amount of human Hig1-1A$_{His}$ and Hig1-2A$_{His}$ protein that was purified on the beads, as determined by western blot using His antiserum, was significantly reduced (~70% reduction), compared to the levels of Rcf1$_{His}$. A similar pattern of reduction was observed in the total mitochondrial fraction (total), and thus, suggests that human Hig1 proteins might be less stable in yeast mitochondria.

First, heterologous Hig1-type2 proteins (Rcf1 and Hig1-2A) were compared in their ability to associate with complex IV, the level of complex IV subunit co-purification was similar between the human Hig1-2A$_{His}$ derivative and the Rcf1$_{His}$ control (FIGURE 19C). However, when the level of complex IV co-purification was compared to the level of Rcf1$_{His}$/Hig1-2A$_{His}$ bound to the Ni-NTA beads, a greater amount of Rcf1$_{His}$ was bound to the beads, suggesting that Hig1-2A$_{His}$ associates with a greater amount of complex IV, relative to Rcf1$_{His}$. When the association with complex IV was compared between Hig1-1A$_{His}$ and Rcf1$_{His}$, a reduced association of complex IV subunits with the Hig1-1A$_{His}$ derivative, relative to the wild type Rcf1$_{His}$ control, was observed. When the level of complex IV association was compared between Hig1-1A$_{His}$ and Hig1-2A$_{His}$, where the amount of His-tagged protein bound to the beads was similar, Hig1-2A$_{His}$ co-purified a significantly greater amount of complex IV protein than Hig1-1A$_{His}$.

Together, these results indicate that Hig1-type1 proteins, which contain a modified [I/V]-HLIHM-R-(X)$_3$-[Q] motif display a weaker interaction with complex IV, relative to Hig1-type 2 proteins, and cannot complement the respiration-based growth

defect of the Δ*rcf1*;Δ*rcf2* yeast strain. These results highlight the importance of the QRRQ motif as a potential basis of functional differences between Hig1-type 1 and -type 2 proteins, and further support the conserved role of the QRRQ motif of Hig1-type 2 proteins in influencing association with complex IV and supporting respiratory growth.

3.2.8 Analysis of the molecular environment of the Rcf1 QRRQ motif

The preceding results suggested an important role for the QRRQ motif in the function of the Rcf1 protein. Yet the molecular environment surrounding the QRRQ motif was unknown. In particular, it was important to identify potential protein partners that may interact with the QRRQ region of Rcf1.

To analyze the molecular environment of the conserved QRRQ motif region and identify potential protein partners, a Cysteine (Cys)-based scanning strategy via a Cys-based crosslinking was adopted. Cysteine site-directed mutagenesis was used to introduce unique Cys residues into the Rcf1 QRRQ motif region in the context of a Cys-less $Rcf1_{His}$ derivative ($rcf1_{His}^{C28A,C38A}$) where the sole Rcf1 cysteines, C28 and C38, have been mutated to Ala. Four distinct Rcf1 mutant derivatives were created, with the location of the "inserted" Cys residues selected on the basis of their position relative to the conserved QRRQ residues (FIGURE 20A). In the first mutant, tryptophan (Trp, W) 58 was mutated to Cys, to create the $rcf1_{His}^{C28A,C38A,W58C}$ (W58C) derivative. In the second mutant derivative Alanine (Ala, A) 60 was mutated to Cys, to create $rcf1_{His}^{C28A,C38A,A60C}$ (A60C). The third and fourth mutants were created by individually mutating Valine (Val,V) 68 and Glycine (Gly, G) 69 to Cys, to create $rcf1_{His}^{C28A,C38A,V68C}$ (V68C) and $rcf1_{His}^{C28A,C38A,G69C}$ (G69C) derivatives, respectively. Rcf1 mutant

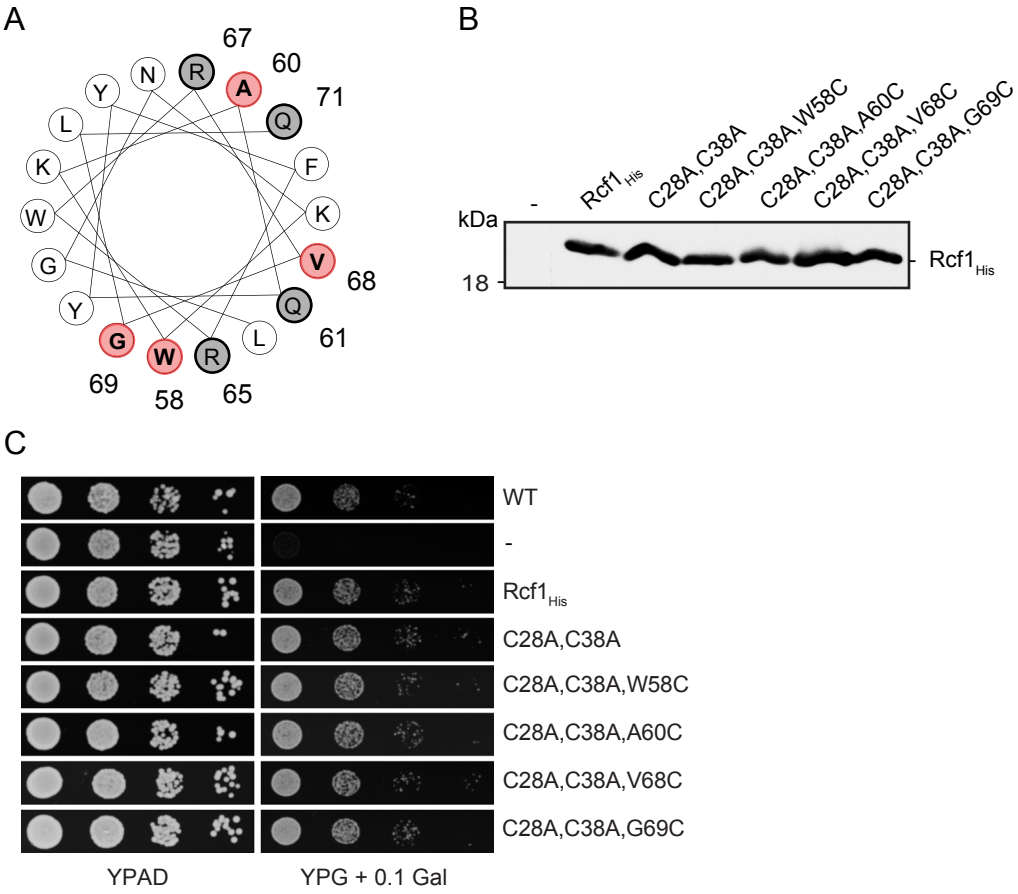

Figure 20. Cysteine mutation of residues within, and adjacent to, the Rcf1 QRRQ motif. (A) α-helical plot of residues Leu(L)54 through Gln(Q)71of Rcf1 depicting the location of cysteine mutated residues (W58, A60, V68 and G69) and their respective positions relative to the QRRQ residues **(B)** Mitochondria were isolated from the Δ*rcf1*;Δ*rcf2* control (-) and the Δ*rcf1*;Δ*rcf2* strain harboring either His-tagged Rcf1 ($Rcf1_{His}$), $rcf1_{His}^{C28A,C38A}$ (C28,C38), $rcf1_{His}^{C28A,C38A,W58C}$ (C28,C38,W58C), $rcf1_{His}^{C28A,C38A,A60C}$ (C28,C38,A60C), $rcf1_{His}^{C28A,C38A,V68C}$ (C28,C38,V68C), or $rcf1_{His}^{C28A,C38A,G69C}$ (C28,C38,G69C) derivatives. Rcf1 levels were analyzed by Western blotting.(*mitochondria were incubated in SH Buffer containing DMSO prior to SDS-PAGE). **(C)** Serial 10-fold dilutions of wild type (WT), and Δ*rcf1*;Δ*rcf2* yeast strains expressing the $Rcf1_{His}$ derivative or cysteine mutant derivatives or not, as indicated, were spotted on YP plates containing glucose (YPAD) or glycerol supplemented with 0.1 % galactose (YPG+0.1% Gal) and grown at 30 °C.

derivatives were expressed as C-terminal His-tagged derivatives in the Rcf1/Rcf2 double null yeast strain (Δ*rcf1*;Δ*rcf2*). Expression was verified by western blot analysis of purified mitochondria fractions isolated from wild type and mutant derivative strains (FIGURE 20B). The Δ*rcf1*;Δ*rcf2* yeast strain displays a respiration-based growth defect (Strogolova et al., 2012). The expression of $rcf1_{\mathrm{His}}^{\mathrm{C28A,C38A,W58C}}$, $rcf1_{\mathrm{His}}^{\mathrm{C28A,C38A,A60C}}$, $rcf1_{\mathrm{His}}^{\mathrm{C28A,C38A,V68C}}$ and $rcf1_{\mathrm{His}}^{\mathrm{C28A,C38A,G69C}}$ derivatives complemented the Δ*rcf1*;Δ*rcf2* respiratory growth defect (growth on the non-fermentable carbon source, glycerol) to a similar extent as the wild type $\mathrm{Rcf1_{His}}$ derivative (FIGURE 20C). From this result it was concluded that these yeast strains were viable and that the loss of C28 and C38, or the Cys insertion mutations do not affect the ability of the resulting Rcf1 derivatives to complement the respiratory growth defect of the Δ*rcf1*;Δ*rcf2* yeast strain.

The molecular environment of the QRRQ motif region was analyzed via sulfhydryl (SH) –specific cross-linking by the SH-specific homobifunctional reagent bismaleimidoethane (BMOE), and subsequently analyzed by SDS-PAGE and immunedecoration with Rcf1 antisera. Following BMOE crosslinking, wild type $\mathrm{Rcf1_{His}}$ formed a number of adducts with partner proteins, the most prominent of which was a 40 kDa adduct (Rcf1+ a 20 kDa partner protein)(FIGURE 21). None of the $\mathrm{Rcf1_{His}}$ BMOE crosslinking adducts were detectable in the $rcf1_{\mathrm{His}}^{\mathrm{C28A,C38A}}$ derivative, indicating that the BMOE (SH-SH) crosslinking observed in the wild type $\mathrm{Rcf1_{His}}$ involved the C28 and C38 residues. When the crosslinking patterns of the Cys insertion Rcf1 mutant derivatives were directly compared to those of wild type $\mathrm{Rcf1_{His}}$ and the $rcf1_{\mathrm{His}}^{\mathrm{C28A,C38A}}$ derivative, a number of novel crosslinking adducts containing Rcf1 and partner proteins were identified (FIGURE 21A). Of particular interest was a significant increase

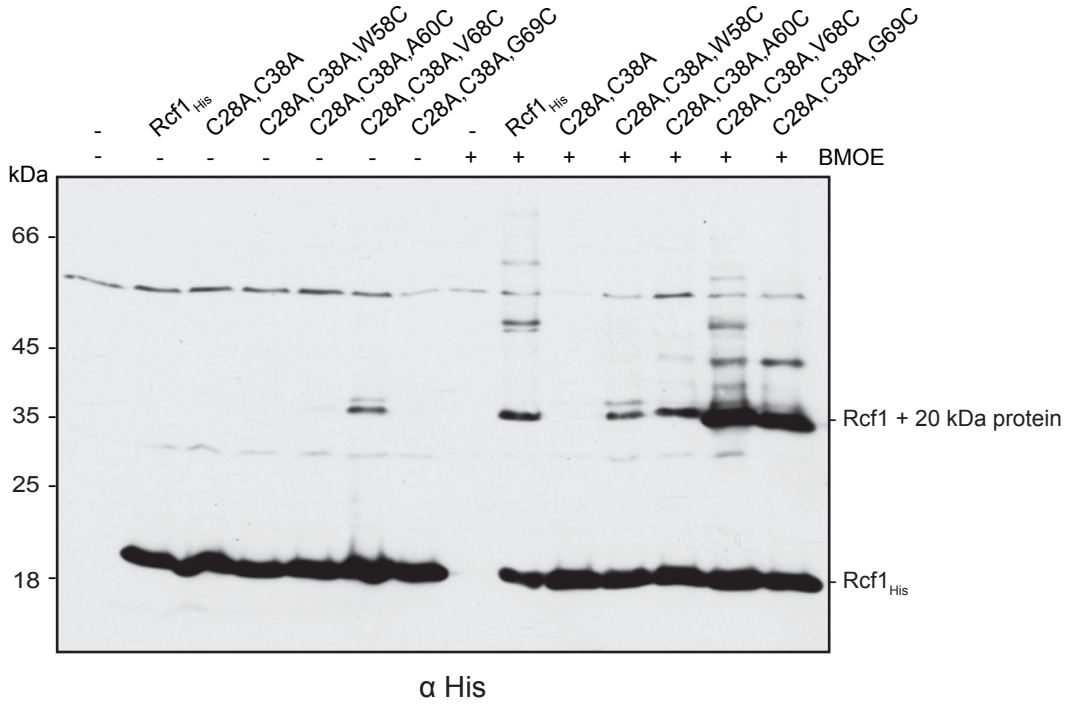

Figure 21. Cysteine -based scanning analysis of the molecular environment of the Rcf1 QRRQ motif. Chemical cross-linking (BMOE) was performed on mitochondria isolated from the Δ*rcf1*;Δ*rcf2* control (-) and Δ*rcf1*;Δ*rcf2* strains harboring the $Rcf1_{His}$ derivative or cysteine mutant derivatives, as indicated. Following SDS-PAGE, and Western blotting, decoration with His-tag epitope (α His12) antiserum was performed. The positions of the dominant 40 kDa (Rcf1+ 20 kDa protein) Rcf1-containing adduct, and the monomeric Rcf1 (Rcf1His) are indicated.

(approximately twice the level observed in wild type $Rcf1_{His}$ mitochondria) in the 40 kDa adduct in the $rcf1_{His}^{C28A,C38A,V68C}$ and $rcf1_{His}^{C28A,C38A,G69C}$ derivatives. Interestingly, in the $rcf1_{His}^{C28A,C38A,V68C}$ derivative the 40 kDa adduct was observed even in the absence of cross-linking reagent, albeit at a significantly lower level compared to the presence of cross-linking reagent. These results suggested that the C68 within the Rcf1 QRRQ motif potentially forms a disulfide bond with an Rcf1 partner protein.

To determine the identity of the protein partner that forms a 40 kDa adduct with Rcf1, BMOE cross-linking was combined with affinity chromatography to affinity purify the Rcf1 crosslinking adduct, and liquid chromatography –tandem mass spectrometry (LC-MS/MS) analysis to identify the partner protein. Cross-linking was performed in $rcf1^{C28A,C38A,V68C}$ mitochondria, and in parallel with a $rcf1^{C28A,C38A}$ mutant control. Following crosslinking, mitochondria were solubilized first in SDS-containing buffer, followed by Triton–X100 solubilization. $Rcf1_{His}$ –containing adducts were purified by Ni-NTA affinity chromatography, and separated by SDS-PAGE. The purified 40 kDa adduct that contained $rcf1^{C28A,C38A,V68C}$ and the 20 kDa partner protein was visualized by silver staining (FIGURE 22), excised and subjected to LC-MS/MS in collaboration with Dr. Kate Noon at the Medical College of Wisconsin Mass Spectrometry Facility. Common contaminants were excluded from the final results and false positives were eliminated from the resulting data set by comparing the LC-MS/MS spectra of $rcf1^{C28A,C38A,V68C}$ to that of the $rcf1^{C28A,C38A}$ derivative. Rcf1was the only protein detected within the excised 40 kDa cross-linking adduct. These results suggest that Rcf1 may form a homodimer, and that the insertion of a Cys at V68 enhances the formation of the Rcf1 homodimer.

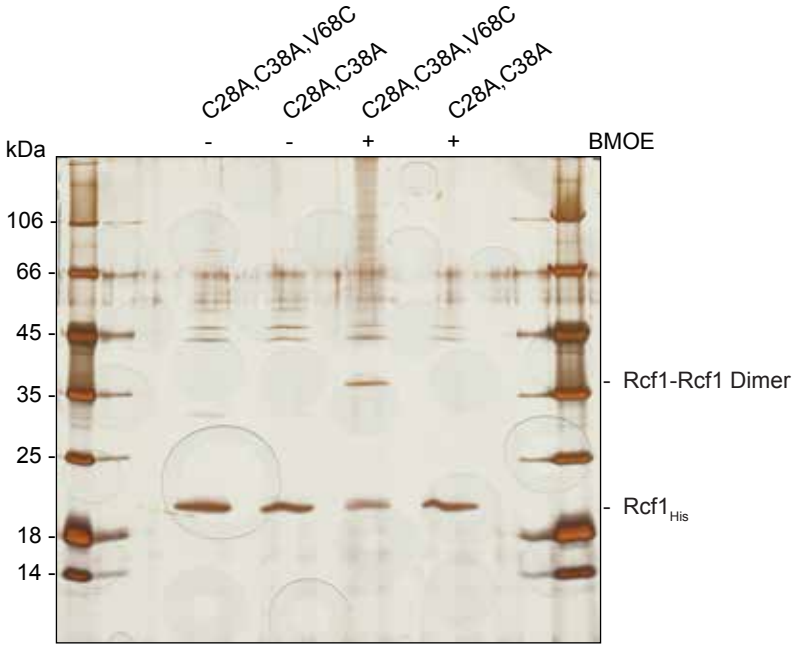

Figure 22. Liquid chromatography- (tandem) mass spectrometry identification of an Rcf1-Rcf1 dimer. Chemical cross-linking (BMOE) was performed on mitochondria isolated from the Δ*rcf1*;Δ*rcf2* strain harboring *rcf1*$_{His}^{C28A,C38A}$ (C28,C38) or *rcf1*$_{His}^{C28A,C38A,V68C}$ (C28,C38,V68C) and the affinity purification of Rcf1-containing adducts following solubilization with Triton X-100 detergent was performed. Following SDS-PAGE, affinity purified Rcf1-containing adducts were visualized by silver stain and the 40 kDa *rcf1*$_{His}^{C28A,C38A,V68C}$ - containing adduct was analyzed by liquid chromatography- (tandem) mass spectrometry (LC-MS/MS).

3.2.9 Investigation of the protonation state of R67 in influencing the molecular interactions of the Rcf1 protein

The mutation of R67 within the QRRQ motif of Rcf1 resulted in a distinct pattern of biochemical and bioenergetic changes within the mitochondria that appeared to be, at the very least, tangentially related to lipid synthesis and/or remodeling within respiratory enzymes. Transmembrane helical prediction algorithms predict that Rcf1 R67 resides at the matrix loop-transmembrane interface of the Rcf1 protein. While R67 is predicted to be protonated at the reported physiological pH of the mitochondrial matrix (pH7.7), the pH within the inner mitochondrial membrane micro-environment may vary (Santo-Domingo and Demaurex, 2012). The mutation of Arg 67 to Ala simultaneously changed the size and protonation state of the amino acid, and introduced a de-protonated residue to the Rcf1 QRRQ motif. Thus, the functional consequences of mutating R67 could be related to the protonation state of Rcf1 R67, an amino acid that is exceptionally conserved among both type1 and type2 Hig1 proteins.

To characterize the Rcf1 R67 protonation state and its potential influence on complex IV and the molecular environment of Rcf1, mutations were introduced that were predicted to change the charge of the residue; R67Q (uncharged), R67H (pH-sensitive), R67K (charged, [+]), R67E (charged, [-]). The resulting Rcf1 R67 mutant derivatives, i.e. $rcf1_{\mathrm{His}}^{\mathrm{R67Q}}$, $rcf1_{\mathrm{His}}^{\mathrm{R67H}}$, $rcf1_{\mathrm{His}}^{\mathrm{R67K}}$ and $rcf1_{\mathrm{His}}^{\mathrm{R67E}}$, were expressed in the Δ*rcf1*;Δ*rcf2* null mutant. Steady state analysis of proteins isolated from the resulting strains indicated that the levels of mutant Rcf1 R67 derivatives were equal to the wild type $\mathrm{Rcf1}_{\mathrm{His}}$ control (FIGURE 23A). Therefore, mutation of R67 in this manner did not appear to adversely affect the stability of the Rcf1 protein.

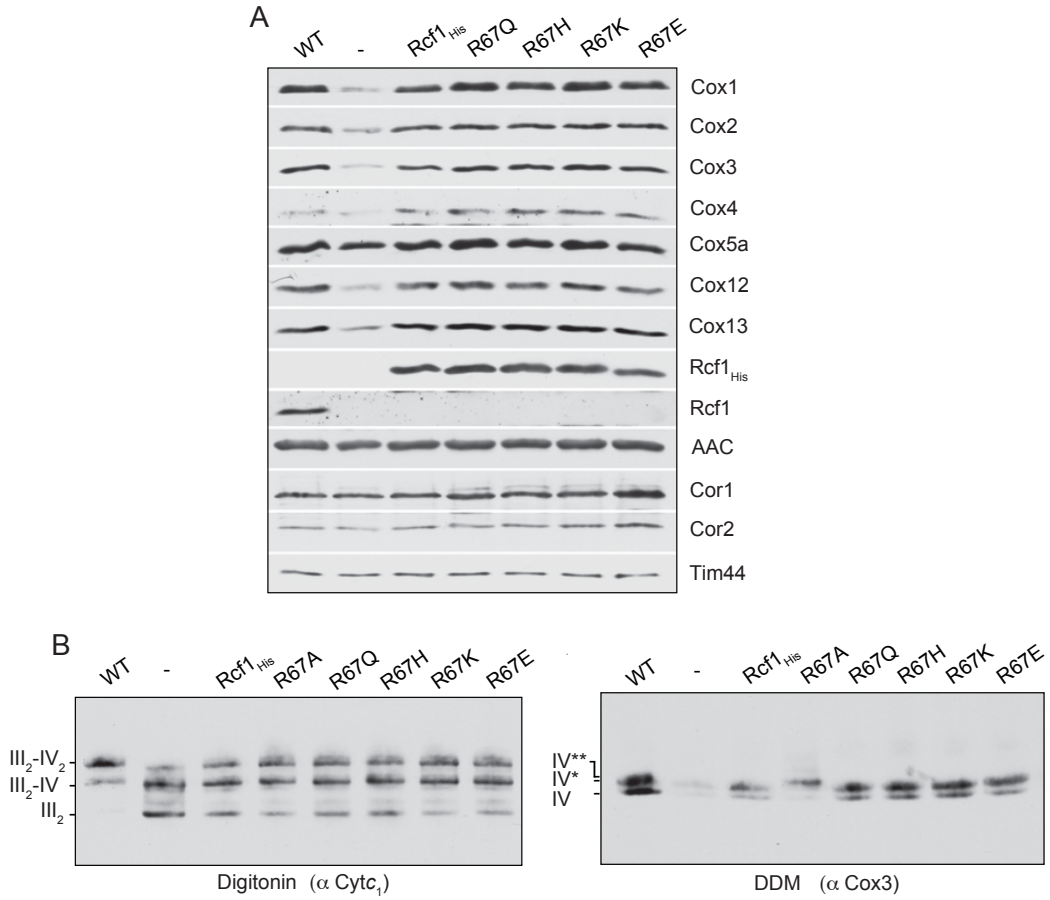

Figure 23. Charge-altering mutations in Rcf1 R67 do not negatively affect the assembly state of complex IV or the assembly of complex IV with complex III, in contrast to the size-altering R67A mutation. (A) Steady state protein levels of OXPHOS subunits in mitochondria (50 µg protein) isolated from the wild type, and the Δ*rcf1*;Δ*rcf2* strain harboring his-tagged Rcf1(Rcf1$_{His}$), *rcf1*$_{His}^{R67Q}$ (R67Q), *rcf1*$_{His}^{R67H}$ (R67H) , *rcf1*$_{His}^{R67K}$ (R67K), and *rcf1*$_{His}^{R67E}$ (R67E) derivatives, or not (-). Mitochondria were analyzed by SDS-PAGE, Western blotting and immune-decoration with antibodies against indicated OXPHOS proteins. Tim44 levels were used as loading controls. **(B)** Mitochondria isolated from WT and indicated Δ*rcf1*;Δ*rcf2* strains were solubilized in digitonin (1%) (left panel) or DDM (0.6%)(right panel) and subjected to BN-PAGE analysis, Western blotting and immunedecoration with antibodies against complex III subunit, cytochrome c_1 (αCytc_1)(left panel) or complex IV subunit Cox3 (α -Cox3)(right panel).

Analysis of the complex IV subunit levels in mutant mitochondria demonstrated that they were similar to that of the $Rcf1_{His}$ control and significantly higher than those observed in the Δ*rcf1*;Δ*rcf2* null mitochondria (FIGURE 23A). BN-PAGE analysis of the III-IV supercomplex indicated that the levels of III_2-$IV_{(1-2)}$ in Δ*rcf1*;Δ*rcf2* harboring the Rcf1 R67 mutant proteins were similar to the III_2-$IV_{(1-2)}$ levels in double mutant harboring the wild type $Rcf1_{His}$ derivative, or $rcf1_{His}^{R67A}$ mutant derivative, which were both analyzed in parallel (FIGURE 23B, left panel). The levels of DDM-solubilized complex IV in the R67Q, R67H, R67K and R67E mitochondria were also similar to those of the wild type $Rcf1_{His}$ control, and in contrast to the strongly reduced levels of assembled complex IV and appearance of the novel IV** form that was observed in the $rcf1_{His}^{R67A}$, which were both analyzed in parallel (FIGURE 23B right panel).

Together, these results suggest that charge-altering mutations in R67 that do not alter the size of the amino acid (in contrast to the R67A mutation), likewise do not negatively affect the assembly state of complex IV or the assembly of complex IV with complex III.

The levels of complex IV that associated with the His-tagged Rcf1 R67 derivatives was also investigated through affinity purification via Ni-NTA chromatography, following solubilization from mitochondria with digitonin (FIGURE 24A). The level of complex IV (and complex III, Cytc_1) subunits that co-purified with the $rcf1_{His}^{R67Q}$, $rcf1_{His}^{R67K}$ and $rcf1_{His}^{R67E}$ derivatives were similar to the control $Rcf1_{His}$ protein, which was analyzed in parallel (FIGURE 24A). Notably, a slight increase in level of association with complex IV (and Complex III) was observed in the $rcf1_{His}^{R67H}$ derivative. In contrast, when complex IV association was analyzed under stronger

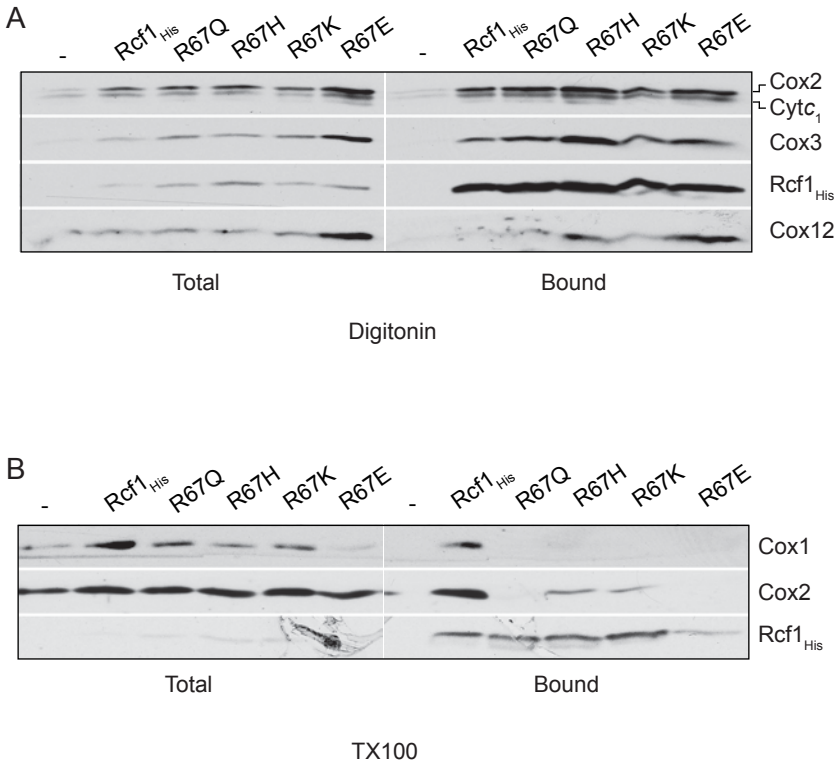

Figure 24. Charge-altering mutations in Rcf1 R67 affect the association of Rcf1 with complex IV. (A) Affinity purification of Rcf1His, *rcf1*$_{His}^{R67Q}$, *rcf1*$_{His}^{R67H}$, *rcf1*$_{His}^{R67K}$, *rcf1*$_{His}^{R67E}$ derivatives following solubilization with 1 % digitonin detergent was performed, followed by SDS-PAGE, Western blotting and immunedecoration, as indicated. Total, 5% of solubilized material; Bound, affinity purified material on the Ni-NTA beads. **(B)** Same as (A), except solubilization was performed with Triton X100.

(Triton-X100) solubilization conditions, the ostensibly similar levels of association with complex IV that were observed under milder detergent solubilization conditions disappeared, and gave way to nuanced changes in complex IV association (as determined by Cox2 immunedecoration) between respective R67 mutant derivatives. Specifically, the level of Cox2 that co-purified with the *rcf1*$_{His}^{R67H}$ and *rcf1*$_{His}^{R67K}$ derivatives was reduced by approximately 50%, compared to wild type Rcf1$_{His}$, which was evaluated in parallel (FIGURE 24B). On the other hand, the *rcf1*$_{His}^{R67Q}$ and *rcf1*$_{His}^{R67E}$ derivatives did not appear to co-purify complex IV under Triton-X100 solubilization conditions.

These results are consistent with initial analysis of the QRRQ motif using the *rcf1*$_{His}^{Q61A\ Q71A}$ and *rcf1*$_{His}^{R67A}$ derivatives, in that they support the conclusion that Rcf1 likely displays a dynamic interaction with complex IV that is influenced, or possibly governed, by the QRRQ motif.

Measurement of the state 4 OCR in Δ*rcf1*;Δ*rcf2* mitochondria harboring Rcf1 R67 mutants indicated that *rcf1*$_{His}^{R67Q}$ and *rcf1*$_{His}^{R67H}$ fully restored state 4 OCR to the levels in the wild type Rcf1$_{His}$ control mitochondria, whereas the rates in the *rcf1*$_{His}^{R67K}$ and *rcf1*$_{His}^{R67E}$ mitochondria were slightly higher, compared to the wild type Rcf1$_{His}$ control mitochondria (FIGURE 25A). The respiratory control ratio was similar across all R67 mutant derivatives and closely matched that of the wild type Rcf1$_{His}$ control (FIGURE 25B). The coupled state of these mitochondria suggests that the elevated state 4 OCR of the R67K and R67E mitochondria is not due to an elevated basal OCR activity caused by a H^+ leaky membrane. Measurement of the complex IV OCR directly in the presence of ascorbate/TMPD in the *rcf1*$_{His}^{R67Q}$ and *rcf1*$_{His}^{R67H}$ mitochondria demonstrated them to be slightly elevated, as compared to the levels in the wild type Rcf1$_{His}$ control

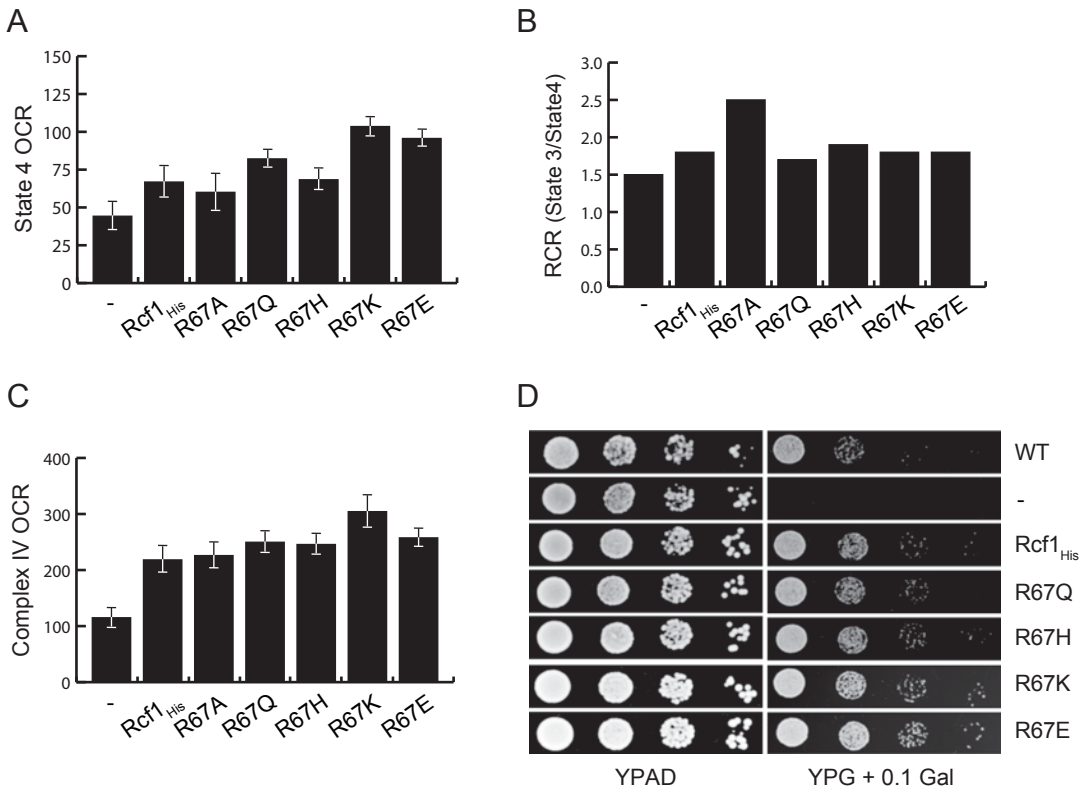

Figure 25. A charged Rcf1 R67 residue affects the catalytic properties of complex IV. (A and B) The oxygen consumption rates (OCR) of the NADH driven state 4 and respiratory control ratio (RCR) - the ratio of state 3 (NADH/ADP) to state 4 (NADH) OCR's - were measured in mitochondria isolated from wild type (WT) or the Δ*rcf1*;Δ*rcf2* strain harboring the $Rcf1_{His}$, $rcf1_{His}^{R67A}$, $rcf1_{His}^{R67Q}$, $rcf1_{His}^{R67H}$, $rcf1_{His}^{R67K}$, $rcf1_{His}^{R67E}$ derivatives, or not (-), n = 3. **(C)** The bioenergetically isolated activity of complex IV was determined by measuring the OCR driven by ascorbate/TMPD, n= 3. **(D)** Serial 10-fold dilutions of indicated strains were spotted on YP plates containing glucose (YPAD) or glycerol supplemented with 0.1 % galactose (YPG+0.1% Gal) and grown at 30 oC.

mitochondria, whereas in the *rcf1*$_{\text{His}}^{\text{R67E}}$ and, to a greater extent, the *rcf1*$_{\text{His}}^{\text{R67E}}$ mitochondria the complex IV OCR was significantly higher than the wild type Rcf1$_{\text{His}}$ control mitochondria (FIGURE 25C). The increased level of complex IV activity in the R67 mutants was sufficient to restore aerobic growth, as expression of each R67 mutant derivative (*rcf1*$_{\text{His}}^{\text{R67Q}}$, *rcf1*$_{\text{His}}^{\text{R67H}}$, *rcf1*$_{\text{His}}^{\text{R67K}}$ and *rcf1*$_{\text{His}}^{\text{R67E}}$), complemented the growth defect phenotype of the Δ*rcf1*;Δ*rcf2* strain (FIGURE 25D).

Together, these results suggest that *rcf1*$_{\text{His}}^{\text{R67Q}}$, *rcf1*$_{\text{His}}^{\text{R67H}}$, *rcf1*$_{\text{His}}^{\text{R67K}}$ and *rcf1*$_{\text{His}}^{\text{R67E}}$ mutant derivatives display the capacity to fully support complex IV activity when expressed in Δ*rcf1;*Δ*rcf2* strain. Furthermore, the state 4 OCR measurements would suggest that the complex IV enzyme in the *rcf1*$_{\text{His}}^{\text{R67K}}$ and *rcf1*$_{\text{His}}^{\text{R67E}}$ mitochondria may display differential enzymatic properties than when the wild type Rcf1 control (or *rcf1*$_{\text{His}}^{\text{R67Q}}$ and *rcf1*$_{\text{His}}^{\text{R67H}}$) protein is present.

To determine whether charge-altering mutations in R67 (R67Q, R67H, R67K, R67E), effect the molecular environment of Rcf1 a chemical cross-linking approach was adopted, using m-maleimidobenzoyl-N-hydroxysuccinimide ester (MBS), an amine-sulfhydryl cross-linker with a 7.3 Å spacer length. Cross-linking was performed in isolated mitochondria harboring the Rcf1 derivatives and subsequently analyzed by SDS-PAGE and immunedecoration with Rcf1 antisera (FIGURE 26, left panel). Previous analysis demonstrated that the mutation R67A influences the proximity between Rcf1- and Cox2 subunit, seen in the gained crosslink between *rcf1*$_{\text{His}}^{\text{R67A}}$ and Cox2 (not shown). Therefore, the affect of charge–related mutations in R67 on the ability of Rcf1 to be cross-linked to Cox2 was determined by immunedecoration of a parallel MBS crosslinking experiment with Cox2-specific-antisera (FIGURE 26, right panel).

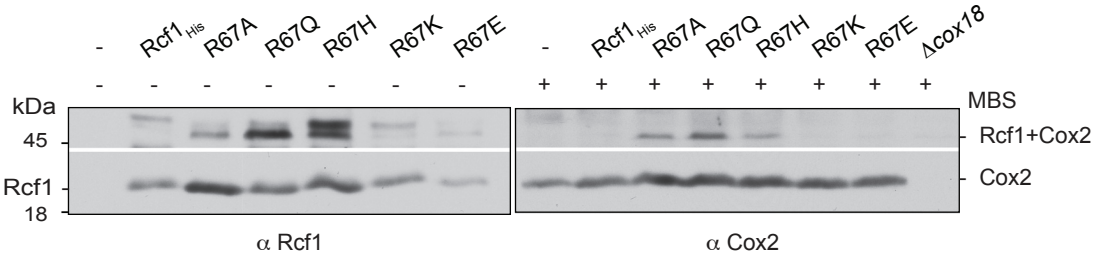

Figure 26. Mutation of R67 Affects the molecular environment of Rcf1 and Cox2. Chemical cross-linking (MBS) was performed on mitochondria isolated from the Δ*rcf1*;Δ*rcf2* control (-) and Δ*rcf1*;Δ*rcf2* strains harboring the $Rcf1_{His}$, $rcf1_{His}^{R67A}$, $rcf1_{His}^{R67Q}$, $rcf1_{His}^{R67H}$, $rcf1_{His}^{R67K}$, $rcf1_{His}^{R67E}$ derivatives, as indicated. Following SDS-PAGE, and Western blotting, immunedecoration with the His-tag epitope (α His12)(left panel) or complex IV subunit 2 (α Cox2)(right panel) antiserum was performed. The positions of the Rcf1-Cox2 adduct, and monomeric Rcf1 and Cox2 are indicated.

Consistent with previous results and observed in parallel with the Rcf1-antibody decoration, no Cox2-containing adduct was detected in Δ*rcf1;*Δ*rcf2* mitochondria harboring His-tagged wild type Rcf1. Additionally, no Cox2 adduct was observed in the Cox2-deficient control strain, Δ*cox18*. The ability of Rcf1 to be cross-linked to Cox2 varied across R67 mutant derivatives expressed in Δ*rcf1;*Δ*rcf2* mitochondria. Similar to the R67A control, which was analyzed in parallel, R67Q and R67H mutant derivatives gained the ability to be cross-linked to Cox2. In contrast, no crosslinking to Cox2 was observed in Δ*rcf1;*Δ*rcf2* mitochondria harboring either the R67K or R67E mutant derivatives. It was therefore concluded that, similar to the R67A mutant, the arrangement of Rcf1 with complex IV is altered in the R67Q and R67H mutants, such that a close proximity between Rcf1-and Cox2 subunit is gained.

These results suggest that the protonation state of R67 may influence the molecular environment of Rcf1 and Cox2/complex IV.

3.3 Chapter 3 Summary

In summary, these results demonstrate the importance of the QRRQ motif in influencing a dynamic interaction between Cox3 and complex IV. It was found that the QRRQ motif impacts the ability of Rcf1 to associate with the assembled complex IV, and the Cox3 and Cox12 protein subunits. In addition, these data reveal that Rcf1 exists in close proximity to Cox2, a catalytically important subunit of complex IV. The mutation of conserved residues within the QRRQ motif lead to the assembly of a novel Rcf1-complex IV subpopulation that displays altered enzymatic properties. The conserved QRRQ motif may further influence the molecular environment of Rcf1 and its potential relationship with the cardiolipin-remodeling enzyme Taz.

Comparative analysis of Hig1-type 1 and type 2 proteins revealed differences in their ability to interact with complex IV. Given the importance of the QRRQ motif for the interactions of Rcf1 stated above, it is tempting to speculate that the differences observed in the association between type 1 and type 2 proteins and complex IV could potentially be related to differences in the amino acid composition of their respective QRRQ motifs.

Finally, it was found that Rcf1 may form a homodimer and that the QRRQ motif might influence the formation, or stability of the Rcf1-Rcf1 dimer.

Based on these findings, a model is proposed where Rcf1 transiently associates with complex IV to modify it, possibly its lipid composition, and by doing so, alters its enzymatic properties.

CHAPTER 4: CHARACTERIZATION OF THE MOLECULAR ENVIRONMENT OF RCF1 AND AAC

4.1 Introduction

Mitochondria are dynamic eukaryotic organelles that operate within and respond to the metabolic context of the cell. Each of the mitochondrial processes, including the regulation of cellular Ca^{2+} flux, ROS homeostasis, the assembly of iron-sulfur clusters, and OXPHOS require a level of interconnectedness between mitochondria and the rest of the cell. Mitochondrial carriers are a family of proteins that connect the biochemical pathways of the mitochondrial matrix to those of the cytoplasm through the transport of amino acids, cofactors, fatty acids, keto acids, inorganic ions, and nucleotides across the mitochondrial membrane (Palmieri, 2013).

In the final steps of OXPHOS, the F_1F_O ATP-synthase utilizes the proton gradient generated by electron transport complexes to synthesize ATP from inorganic phosphate and ADP. This metabolically critical process relies on a sufficient ADP/ATP exchange carried out by the adenine nucleotide translocase, commonly referred to in yeast as the ADP/ATP carrier (AAC) (Gawaz et al., 1990; Klingenberg, 1989; Nury et al., 2006; Pebay-Peyroula and Brandolin, 2004). Under normal respiratory conditions the AAC protein imports ADP^{3-} into the mitochondrial matrix and exports ATP^{4-} into the cytosol for use in cellular functions. Under severe mitochondrial damage the reversal of the translocase facilitates the export of mitochondrial ADP and import of cytosolic ATP into the mitochondria, thereby maintaining the mitochondrial membrane potential and biosynthesis processes that are critical for cell viability (Chen, 1995; Chen and Clarke-Walker, 1996; Giraud and Velours, 1997). The importance of AAC proteins in cellular

metabolism is underscored by the fact that the AAC protein accounts for nearly 10% of the total mitochondrial protein content, and is therefore considered the most abundant protein within the mitochondria (Brand, 2005).

A number of isoforms of AAC proteins have been identified in different organisms. The yeast *Saccharomyces cerevisiae* contains the ADP/ATP carrier (AAC), a homolog of AAC proteins and a classic member of the mitochondrial carrier family with an essential role in the translocation of adenine nucleotides across the mitochondrial membrane system (Klingenberg, 2008). Yeast contain 3 distinct AAC isoforms: Aac1, Aac2 and Aac3 (Kolarov et al., 1990; Lawson and Douglas, 1988; O'Malley et al., 1982). Aac2 is the primary isoform expressed in aerobically growing yeast, Aac3 is expressed largely in anaerobically growing yeast, and Aac1 is expressed at low levels regardless of oxygen availability (Gawaz et al., 1990; Kolarov et al., 1990; Lawson et al., 1990).

Encoded by nuclear DNA, AAC proteins are synthesized in the cytosol prior to being imported into the mitochondria and inserted in the inner membrane (Endres et al., 1999; Pfanner et al., 1987; Ryan et al., 1999). AAC proteins have six transmembrane α helical domains (H1-H6) that span the inner mitochondrial membrane and form alpha helices, with short hydrophobic N- and C- terminal tails located in the intermembrane space (Pebay-Peyroula et al., 2003). Two specific inhibitors, carboxyatractyloside (CATR,AT) and bongkrekic acid (BA), have significantly aided functional analysis of AAC. AT binds to the IMS side of AAC locking the translocase in a cytosol-open state referred to as “c-state”, and BA binds to the matrix side locking AAC in a matrix-open state referred to as “m-state” (FIGURE 27) (Aquila et al., 1978; Brandolin et al., 1993; Riccio et al., 1975). The crystal structure of the yeast Aac2 protein bound to AT has been

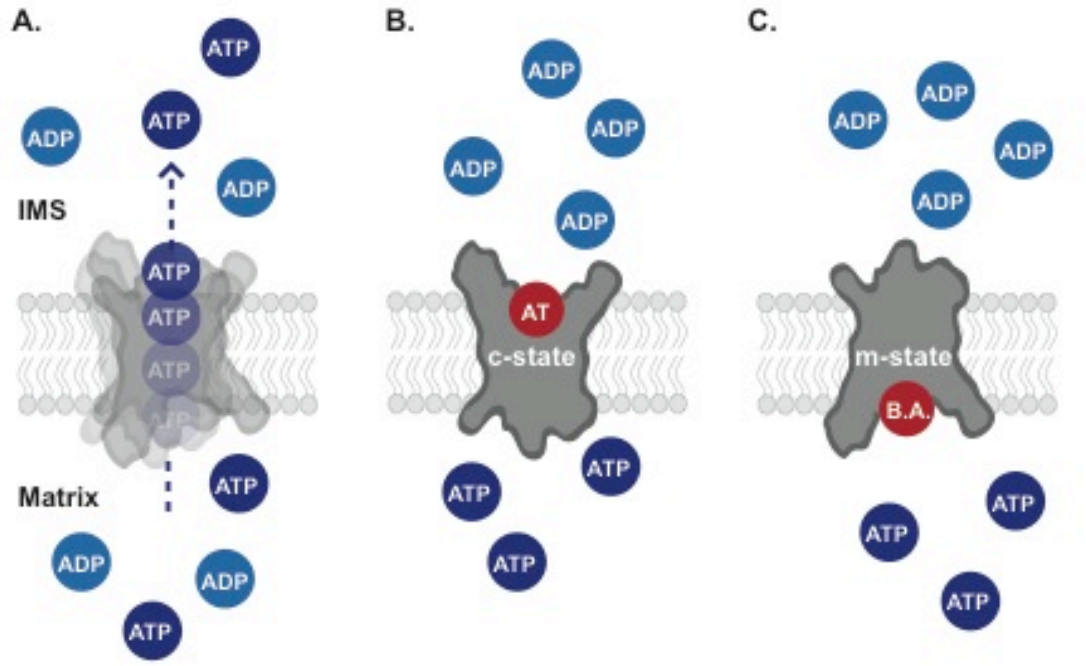

Figure 27. Inhibitors of AAC lock the translocase in specific conformational states. (A) AAC catalyzes the transfer of adenine nucleotides (ADP/ATP) across the inner mitochondrial membrane. **(B)** The inhibitor atractyloside (AT) binds to the intermembrane space side of AAC, locking the enzyme in a cytosolic state (c-state), in which the translocase is in a conformation that is open to the cytosol/intermembrane space (IMS). **(C)** Bongkrekic acid (B.A.) binds to the matrix side of AAC, locking the enzyme in a matrix state (m-state), where the conformation of AAC is open to the matrix.

solved and structural and functional analyses support a domain-based alternating-access transport mechanism that underlies mitochondrial AAC function (Pebay-Peyroula et al., 2003; Ruprecht et al., 2014). In short, AAC contains three domains that surround a central substrate-binding site. The rotation of these domains mediates the dynamic formation and disruption of interdomain salt bridge networks that regulate access to either side of the membrane, and allow equimolar nucleotide exchange between the cytosol and mitochondrial matrix (Ruprecht et al., 2014). The matrix salt bridge interactions are braced by highly conserved glutamine (Q) residues, that are located in a [K/R]-$(X)_3$-[Q] motif, and serve as charged, integral components of the salt bridge. Specifically, the Q residues function to stabilize an otherwise dynamic region of AAC by increasing the magnitude of the energy barrier, thereby preventing conversion to the matrix-open conformation in the absence of substrate binding (Ruprecht et al., 2014). A similar salt bridge network, found in the IMS region of AAC, stabilizes the IMS-closed conformation state during the dynamic ADP/ATP translocation cycle. The formation and disruption of IMS-localized salt bridge networks result in dynamic conformational changes within the IMS-exposed, H2-L-H3 (helix2-loop-helix3) region of AAC, and result in the subsequent opening and closing of the channel (FIGURE 28). While the importance of salt bridge networks and Q braces (in the matrix) for supporting AAC in its "closed" conformational states has been shown, it is unclear how the respective "open" states of AAC are stabilized.

Yeast Aac2 has been shown to physically interact with the translocase of the inner mitochondrial membrane complex (TIM23), and the complex III-complex IV

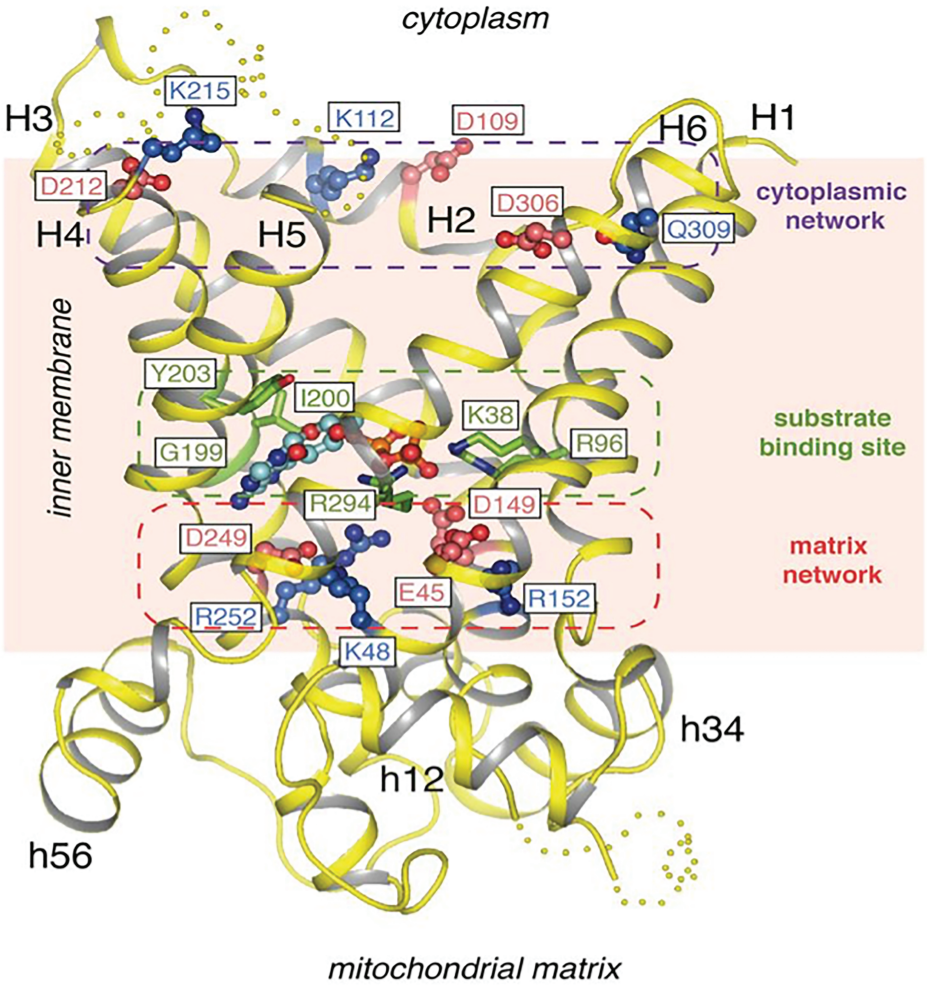

Figure 28. The yeast ADP/ATP carrier, Aac2. The Aac2 protein contains 6 transmembrane helices (H1-H6) that comprise 3 domains. The rotation of the Aac2 domains mediates the dynamic formation and disruprion of cytoplasmic salt-bridge networks that support equimolar nucleotide transport across the inner mitochondrial membrane, and matrix-localized salt-bridges are stabilized by highly conserved Q residues. Image from Ruprecht et al,. 2014.

supercomplex and associated TIM23 (Dienhart and Stuart, 2008). Additionally, it was shown that the loss of Aac2 results in changes in the supercomplex assembly state, with a shift from the III_2-IV_2 form to the III_2-IV form. These changes were hypothesized to be due to limiting levels of complex IV, which were also reduced in the absence of Aac2. These results suggest that AAC does not exist in isolation in the mitochondrial inner membrane, but is rather physically and, possibly functionally, associated with other respiratory proteins and complexes to facilitate the transport of ADP and ATP. The current model of AAC function is heavily dependent upon dynamic structural flexibility. Therefore, molecular interactions between AAC and nearby proteins might influence the activity of the carrier. Furthermore, it can be inferred that any such changes could have consequences for mitochondrial energy production and cellular metabolic activity.

Rcf1 has previously been shown to physically associate with respiratory supercomplexes, including the complex III- complex IV – AAC supercomplex, (III-IV-AAC). 2-dimension BN/SDS-PAGE analysis of mitochondrial respiratory supercomplexes showed that AAC and Rcf1 are components of III-IV respiratory supercomplexes (Dienhart and Stuart, 2008; Strogolova et al., 2012). Affinity purification of III-IV-AAC using histidine (His)-tagged complex III and AAC derivatives, cytochrome c_{1His} or $_{His}$AAC, both resulted in the co-purification of Rcf1 (Strogolova et al., 2012). In an independent study, the two-step purification of Rcf1-His_6 /HA_3 resulted in the co-purification of AAC (Chen et al., 2012). Additionally, Rcf1 and AAC proteins have been shown to exist in close physical proximity within the inner mitochondrial membrane. MBS can facilitate the conjugation of wild type and his-tagged derivatives of Rcf1 and AAC (Strogolova et al., 2012). This partnership was enhanced in [rho^0]

(mtDNA-deficient) mitochondria where the co-assembly of Rcf1 with the complex III-complex IV supercomplex is abolished, as neither complex III or complex IV assemble in the absence of mtDNA. It was subsequently demonstrated that the ability of Rcf1 to form the 45 kDa crosslinking adduct was lost in a mutant where the most prominent isoform of AAC (Aac2) had been genetically deleted (*Δaac2* mutant). The Rcf1-AAC interaction was restored when $_{His}$Aac2 was expressed in the *Δaac2* mutant, and again enhanced in a [*rho*^{0}] *Δaac2* mutant expressing $_{His}$Aac2. Likewise, in a *Δaac1 Δaac2* double mutant Rcf1 lost the ability to form the 45 kDa adduct and the expression of Aac1$_{His}$ or Aac3$_{His}$ under the control of a galactose-inducible promoter (GAL10) restored the adduct and changed the size; to a slightly larger form when Aac1$_{His}$ was expressed and to a slightly smaller form when Aac3$_{His}$ was expressed (Strogolova et al., 2012). It was therefore concluded that the 45 kDa Rcf1 –containing adduct was Rcf1 cross-linked to AAC. However, the formation of the purported Rcf1$_{His}$-AAC cross-linked adducts could be detected by western blotting and immunedecoration using either Rcf1 or His antisera, but was not detected by immunedecoration using an AAC-specific antibody (Stuart lab unpublished results). Thus, the validity of the Rcf1-AAC crosslink, i.e. that AAC is truly a partner to Rcf1, requires further characterization, ideally by an alternative methodology. This independent validation of the Rcf1-AAC adduct was an initial goal of this study.

In the previous chapter of this dissertation, results were presented that support a hypothesized role of Rcf1/Hig1 in regulating complex IV activity in response to metabolic changes. However, the relationship between Rcf1 and AAC is much less understood, and a number of fundamental aspects of the Rcf1-AAC interaction remain uncharacterized. Therefore, the 2 main aims of this chapter were to (1) characterize Hig1

family conserved regions of the Rcf1 protein in their ability affect the interaction between Rcf1 and AAC, and (2) determine whether dynamic conformational changes and/or structural characteristics of the AAC protein influence the relationship between AAC and Rcf1.

In characterizing the Rcf1-AAC interaction using a C-terminal deletion mutant of Rcf1, it was shown that the Hig1 domain of Rcf1 and not the fungal-specific C-terminal domain is important for the ability of Rcf1 to associate with AAC proteins (Strogolova et al., 2012). Furthermore, in mitochondria harboring an Aac2 derivative, *aac2*^{A113C} (where A113, located in the IMS-localized H2-L-H3 domain of Aac2, has been exchanged for Cys), disulfide bond formation between Rcf1 and *aac2*^{A113C} could be promoted by 5,5-dithio-bis-(2-nitrobenzoic acid (DTNB, Ellman's reagent). Rcf1 contains just 2 Cys residues, C28 and C38, that are located in the IMS and TM1 region of the Rcf1 protein (Figure 4), and wild type Aac2 contains 4 Cys residues that are located in matrix or TM regions of the AAC protein. Therefore, the DNTB-facilitated disulfide bond formation between the *aac2*^{A113C} derivative and Rcf1 demonstrates that the N-terminal IMS region of Rcf1 exists in close physical proximity to the H2-L-H3 domain of the AAC protein. Mitochondrial Rcf1/Hig1 proteins contain a [P^{32}]-X-[V^{34}]-[P^{35}]-X-[G^{37}] (S.c. Rcf1 numbering) motif located at the N-terminal tail region near the IMS/TM1 interface that is conserved specifically among mitochondrial Hig1 proteins, i.e. the [P]-X-[V]-[P]-X-[G] motif is not a feature of prokaryotic Hig1 proteins, where AAC is also absent. In the Rcf1 protein, the [P]-X-[V]-[P]-X-[G] motif is flanked by 2 cysteines, C28 (Rcf1-specific) and C38 (conserved among mammalian Hig1-type2), and at least one of these cysteines can be cross-linked to AAC proteins. A recently published NMR structure of the human

Hig1-type1 protein indicates that the N-terminal tail of Hig1 proteins contain a short amphiphilic helix that is oriented parallel to the surface of the membrane (Lindert et al., 2014). The analogous region in the yeast Rcf1 protein would be comprised of amino acid residues F20-Y26, encompassing a region that is in close proximity to the cysteines of Rcf1 that have been shown to interact with the H2-L-H3 domain of AAC. Thus, the proline and glycine residues within the [P]-X-[V]-[P]-X-[G] motif potentially provide a level of conformational flexibility that might affect the association of the putative N-tail amphiphilic helix of Rcf1 with the H2-L-H3 domain of AAC. Therefore, the potential influence of the Rcf1/Hig1 [P]-X-[V]-[P]-X-[G] motif and flanking cysteine residues on the interaction between Rcf1 and AAC was explored here.

The Hig1/Rcf1 conserved QRRQ motif, by its putative location within the matrix loop of the Rcf1 protein, represents a potential point of interaction between Rcf1 and AAC. Moreover, Rcf1 Q61 and Q71 each form Q/R pairs, seen in a helical wheel plot of the Rcf1 amino acids that comprise the matrix loop of the Rcf1 protein (FIGURE 16A), that are separated by 3 residues i.e. $[Q^{61}]$-$(X)_3$-$[R^{65}]$ and $[R^{67}]$-$(X)_3$-$[Q^{71}]$, and closely resemble the salt-bridge bracing Q residues of the AAC [K/R]-$(X)_3$-[Q] motif. However, the ability of the Rcf1 QRRQ motif to directly interact with AAC, or possibly influence the interaction between Rcf1 and AAC, has not been characterized. Of particular interest is the possible role of conserved Q residues (Q61 and/or Q71) of the Hig1/Rcf1 QRRQ motif in supporting the m-state conformation of AAC by bracing the matrix-localized residues of AAC that participate in salt bridge formation. The molecular environment of the Rcf1 QRRQ motif and its relationship to the functional state of the AAC protein will be explored in this chapter.

The H2-L-H3 domain forms a structurally dynamic gating region within AAC, and the conformational flexibility of this region is critical for transport activity of the carrier. Additionally, the H2-L-H3 region has been shown to affect the transport of H^+ across the inner mitochondrial membrane by AAC, i.e. the H2-L-H3 domain of AAC could significantly contribute to H^+ leak across the membrane, thereby demonstrating that this domain can influence the mitochondrial membrane potential, and thus, membrane potential dependent mitochondrial functions. In agreement with its importance for AAC function, the H2-L-H3 region of AAC is the site of a number of pathogenic mutations that have been proposed to dominantly uncouple respiration. Therefore, the interaction between Rcf1 and a functionally critical, pathogenically relevant region of AAC could potentially influence the activity of the carrier under different mitochondrial energetic states. In support of this prediction, preliminary results from the Stuart lab suggest that the interaction between Rcf1 and AAC may be dependent upon the conformational state of the carrier. When disulfide bond formation was tested in the presence of specific inhibitors of AAC, it was found that AT (which locks AAC into c-state with the substrate binding site accessible to the IMS), but not BA (locks AAC into m-state with the substrate binding site accessible to the matrix), adversely affected disulfide bond formation between the *aac2*^{A113C} derivative and Rcf1. It is unknown whether the conformational state -dependent interaction between Rcf1 and the *aac2*^{A113C} derivative exists between Rcf1 and wild-type AAC, i.e. via MBS chemical cross-linking. Therefore, specific inhibitors of AAC were utilized to determine whether the conformation of AAC influences formation of the Rcf1-AAC cross-link adduct. Determining whether the formation of the Rcf1-AAC cross-linked adduct occurs preferentially in one AAC

conformational state over the other, i.e. the c-state (substrate binding site accessible to the IMS) or m-state (substrate binding site accessible to the mitochondrial matrix), could shed light on the functional significance of the Rcf1-AAC interaction, and may provide insight into whether Rcf1 could stabilize AAC in a particular state (matrix open or IMS open).

The proposed Rcf1-AAC interaction can occur independent of assembled complex IV (or complex III), seen in the enhanced level of Rcf1-AAC crosslinking in the absence of mitochondrial DNA in *rho*^{0} mitochondria (Strogolova et al., 2012). The observed cross-linking of Rcf1 to AAC in *rho*^{0} mitochondria indicates that these two proteins may interact independently of their association with the III-IV supercomplex. Given the interactions between Rcf1 and both complex IV and AAC, Rcf1 might be centrally positioned to function in the communication between AAC and IV/III-IV, thereby providing a level of regulation to coordinate the activity of these two critical OXPHOS enzymes in response to the metabolic need of the cell. However, it is not known whether the dynamic conformational changes in AAC that are associated with an increase in its activity level, i.e. during state 3 respiration where the presence of exogenously supplied ADP in the presence of substrate (NADH) increases the level of adenine nucleotide transport, affects the ability of Rcf1 to be cross-linked to AAC. It was therefore addressed in this study whether the Rcf1-AAC interaction could be modulated through alterations in the bioenergetic status of the mitochondria.

AAC contains 3 bound cardiolipin molecules that have been shown to be required for transport in reconstituted vesicles (Klingenberg, 2009). It is unknown however, whether the presence of cardiolipin, a proposed structural and functional component of

AAC, influences the interaction between Rcf1 and AAC. It was therefore addressed in this chapter whether the absence of cardiolipin affects the ability of Rcf1 and AAC to be cross-linked.

In wild-type mitochondria, AAC has been reported to form a digitonin-stable dimer that migrates to approximately 80 kDa on a blue native gel (Ryan et al., 1999). In contrast, in mitochondria that are deficient in cardiolipin synthesis (i.e. the *Δcrd1* mutant), AAC BN-PAGE mobility is altered, and migrates to a position below 80 kDa (Jiang et al., 2000). The authors of the latter study attribute the AAC mobility shift in the Δ*crd1* mutant to the absence of bound cardiolipin, and propose that AAC in the *Δcrd1* mutant exists in a sub-optimally folded conformation, thereby resulting in altered BN-PAGE mobility. It is not known whether the presence of Rcf1 (or Rcf2) affects the native gel mobility of AAC and this will be explored in this chapter.

This chapter details the characterization of the Rcf1-AAC interaction. The primary focus of the experiments herein was to answer specific questions underlying the basis of the Rcf1 -AAC interaction. The aim of these experiments was to analyze the functional relationship between Rcf1 and AAC by characterizing the role of conserved regions of the Rcf1 protein in the Rcf1-AAC interaction, and also by examining whether conformational dynamics or structural characteristics of AAC influence the molecular environment of Rcf1 and AAC.

4.2 Chapter 4 Results

4.2.1 Independent Verification of the $Rcf1_{His}$-AAC MBS Cross-link Via LC-MS/MS

The relationship between Rcf1 and AAC is not fully understood; therefore one of the aims of this dissertation was to characterize the molecular interaction and potential functional relationship between Rcf1 and AAC.

The close proximity between Rcf1 and AAC was initially discovered through chemical cross-linking analysis, where MBS appeared to facilitate the conjugation of wild type and his-tagged derivatives of Rcf1 and all three isoforms of AAC (Strogolova et al., 2012). While the 45 kDa adduct could be detected using Rcf1 or His antisera, it was not detected when the AAC antibody was used. Thus, theoretically it remained a possibility that the 45 kDa adduct does not actually represent Rcf1 cross-linked to AAC, but rather, that the ability of Rcf1 to be cross-linked to a different (unidentified) protein and form the 45 kDa adduct, is contingent upon the presence of AAC. An initial goal therefore was to verify that the MBS adduct truly represented a partnership between Rcf1 and AAC.

To determine the composition of the MBS-dependent 45 kDa adduct containing Rcf1, crosslinking was performed in mitochondria isolated from the *Δrcf1,Δrcf2* double mutant harboring His-tagged Rcf1 in parallel with a *Δrcf1,Δrcf2* double mutant control. Following cross-linking, mitochondria were solubilized using buffer containing Triton X-100 and $Rcf1_{His}$ –containing adducts were purified by Ni-NTA affinity chromatography, and separated on a gel by SDS-PAGE. The purified 45 kDa adduct that contained $Rcf1_{His}$

was visualized by silver staining, excised and subjected to LC-MS/MS by our collaborator Dr. Kate Noon at the Medical College of Wisconsin Mass Spectrometry Facility. False positives were eliminated from the resulting data set by comparing the LC-MS/MS spectra of the *Δrcf1,Δrcf2* + $Rcf1_{His}$ to that of the *Δrcf1,Δrcf2* double mutant. The two most abundant proteins within the excised 45 kDa crosslinking adduct were Aac2 and Rcf1.

It can therefore be concluded that Rcf1 is cross-linked to Aac2 via MBS, independently verifying that Rcf1 and Aac2 exist in close proximity within the inner mitochondrial membrane.

4.2.2 Characterization of N-terminal amino acid residues of Rcf1 and their influence on the molecular environment of Rcf1 and AAC

The highly conserved Rcf1/Hig1 PXVPXG motif represents a potential point of interaction between Rcf1 and AAC. At least one of two cysteine residues (C28 and C38) that flank this region can be crosslinked to AAC, and the proline residues (and possibly the glycine) that comprise the PXVPXG motif may be a conformational feature that would allow a dynamic interaction between Rcf1 and AAC that may be dependent upon the bioenergetic state of the mitochondria.

Mutational analysis of the PXVPXG motif of Rcf1 was performed in part, through a collaboration with students in the upper level Experimental Molecular Biology course at Marquette University, taught by Dr. Ben Kemp. Students created and analyzed Rcf1 PXVPXG mutants, where conserved residues of the PXVPXG motif were individually mutated to alanine. One student, Hanting Tsai, subsequently joined the Stuart lab and continued the project under the joint supervision of Dr. Rosemary Stuart

and myself. Thus, the growth analysis and MBS cross-linking results of the *rcf1*$_{His}^{P32A}$ and *rcf1*$_{His}^{P35A}$ mutant derivatives represent experiments completed by Hanting Tsai.

To determine whether the conserved prolines P32 and P35 of the PXVPXG motif of Rcf1 support the Rcf1-AAC interaction, MBS crosslinking was performed in isolated Δ*rcf1*;Δ*rcf2* mitochondria harboring *rcf1*$_{His}^{P32A}$ or *rcf1*$_{His}^{P35A}$ mutant derivatives, and analyzed by SDS-PAGE and immunedecoration with Rcf1 antisera (FIGURE 29A). Both the *rcf1*$_{His}^{P32A}$ and *rcf1*$_{His}^{P35A}$ derivatives maintained the ability to be cross-linked to AAC as evidenced by the presence of the 45 kDa Rcf1 adduct which was detected in the mutant mitochondria at a similar level to that in the wild type Rcf1$_{His}$ control. Thus, it was concluded that P32 and P35 of the conserved Rcf1 PXVPXG motif, are not required for the interaction between Rcf1 and AAC

Rcf1 cysteines C28 and C38 flank the PXVPXG motif and have been shown to participate in DTNB-facilitated disulfide bond formation between Rcf1 and the *aac2*^{A113C} derivative. As the only cysteine residues within the Rcf1 polypeptide, C28 and C38 represent the only residues of Rcf1 that could participate in the observed SH-SH disulfide bond with AAC. It was therefore concluded that Rcf1 C28 and C38 and thus, the N-tail of the Rcf1 protein, is in close proximity to the functionally relevant H2-L-H3 domain of AAC. Here, the importance of the Rcf1 N-tail cysteines in supporting the Rcf1-AAC interaction was further analyzed.

Rcf1 C28 and C38 were simultaneously mutated to alanine, and the resulting *rcf1*$_{His}^{C28A\ C38A}$ mutant derivative was expressed in Δ*rcf1*;Δ*rcf2* mitochondria. First, it was tested whether Rcf1 C28 and C38 were required for the cross-linking of Rcf1 and AAC through the heterobifunctional (SH-NH_3) cross-linking reagent MBS, i.e. whether C28

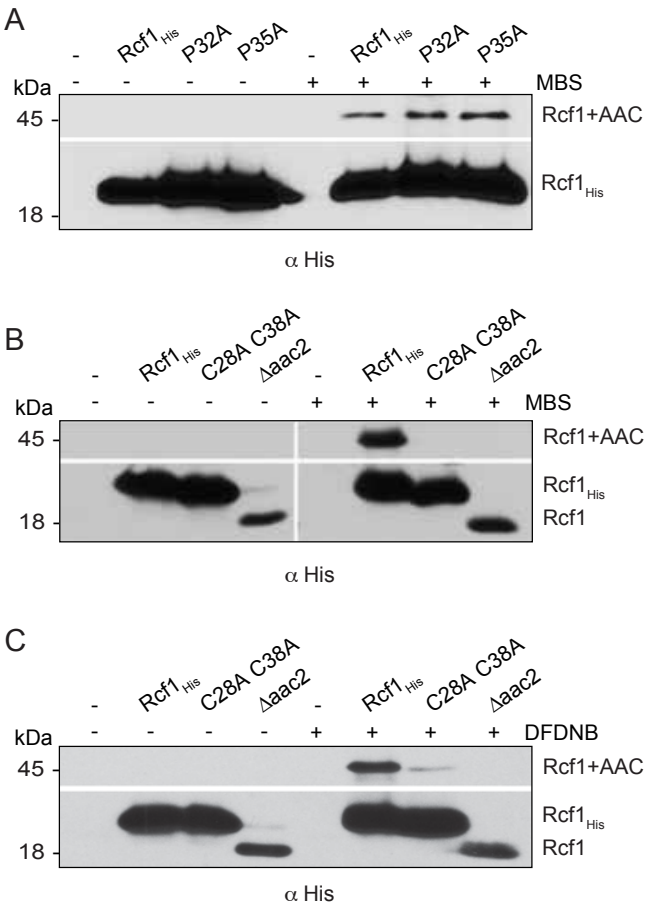

Figure 29. Rcf1 cysteine residues influence the molecular environment of Rcf1 and AAC. (A) Chemical cross-linking (MBS) was performed on mitochondria isolated from the Δ*rcf1*;Δ*rcf2* control (-) and Δ*rcf1*;Δ*rcf2* strains harboring the Rcf1$_{His}$, *rcf1*$_{His}^{P32A}$ (P32A), or *rcf1*$_{His}^{P35A}$ (P35A) derivatives, as indicated. Following SDS-PAGE, and Western blotting, immunedecoration with the His-tag epitope (α His12) was performed. The positions of the Rcf1-AAC adduct, and monomeric Rcf1 are indicated. **(B)** Chemical cross-linking (MBS) was performed on mitochondria isolated from the Δ*rcf1*;Δ*rcf2* (-) and Δ*aac2* controls and the Δ*rcf1*;Δ*rcf2* strain harboring the Rcf1$_{His}$ or *rcf1*$_{His}^{C28A\ C38A}$ (C28A C38A) derivatives, as indicated. SDS-PAGE, Western blotting and immunedecoration was performed as in (A). **(C)** Chemical cross-linking (DFDNB) was performed as in (B) in the indicated strains, and analyzed as in (B).

and/or C38 represent the sole sulfhydryl components of the MBS-facilitated Rcf1-AAC cross-link. MBS crosslinking was performed in isolated Δ*rcf1*;Δ*rcf2* mitochondria harboring the *rcf1*$_{His}^{C28A,C38A}$ mutant derivative, and analyzed by SDS-PAGE and immunedecoration with Rcf1 antisera (FIGURE 29B). A 45 kDa Rcf1 adduct, i.e. Rcf1 cross-linked to AAC, was observed in the wild type control, but was not detected in *rcf1*$_{His}^{C28A,C38A}$ mitochondria. Therefore it was concluded that Rcf1 C28 and C38 are required for the crosslinking of Rcf1 to AAC by the SH-NH_3 cross-linking reagent MBS, and thus, that C28 and/or C38 represent the sulfhydryl component of the MBS-facilitated Rcf1-AAC cross-link.

Next, to determine whether Rcf1 C28 and C38 *influence* the molecular environment of Rcf1 and AAC, crosslinking was performed using the amine-amine homobifunctional crosslinking reagent, 1,5-difluro-2-4 dinitrobenzene (DFDNB). DFDNB facilitates the cross-linking of two proteins through amine groups on either protein partner, and thus does not rely on the direct participation of cysteines to cross-link two proteins. Therefore, the use of DFDNB as a cross-linking reagent provides a means to determine whether Rcf1 C28 and C38 *influence* the amine-amine crosslinking between Rcf1 and AAC, and thus the molecular environment of Rcf1 and AAC. Crosslinking was performed using DFDNB and analyzed by SDS-PAGE and immunedecoration with Rcf1 antisera (FIGURE 29C). A DFDNB-specific 45 kDa adduct, i.e. Rcf1 cross-linked to AAC, was observed in wild type Rcf1$_{His}$ mitochondria and was absent in mitochondria deficient in Aac2 (Δ*aac2*). In contrast to wild type Rcf1$_{His}$, a strong reduction of the 45 kDa Rcf1-AAC adduct was observed in *rcf1*$_{His}^{C28A\ C38A}$ mitochondria.

These results demonstrate that Rcf1 C28 and/or C38 directly participate in an MBS facilitated SH-NH_3 cross-link between Rcf1 and AAC, and additionally *influence* the ability of Rcf1 to be cross-linked to AAC via DFDNB facilitated NH_3-NH_3 conjugation. Thus, it can be concluded that C28 and C38, located in the N-tail of Rcf1 and predicted to reside adjacent to the IMS-membrane interface near the functionally relevant H2-L-H3 domain of AAC, impact the molecular environment of Rcf1 and AAC.

4.2.3 The integrity of the Rcf1 QRRQ motif alters the molecular interaction between Rcf1 and AAC

To probe the consequence of mutation of the QRRQ motif on the molecular environment of Rcf1 and AAC, an MBS chemical cross-linking approach was adopted. Cross-linking was performed in isolated mitochondria harboring the Rcf1 derivatives and subsequently analyzed by SDS-PAGE and immunedecoration with Rcf1 antisera and the ability of Rcf1 derivatives to form the AAC 45 kDa adduct was analyzed (FIGURE 30A). Formation of the 45 kDa Rcf1-AAC adduct was observed in *rcf1*$_{His}^{Q61A,Q71A}$ mitochondria to a similar level as the 45 kDa Rcf1-AAC adduct in wild type Rcf1$_{His}$ mitochondria, indicating the *rcf1*$_{His}^{Q61A,Q71A}$ mutant derivative maintained the ability to be cross-linked to AAC. On the other hand, cross-linking between *rcf1*$_{His}^{R67A}$ and AAC was markedly reduced, despite normal levels of Rcf1 and AAC in these mitochondria (FIGURE 9A). This observation suggests that the mutation of R67 to alanine interfered with Rcf1's association with the AAC protein.

Given that the mutation of Rcf1 R67 to alanine affected the molecular environment of Rcf1 and AAC, charge-altering Rcf1 R67 mutant derivatives (R67Q,

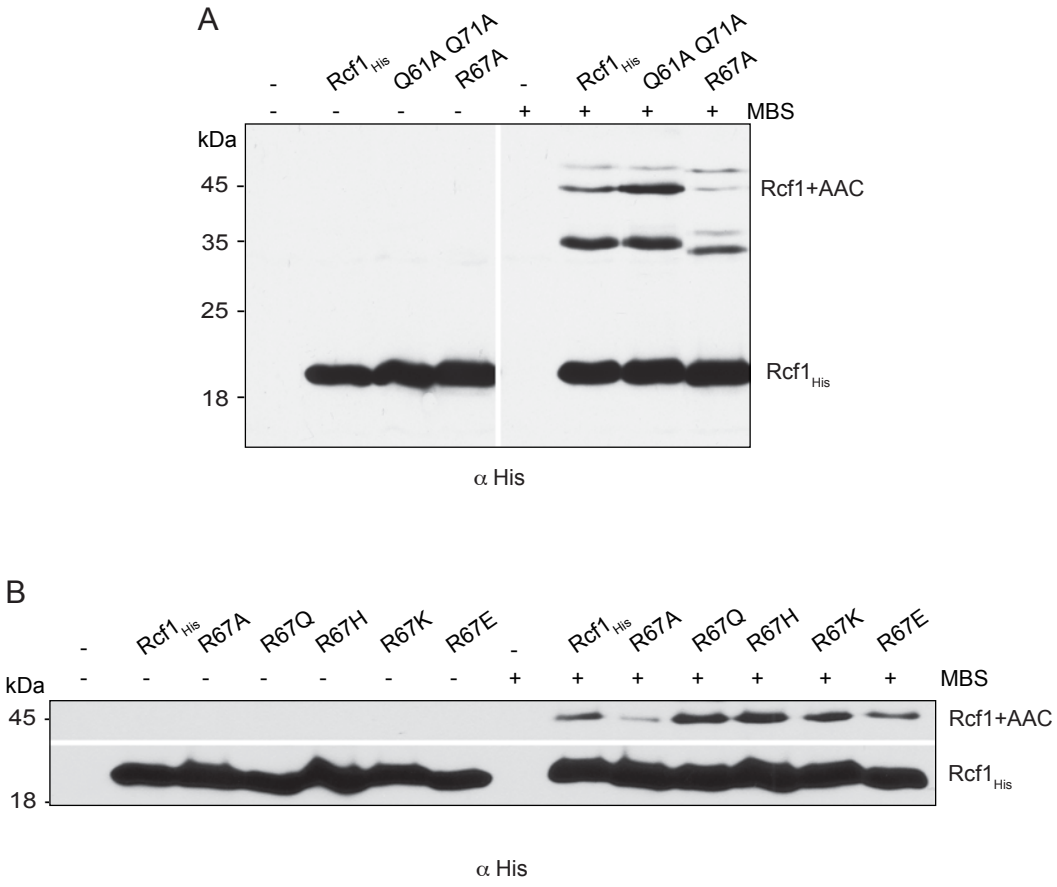

Figure 30. Rcf1 R67 influences the molecular environment of Rcf1 and AAC. (A) Chemical cross-linking (MBS) was performed on mitochondria isolated from the Δ*rcf1*;Δ*rcf2* control (-) and Δ*rcf1*;Δ*rcf2* strains harboring the $Rcf1_{His}$, $rcf1_{His}^{Q61A,Q71A}$ (Q61A Q71A), or $rcf1_{His}^{R67A}$ (R67A) derivatives, as indicated. Following SDS-PAGE, and Western blotting, immunedecoration with the His-tag epitope (α His12) was performed. The positions of the Rcf1-AAC adduct, and monomeric Rcf1 are indicated. **(B)** Chemical cross-linking (MBS) was performed on mitochondria isolated from the Δ*rcf1*;Δ*rcf2* (-) control and the Δ*rcf1*;Δ*rcf2* strain harboring the $Rcf1_{His}$, $rcf1_{His}^{R67A}$ (R67A),$rcf1_{His}^{R67Q}$ (R67Q),$rcf1_{His}^{R67H}$ (R67H),$rcf1_{His}^{R67K}$ (R67K),$rcf1_{His}^{R67E}$ (R67E) derivatives, as indicated. SDS-PAGE, Western blotting and immunedecoration was performed as in (A).

R67H, R67K, R67E) were next examined in their ability to associate with AAC. Charge-altering Rcf1 R67 mutant derivatives were examined in their ability to form the 45 kDa Rcf1-AAC adduct by MBS cross-linking, and analyzed by SDS-PAGE and immunedecoration with Rcf1 (anti-His) antiserum (FIGURE 30B). The 45 kDa Rcf1-AAC adduct was observed in wild type $Rcf1_{His}$ mitochondria and in each of the charge-altering Rcf1 R67 mutant mitochondria, in contrast to R67A, where a reduction in crosslinking to AAC was consistently observed (FIGURE 30B).

These results suggest that Rcf1 R67, a signature QRRQ motif residue that is highly conserved among Hig1 proteins, influences the association between Rcf1 and AAC, and in a manner that appears to be independent of the protonation state of R67.

4.2.4 The Bio-Energetic State of the Mitochondria Influences the Ability of Rcf1 and AAC Proteins to be Cross-linked

In isolated mitochondria, in the absence of substrate for the electron transport chain and exogenously added nucleotides (ADP/ATP), it is presumed that the structure of AAC is static, and under these conditions Rcf1 can be cross-linked to AAC by MBS. However, it is not known whether a conformationally dynamic AAC, as predicted to exist under different mitochondrial bioenergetic states, affects the interaction between Rcf1 and AAC, as judged by its ability to form an MBS facilitated adduct with Rcf1.

To determine whether the mitochondrial bioenergetic state influences the ability of Rcf1 to be chemically cross-linked to AAC, cross-linking was performed in Δ*rcf1;*Δ*rcf2* mitochondria harboring $Rcf1_{His}$ during state 4 and state 3 respiration. Isolated mitochondria were incubated in the presence of NADH alone (state 4), or with NADH and ADP (state 3) and crosslinking was subsequently performed with MBS.

Mitochondria were re-isolated and analyzed by SDS-PAGE and western blotting using Rcf1 antisera (FIGURE 31). Formation of the Rcf1-AAC adduct was observed in state 4 respiration, and at a level that was similar to crosslinking in the absence of substrate. In contrast, crosslinking between Rcf1 and AAC was lost when state 3 respiration was induced. From these results it can be concluded that the bioenergetic state of the mitochondria affects the ability of Rcf1 to be cross-linked to AAC, whereby a higher bioenergetic state that confers AAC that is dynamic in conformation, results in the loss of interaction between Rcf1 and AAC. Furthermore, these results suggest that the Rcf1-AAC interaction captured by MBS cross-linking might be influenced by the conformation of AAC.

4.2.5 The ability of Rcf1 to be cross-linked to AAC is dependent upon the conformational state of AAC

Determining that the bioenergetic state of the mitochondria influences the ability of Rcf1 to be cross-linked to AAC was an important step towards characterizing a potential dynamic relationship between Rcf1 and AAC. However, it remained unclear whether a specific conformational state of AAC confers the ability to form the Rcf1-AAC cross-linked adduct.

To determine whether the ability of Rcf1 to be cross-linked to AAC is dependent upon the conformation of AAC, MBS cross-linking was performed in isolated wild type mitochondria during state 4 respiration in the presence of the specific inhibitors AT (which locks AAC in the cytosol open ‘c-state’) or B.A., (which locks AAC in the matrix open ‘m-state’)(FIGURE 27). Mitochondria were re-isolated and analyzed by SDS-PAGE and western blotting using Rcf1 antisera (FIGURE 32). When inhibitor was added

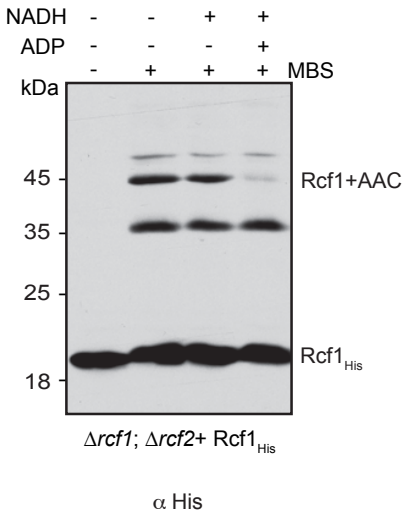

Figure 31. The bio-energetic state of the mitochondria influences the ability of Rcf1 AAC proteins to be cross-linked. Chemical cross-linking (MBS) was performed on mitochondria isolated from the Δ*rcf1*;Δ*rcf2* strain harboring the $Rcf1_{His}$ derivative. Prior to the addition of MBS, mitochondria were incubated in NADH (state 4), NADH followed by ADP (state 3) , or not, as indicated. Following SDS-PAGE, and Western blotting, immunedecoration with the His-tag epitope (α His) was performed. The positions of the Rcf1-AAC adduct, and monomeric Rcf1 are indicated.

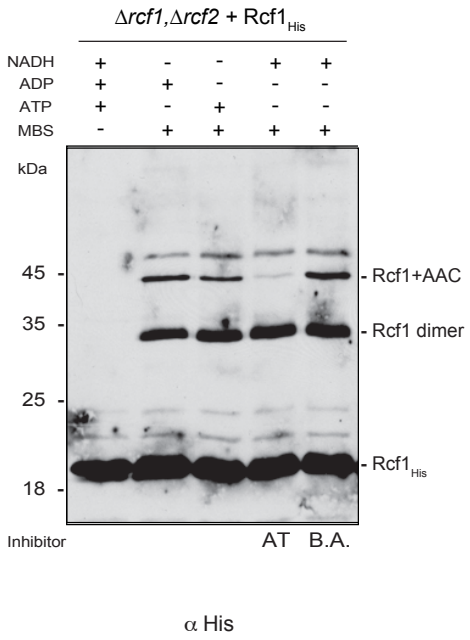

Figure 32. The ability to cross-link Rcf1 and AAC is dependent upon the structural conformation of the AAC protein. Chemical cross-linking (MBS) was performed on mitochondria isolated from the Δ*rcf1*;Δ*rcf2* strain harboring the $Rcf1_{His}$ derivative. Prior to the addition of MBS, mitochondria were incubated in ADP, ATP, or NADH and atractyloside (AT), or bongkrekic acid (B.A.) as indicated. Following SDS-PAGE, and Western blotting, immune-decoration with the His-tag epitope (α His) was performed. The positions of the Rcf1-AAC adduct, and monomeric Rcf1 are indicated.

to mitochondria in state 4 respiration, formation of the 45 kDa Rcf1-AAC adduct was observed when AAC was locked in the m-state i.e. in the presence of BA, but was abolished when AAC was locked in the c-state by AT. In contrast, the ability of Rcf1 to form a 40 kDa Rcf1-Rcf1 homodimer was unaffected by the conformation of AAC, as evidenced by detection of equal levels of the Rcf1-Rcf1 homodimer in the presence and absence of AAC inhibitors AT and B.A., and supports that the altered molecular environment of Rcf1 in the presence of AT is specific for the Rcf1-AAC interaction.

These results suggest that the ability of Rcf1 to be cross-linked to AAC via MBS is dependent upon the structural conformation of AAC, whereby AAC with its channel open to the mitochondrial matrix can be cross-linked to Rcf1, and AAC with its channel open to the IMS (cytosol) cannot be cross-linked to Rcf1. The IMS exposed H2-L-H3 region of AAC has been shown to undergo significant conformational changes in response to the dynamic remodeling of the transport-regulating cytosolic salt-bridge network of AAC during the ADP/ATP transport cycle (Ruprecht et al., 2014). The H2-L-H3 region of AAC has been shown to interact with C28 and/or C38 of the N-tail of Rcf1, a region of Hig1 proteins that has been modeled to be oriented parallel to the surface of the membrane (Lindert et al., 2014). Thus, the conformation-dependent ability to cross-link Rcf1 and AAC via MBS, might reflect a functional role for Rcf1 in its interaction with AAC.

4.2.6 The molecular environment of Rcf1 and AAC is altered in the absence of cardiolipin

Cardiolipin has been shown to bind tightly to AAC where it is important, but not essential for AAC function (Beyer and Klingenberg, 1985; Brandolin et al., 1980; Jiang

et al., 1997; Kramer and Klingenberg, 1980; Ruprecht et al., 2014). A possible role for the Rcf1 protein in the insertion/remodeling of cardiolipin associated with complex IV proteins was supported by results from the characterization of the Rcf1 QRRQ motif, and in particular, the Rcf1 R67A mutant (reported in Chapter 3 of this dissertation). Consistent with the important role of R67 in the molecular interactions of Rcf1, as previously shown between Rcf1 and Cox3/complex IV, R67 was found to influence the association of Rcf1 with AAC (FIGURE 30A,B). Therefore, the relationship between Rcf1 and AAC was analyzed in the absence of cardiolipin.

To determine whether the association between Rcf1 and AAC is affected by the absence of cardiolipin, MBS cross-linking of the Rcf1 protein was performed in mitochondria isolated from mutants displaying defective cardiolipin biosynthesis, such as the cardiolipin synthase mutant, Δ*crd1*, and the Tam41 null mutant, Δ*tam41* (FIGURE 33). Tam41 is a CDP-diacylglycerol synthase required for cardiolipin biosynthesis in mitochondria and thus like Δ*crd1*, Δ*tam41* mitochondria are deficient in cardiolipin (Tamura et al., 2013). When analyzed in parallel to wild type mitochondria, a complete loss of Rcf1-AAC formation was observed in Δ*tam41* mitochondria, and a partial loss of Rcf1-AAC formation was observed in Δ*crd1* mitochondria. The level of Rcf1-AAC reduction in Δ*crd1* and Δ*tam41* mitochondria was similar to that observed in Rcf1 R67A mutant mitochondria, which was analyzed in parallel (not shown).

The altered environment of Rcf1 with respect to AAC proteins in cardiolipin-deficient mitochondria mirrors that of the $rcf1_{\mathrm{His}}^{\mathrm{R67A}}$ protein, and further supports a role of Rcf1 in the lipid modification of partner proteins, including AAC.

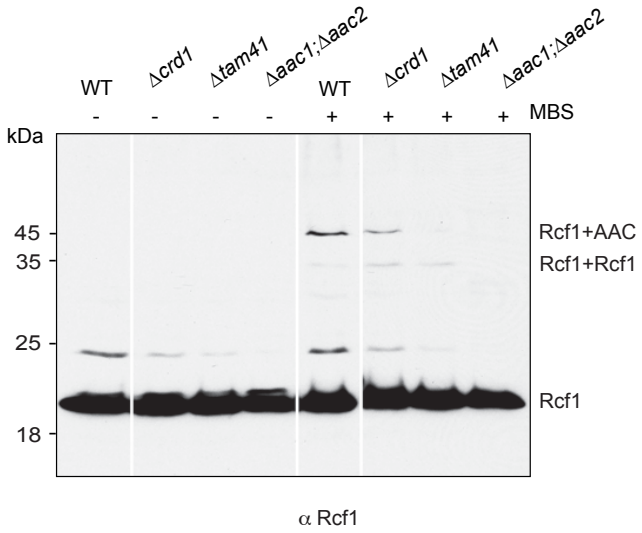

Figure 33. The molecular environment of Rcf1 and AAC is altered in the absence of cardiolipin. Chemical cross-linking (MBS) was performed on mitochondria isolated from the wild type (WT) and Δ*aac1*;Δ*aac2* controls and the Δ*crd1* and Δ*tam41* mutant strains, as indicated. Following SDS-PAGE, and Western blotting, immunedecoration with Rcf1 antiserum (α Rcf1) was performed. The positions of the Rcf1-AAC adduct, the Rcf1-dimer and monomeric Rcf1 are indicated.

4.2.7 The native gel mobility of AAC is influenced by the presence of Rcf1 and Rcf2

The absence of cardiolipin synthase (*CRD1*) has been shown to result in the altered native gel migration of AAC, and the authors of this study speculate that the AAC mobility shift in Δ*crd1* mitochondria is the result of a conformational change in AAC that is attributed to the absence of bound cardiolipin (Jiang et al., 2000). Evidence has been presented in chapter 3 of this dissertation that supports a role of Rcf1/Hig1 proteins in modifying complex IV, possibly its lipid composition, in a manner that alters the structure of the enzyme.

To determine whether Rcf1 (and/or Rcf2) influence the native gel mobility of AAC similar to the reported gel mobility shift in Δ*crd1* mitochondria, mitochondria were subjected to BN-PAGE following solubilization in digitonin-containing buffer, and AAC was detected by western blot analysis using AAC antisera (FIGURE 34). The mobility of AAC in Rcf1, Rcf2 and double null Δ*rcf1*;Δ*rcf2* mitochondria was directly compared to AAC from wild-type mitochondria, which was calculated to migrate to approximately 80 kDa. Compared to AAC from wild type mitochondria, AAC from the Δ*crd1* mutant displayed an increased mobility, similar to the results published by Jiang and colleagues, while no AAC band was detected at or below 80 kDa in Δ*aac2* mitochondria (analyzed separately, not shown) (Jiang et al., 2000). In the Δ*rcf1,*Δ*rcf2* double mutant the detection of AAC was greatly diminished. The levels of AAC are not reduced in Δ*rcf1,*Δ*rcf2* or Δ*crd1* mitochondria compared to wild type, as evidenced by SDS-PAGE analysis (FIGURE 9A, Δ*crd1* not shown). However, the ability to detect AAC by the antibody following BN-PAGE in Δ*rcf1,*Δ*rcf2* and Δ*crd1* mitochondria is significantly

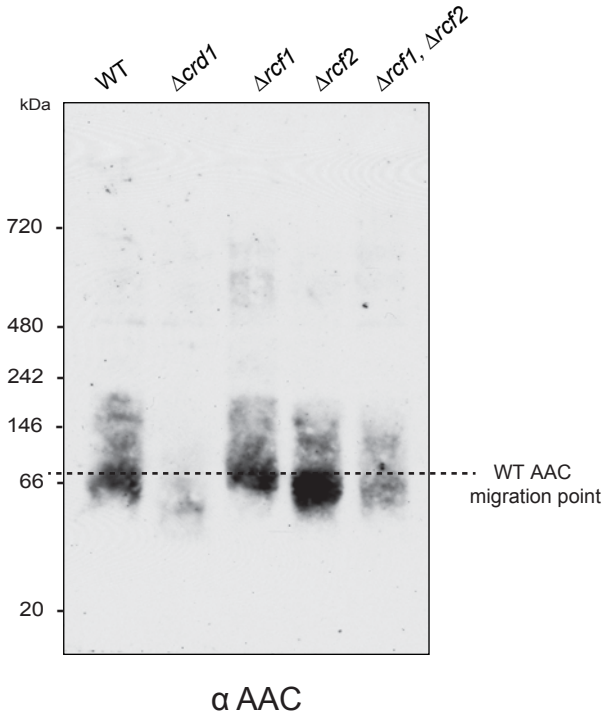

Figure 34. The native gel mobility of AAC is altered in the absence of Rcf1 and Rcf2. Mitochondria isolated from wild type (WT) and Δ*crd1* controls, and the Δ*rcf1*, Δ*rcf2, or* Δ*rcf1*;Δ*rcf2* mutant strains were solubilized in digitonin (1%) and subjected to BN-PAGE analysis, Western blotting and immunedecoration with antibodies against AAC (α Rcf1) was performed. The position of the native gel mobility of AAC from WT mitochondria is indicated.

reduced. Thus, it could be speculated that the altered detection of AAC in the absence of Rcf1 (and Rcf2) or cardiolipin may be due to an altered AAC native structure that reduces accessibility to the epitope by the AAC antibody. The very small amount of AAC that was detected in the Δ*rcf1;*Δ*rcf2* double mutant displayed an increase in mobility, however the extent of the mobility shift was not as large as observed in the Δ*crd1* mutant. AAC in the single Δ*rcf2* mutant displayed a mobility shift equal to that of the double mutant. In contrast, AAC from Δ*rcf1* mutant mitochondria did not display a significant shift in mobility compared to wild-type AAC.

From these results it can be concluded that the absence of Rcf2, and not Rcf1, results in a BN-PAGE mobility shift in AAC. However, the BN-PAGE mobility shift in the Δ*rcf1;*Δ*rcf2* double mutant and single Δ*rcf2* mutant, was not equal to the shift observed in the Δ*crd1* mitochondria, and therefore is not likely to represent a complete absence of cardiolipin assembled with AAC, as in the Δ*crd1* mitochondria.

4.3 Chapter 4 Summary

In summary, these results provide further characterization of the molecular environment of Rcf1 and AAC and in particular, the molecular, bioenergetic and conformational factors that influence the Rcf1-AAC relationship. The identity of the previously identified Rcf1-AAC cross-link adduct was independently verified by combining MBS cross-linking and Ni-NTA chromatography with LC-MS/MS.

Two regions of the Rcf1 protein that are highly conserved among the Hig1 family were analyzed in their ability to influence the molecular environment of Rcf1 and AAC. First the N-tail region of Rcf1 was analyzed and it was concluded that the mutation of prolines P^{32} and P^{35} in the conserved Rcf1 PXVPXG motif do not adversely affect cross-

linking between Rcf1 and AAC. However, in addition to being required for the ability of Rcf1 to cross-link to the functionally relevant H2-L-H3 domain of AAC via MBS, Rcf1 Cys residues C^{28} and C^{38} were found to influence the NH_3-NH_3 cross-linking between Rcf1 and AAC by DFDNB. Analysis of the Hig1 QRRQ motif of Rcf1 indicates that arginine residues, R^{65} and R^{67} support the ability of Rcf1 to be cross-linked to AAC via MBS, whereas the mutation of glutamine residues Q^{61} and Q^{71} to alanine appear to be dispensable in influencing the molecular environment between Rcf1 and AAC.

Together, these results suggest that two different regions of the Rcf1 protein, one predicted to be located on the IMS side of the IMM and the other on the matrix side of the IMM, each can influence the molecular environment between Rcf1 and AAC. Given the difference in the predicted location of R^{67} (mitochondrial matrix) relative to C^{28} and C^{38} (IMS), it is possible that the relationship between Rcf1 and AAC may involve long-range structural changes in the Rcf1 protein. Such long-range structural changes in Rcf1 could be predicted to affect potential roles of Rcf1 in stabilizing AAC salt bridge networks in the matrix, via Q/R pairs of the Rcf1 QRRQ motif, or influencing dynamic structural changes within the IMS H2-L-H3 region of AAC via Rcf1 C^{28} and/or C^{38}.

Following the analysis of conserved Rcf1 regions, a number of conformational and structural characteristics of the AAC protein were analyzed in their ability to influence the molecular environment of Rcf1 and AAC. The ability of Rcf1 to be cross-linked to AAC via MBS was shown to be dependent upon the bioenergetic state of the mitochondria, where Rcf1 and AAC can be cross-linked during bioenergetically inactive conditions, in the presence of ADP or ATP alone, and during state 4 (basal) respiration, but the Rcf1-AAC interaction is abolished during state 3 respiration where AAC is active.

The ability of Rcf1 to be cross-linked to AAC was found to be affected by structural conformation changes in the AAC protein, seen in the cross-linking between Rcf1 and AAC that is open to the matrix, and the loss of cross-linking between Rcf1 and AAC that is open to the IMS.

Finally, it was demonstrated that the ability to cross-link Rcf1 and AAC is influenced by the presence of cardiolipin, as evidenced by the loss of MBS crosslinking between Rcf1 and AAC in cardiolipin deficient mitochondria (Δ*crd1* and Δ*tam41*). Native gel mobility analysis suggested that in the absence of Rcf2, and possibly the absence of both Rcf1 and Rcf2, the native gel mobility of AAC is altered, a result that further suggests a potential cooperative role of the two yeast Hig1 proteins Rcf1 and Rcf2 in their relationship with AAC. However, the native gel mobility shift of AAC in the absence of Rcf2 (and both Rcf1 and Rcf2) did not appear to be equal to the shift seen in a cardiolipin deficient mutant, and thus may indicate that the arrangement or number of cardiolipin molecules bound to AAC, rather than the complete absence of bound cardiolipin, is altered in the absence of Rcf1 and Rcf2.

Taken together, these results suggest that a functional relationship may exist between Rcf1 and AAC, where their molecular environment is dynamic and the Rcf1 – AAC relationship is influenced by conserved regions of Rcf1/Hig1 protein, the structural conformation of AAC, the bioenergetic state of the mitochondria.

CHAPTER 5: DISCUSSION

5.1 Introduction

Hig1 proteins have emerged as important factors regulating complex IV assembly and respiratory supercomplex organization (Chen et al., 2012; Fischer et al., 2016; Strogolova et al., 2012; Vukotic et al., 2012). Members of the Hig1 family of proteins have also been linked to a number of mitochondrial processes including apoptosis, mitochondrial fusion and fission, mediation of oxidative damage, hypoxic growth, tumor growth and viability and aging (Ameri et al., 2015; An et al., 2013; 2011; Chen et al., 2012; Fischer et al., 2016; Vukotic et al., 2012). The reported interactions between Hig1 proteins and critical regulatory components of OXPHOS, including independent association with separate components of complex III and complex IV respiratory supercomplexes, and their close physical proximity to the ADP/ATP carrier protein (AAC), place Hig1 proteins at a pivotal regulatory position with the potential to modulate OXPHOS activity. While it is clear that this evolutionarily conserved family of proteins is important for mitochondrial function, a common mechanism underlying their function is currently unknown. Furthermore, the possible physiological significance of the two groups of isoforms, the Hig1-type 2 and Hig1 type 1 subgroups, is not known.

In this dissertation study the yeast Hig1 protein Rcf1, a member of the Hig1-type 2 subgroup has been studied. The functional importance of conserved motifs within the Hig1 domain of Rcf1, including the QRRQ motif and residues within, and adjacent to, the N-terminal PXVPXG motif, have been probed in their ability to support the association of Rcf1 with partner proteins and influence Rcf1's potential to modulate OXPHOS activity.

5.2 The role of Rcf1 in supporting complex IV activity

The Rcf1 protein supports the assembly of complex IV, and the abundance and functional capacity of the complex IV enzyme are reduced in the absence of Rcf1. Yet the mechanistic underpinnings of the role that Rcf1/Hig1 family proteins play in supporting complex IV assembly and activity have not been thoroughly characterized prior to this study. Therefore, a major focus of this dissertation study was to identify the potential molecular mechanism by which Rcf1 (and Hig1 proteins) influence the assembly and activity of the complex IV enzyme.

A number of recent studies have suggested that Hig1 proteins (including Rcf1) may function to secure the correct assembly of a subpopulation of complex IV, thereby regulating the activity of the enzyme and its level of organization into supercomplexes (Chen et al., 2012; Fischer et al., 2016; Strogolova et al., 2012; Vukotic et al., 2012). Furthermore, it was shown that the binding of the Hig1-type 1 protein, Higd1a, to complex IV enhances the activity of the enzyme (Hayashi et al., 2015). The authors of the latter study speculated that the enhanced complex IV activity occurs through structural changes near the catalytic center of the enzyme caused by the direct binding of the Higd1a protein to the complex IV enzyme (Hayashi et al., 2015). Therefore, one hypothesized role of Rcf1 (and Hig1 proteins) was that Rcf1 potentially functions as stoichiometric subunit of complex IV where it functions to regulate the activity of the enzyme either as structural component, or through securing the correct assembly of peripheral subunits of the complex IV enzyme and its organization into supercomplexes.

In agreement with previous studies, several lines of evidence presented here support a role of the Rcf1 protein in regulating the assembly or maturation of complex IV

in a manner that influences the catalytic activity of the enzyme. However, a distinctive feature of the evidence presented in this dissertation study is that it supports a speculative role of Rcf1 in exerting regulatory control on a subpopulation of complex IV in a transient and dynamic relationship with the enzyme, rather than acting as a stoichiometric or structural component of complex IV.

First, the affinity purification results presented here suggest that only a small fraction of complex IV is found in association with Rcf1, and these results were supported by the 1D BN-PAGE /2D-SDS-PAGE (LC-MS/MS) analysis of complex IV. Similarly, it has been reported that only a small percentage of complex IV is found in association with Rcf1 (Strogolova et al., 2012; Vukotic et al., 2012). These results are in agreement with previously reported purification of sub-stoichiometric amounts of Rcf1 with complex IV (i.e. Rcf1 that co-purifies with the III_2-IV_2), which led the authors of the study to speculate that Rcf1 may function as a non-stoichiometric factor in securing the proper late-stage assembly of individual respiratory complexes (Mileykovskaya and Dowhan, 2014). Additionally, these results are in agreement with a recent study that presents a speculative role of Rcf1 in the modulation of cytochrome *c* binding in the III-IV supercomplex, where the absence of Rcf1 is reported to affect only a fraction of complex IV in the mitochondria (Rydström Lundin et al., 2016). Second, it is reported here that in *rcf1*$_{\text{His}}^{\text{R67A}}$ mitochondria both the IV and IV** populations display enhanced catalytic activity, as evidenced by the in-gel activity of the IV and IV** sub-populations. However, the 1D-BN-PAGE/2D SDS-PAGE (LC-MS/MS and immunodecoration) experiments indicate that *rcf1*$_{\text{His}}^{\text{R67A}}$ is only found in association with IV**, indicating that the enhanced activity of the IV population is not due to the direct association of

Rcf1, but rather, Rcf1's molecular "imprint" on the enzyme. Finally, it was shown here that, despite a strong reduction in the steady state levels of the Rcf1 Q/R pair mutant derivatives (i.e. *rcf1*$_{\text{His}}^{\text{Q61A,R65A}}$ and *rcf1*$_{\text{His}}^{\text{R67A,Q71A}}$), the O_2 consumption rate of complex IV was comparable between the Δ*rcf1,*Δ*rcf2* double mutant harboring Rcf1 Q/R pair mutant derivatives and wild type Rcf1, (all of which contained O_2 consumption rates that were significantly greater than in the double null), and suggests that Rcf1 does not act as a stoichiometric subunit to influence the activity of complex IV.

The results presented here support a role of the Rcf1 protein in regulating the assembly or maturation of complex IV in a manner that influences the catalytic activity of the enzyme. Moreover, these results suggest that Rcf1 may exert regulatory control on a subpopulation of complex IV through a transient and dynamic relationship with the enzyme, rather than acting as a stoichiometric or structural component of the complex IV enzyme.

5.3 The role of Rcf1 in supporting AAC

The Rcf1 and AAC proteins are components of III-IV supercomplexes that have been shown to exist in close physical proximity within the inner mitochondrial membrane (Strogolova et al., 2012). Yet the molecular environment between Rcf1 and AAC was largely uncharacterized prior to this study. Specifically, it was unknown whether the structural characteristics and dynamic conformational changes that underlie the adenine nucleotide transport function of AAC influence the molecular environment of AAC and Rcf1. Likewise, the role of conserved regions of the Rcf1 protein in affecting the Rcf1-AAC environment was unknown.

Evidence presented here suggests the molecular environment of Rcf1 and AAC is dynamic, and is influenced by physical aspects of both partners, including conserved regions of Rcf1/Hig1 protein and the structural conformation of AAC. First, it was shown that two different regions of the Rcf1 protein that are predicted to be physically separated by the lipid bilayer influence the molecular environment between Rcf1 and AAC. It was shown that the alanine mutation of Rcf1 cysteine residues, C28 and C38, abolishes MBS ($SH\text{-}NH_3$) cross-linking between Rcf1 and AAC, and strongly reduced the $NH_3\text{-}NH_3$ cross-linking between Rcf1 and AAC by DFDNB. Additionally, the alanine mutation of conserved arginines within the Rcf1 QRRQ motif negatively impacts the ability to cross-link Rcf1 and AAC by MBS. The regions of the Rcf1 protein that contain C28/C38 and the QRRQ motif are predicted to be physically separated by the lipid bilayer. Thus, taken together these results suggest that the Rcf1 QRRQ motif may contain the ability to influence the structural conformation of the Rcf1 protein, and thereby affect the molecular environment between Rcf1 and the AAC protein. Second, the structural conformation of the AAC protein was shown to influence the molecular environment between Rcf1 and AAC. Two specific inhibitors of AAC, AT and B.A. lock the translocase in opposing structural conformations. When AAC was locked in a matrix open state (m-state) by B.A., it could be cross-linked to Rcf1 via MBS. However, when AAC was locked in a cytosol open state (c-state) by AT, it was shown that cross-linking between Rcf1 and AAC was inhibited. These results suggest that the molecular environment between Rcf1 and AAC may be dynamic, and is possibly influenced by both the Rcf1 QRRQ motif and the activity of the AAC protein. In support of this speculation, evidence is presented here that demonstrates the Rcf1 and AAC molecular environment is

influenced by the bioenergetic state of the mitochondria, as shown in the ability to cross-link AAC and Rcf1 under bioenergetically inactive conditions, (i.e. in the presence of ADP or ATP alone, and during state 4 (basal) respiration), and the strong reduction in Rcf1-AAC cross-linking that was detected during state 3 respiration where AAC is active.

Together, these results support the speculation that a functional relationship may exist between Rcf1 and AAC, where Rcf1 may function to stabilize the AAC protein in a specific structural conformation, possibly by bracing residues of the AAC protein that participate in conformation stabilizing salt-bridges, such as the salt-bridge residues of the H2-L-H3 region of AAC (located in the IMS-side of the inner membrane). Studies currently ongoing in the lab are aimed at determining if the catalytic properties of the AAC protein are altered in mitochondria deficient in the Rcf1/Rcf2 proteins or in those harboring Rcf1 mutant derivatives (Vera Strogolova, PhD dissertation). Furthermore, it is possible that the speculated functional relationship between Rcf1 and AAC may be dependent upon the ability of Rcf1 to form a homo-dimer. Mutations in the Rcf1 protein that negatively impact the formation of the Rcf1-Rcf1 homo-dimer (i.e. C28A/C38A, R65A, and R67A) were the same mutations that resulted in a strong reduction in the amount of cross-linking between Rcf1 and AAC. Therefore, it will be important to determine whether the Rcf1 dimer represents a functional form of the Rcf1 protein.

Finally, evidence was presented here that suggests the relationship between Rcf1 and AAC may be influenced by cardiolipin. It was shown that the ability to cross-link Rcf1 and AAC was strongly reduced in cardiolipin deficient mitochondria (Δ*crd1* and Δ*tam41*). Furthermore, a shift was observed in the native gel mobility of AAC in the

absence of Rcf1 and Rcf2 (and Rcf2 alone). However, the AAC native gel mobility shift in Δ*rcf1*Δ*rcf2* mitochondria did not appear to be equal to the shift seen in a cardiolipin-deficient mutant, and suggests that in the absence of Rcf1 and Rcf2 (Δ*rcf1* Δ*rcf2)*, the arrangement or number of cardiolipin molecules bound to AAC might be altered, rather than the complete absence of cardiolipin bound to AAC. It will be important for future studies to compare the lipid composition of AAC between wild type and Δ*rcf1* Δ*rcf2* mitochondria to determine whether there are differences in the composition of cardiolipin species bound to AAC. Additionally, it will be important to determine whether potential differences in the lipid composition of AAC in Δ*rcf1* Δ*rcf2* mitochondria has functional consequences for the nucleotide transport of AAC, and whether any altered AAC function might contribute to the apparent complex IV-independent growth phenotype of the Δ*rcf1* Δ*rcf2* mutant yeast strain.

5.4 Rcf1 and the Lipids associated with Complex IV and AAC

Evidence presented here suggests that Rcf1 may play a role in modifying the lipid content of OXPHOS enzymes. The majority of this evidence supports a role of Rcf1 in securing the correct integration or modification of the signature mitochondrial phospholipid cardiolipin into complex IV. However, results presented here also suggest that Rcf1 may play a more general role in facilitating the assembly or modification of lipids (i.e. cardiolipin and/or other lipid species) that are associated with multiple OXPHOS enzymes.

Each of the proteins that comprise the Rcf1 interactome have been proposed to associate with cardiolipin. Complex IV contains two distinct types of cardiolipin binding sites, two high affinity binding sites that have been implicated in the electron transfer

process and two lower affinity sites that have been proposed to contribute to the structural integrity or possible dimerization of the complex (Arnarez et al., 2013; Sedlák and Robinson, 2015; Sedlák et al., 2006; Shinzawa-Itoh et al., 2007; Yoshikawa et al., 2012). The cardiolipin binding sites within the complex IV enzyme have been mapped to the Cox3 protein and to the Cox12 and Cox13 proteins, and these specific proteins have been shown to be intimately connected to Rcf1 and its functional relationship with complex IV (Strogolova et al., 2012; Vukotic et al., 2012).

Several lines of evidence presented in this dissertation study support a speculative role of Rcf1 in facilitating the integration or remodeling of cardiolipin that is associated with complex IV. First, it has been shown that the stability of complex IV is altered in mitochondria harboring *rcf1*$_{\text{His}}^{\text{R67A}}$, as evidenced by an increased susceptibility to detergent. Additionally, it was previously shown that the steady state levels of complex IV are reduced in the absence of Rcf1 (Strogolova et al., 2012). Second, evidence is presented here that suggests the catalytic properties of complex IV are altered in *rcf1*$_{\text{His}}^{\text{R67A}}$ mitochondria, and include the enhanced 'in-gel' activity of complex IV and increased sensitivity to the inhibitor DCCD. Third, it is shown here that the cardiolipin remodeling enzyme, Taz1, co-purifies with the *rcf1*$_{\text{His}}^{\text{R67A}}$ mutant derivative.

Together, these results support the speculation that Rcf1 may function to facilitate the correct species, or arrangement of cardiolipin into the complex IV enzyme. Furthermore, evidence obtained from this dissertation study supports the possibility that Rcf1 may play a more generalized role in securing the correct lipid composition of multiple OXPHOS enzymes.

In addition to the close physical relationship between Rcf1 and the cardiolipin-associated proteins of complex IV, results presented here suggest that Rcf1 displays an intimate interaction with the cardiolipin-associated complex III protein, cytochrome c_1, as evidenced by the co-purification of cytochrome c_1 with Rcf1 in the absence of assembled complexes III and IV (i.e. ρ^0 mitochondria). This result supports the previously published association between Rcf1 and cytochrome c_1 when the assembly of a single complex (III or IV) is inhibited or strongly defective (Chen et al., 2012; Strogolova et al., 2012). Similar to proteins of complex IV that interact with Rcf1, an interaction between cytochrome c_1 and cardiolipin has been demonstrated, and the cytochrome c_1 –associated cardiolipin has been implicated in the stability and functional integrity of the complex III enzyme (Lange et al., 2001). Further evidence to suggest a role of Rcf1 in the incorporation or remodeling of cardiolipin that is associated with OXPHOS enzymes was observed in the reduced capacity of Rcf1 to be cross-linked to AAC in the absence of cardiolipin, as shown by the strong reduction in the cross-linking of Rcf1 to AAC in the cardiolipin-deficient mutants, Δ*crd1* and Δ*tam41*. Finally, the speculated role of Rcf1 in facilitating the correct integration or remodeling of cardiolipin that is associated with OXPHOS enzymes presented here, is consistent with the speculation that the Rcf1 and the cardiolipin synthase protein, Crd1, may act in the same pathway to promote respiration (Chen et al., 2012).

The proposed role of Rcf1 in the integration or modification of lipids that are associated with OXPHOS enzymes is based, in part, by the observation that the Rcf1 interactome is almost exclusively comprised of proteins that specifically associate with cardiolipin molecules (i.e. Cox3, Cox12, Cytc_1, AAC, and Taz1). Therefore, it is possible

that Rcf1 functions to facilitate the correct assembly or remodeling of cardiolipin within OXPHOS complexes, and may represent an underlying function of Hig1 proteins.

On the other hand, it is possible that Rcf1 may play an even more general role in the incorporation of lipids (i.e. not exclusively cardiolipin) into respiratory complexes. In support of this speculation is the evidence presented here that indicates the DCCD inhibition of complex IV is elevated in *rcf1*$_{\text{His}}^{\text{R67A}}$ mitochondria. While DCCD is predominantly known as an inhibitor of the F_1F_O ATP-synthase (complex V), it has been shown that at high concentrations DCCD can negatively impact the activity of complex IV (Shinzawa-Itoh et al., 2007). Structural characterization of DCCD bound to complex IV indicates that DCCD interacts with a conserved glutamate of the Cox3 protein (Glu90 in bovine Cox3, equivalent to Glu98 of yeast Cox3), where the binding of DCCD to Cox3 Glu90 induces the migration of the palmitate tails of Cox3-associated phosphatidylglycerol lipids, PG1 and PG2, into the proposed O_2 uptake channel of complex IV, blocking the access of O_2 to the heme a_3-Cu_B catalytic center of the complex IV enzyme. Therefore, the altered DCCD inhibition of complex IV OCR that was observed in *rcf1*$_{\text{His}}^{\text{R67A}}$ mitochondria may reflect a function of Rcf1 in the incorporation of Cox3-associated PG molecules, in addition to, or together with, the Cox3- associated cardiolipin. Furthermore, the speculated altered lipid composition of Cox3/complex IV may underlie the detergent instability of complex IV that is observed in *rcf1*$_{\text{His}}^{\text{R67A}}$ mitochondria.

In summary, several lines of evidence presented here support a role of Rcf1 in the lipid integration or remodeling of respiratory enzymes. Due to the largely speculative nature of this proposed role of Rcf1, future studies are needed to more fully characterize

the relationship between Rcf1 and the lipids associated with respiratory enzymes. In particular, it will be import to analyze whether Rcf1 is capable of binding lipids, and to further characterize the relationship between Rcf1 and the Glu98 residue of Cox3. The lipid profile of wild type, single mutant (Δ*rcf1* and Δ*rcf2*) and double mutant (Δ*rcf1*; Δ*rcf2*) mitochondria was analyzed by Dr. Steven Claypool (Johns Hopkins University School of Medicine) (results not shown), and no significant differences in the total mitochondrial lipid profile were observed between either of the two single mutants (Δ*rcf1* and Δ*rcf2*) or the double mutant (Δ*rcf1*; Δ*rcf2*), compared to the wild type. However, Rcf1 appears to associate with only a fraction of complex IV, and it will be important to characterize the lipid composition of Rcf1-associated enzyme complexes to determine whether there are characteristic hallmarks in the lipid composition of Rcf1-associated respiratory enzyme complexes.

5.5 The role of the Rcf1/Hig1 QRRQ motif

The current Rcf1 model predicts that Rcf1 contains 2 transmembrane domains that are oriented with both N and C tails exposed to the IMS, and connected by a short, matrix localized-loop. However, the latest unpublished data from Peter Brzezinski and Pia Ädelroth (Stockholm University) indicate that Rcf1 may contain 5 transmembrane domains and, contrary to the currently understood Rcf1 model, places the QRRQ motif in the IMS, with C28 and C38 near the matrix. Therefore, when appropriate, consideration of the proposed 5-transmembrane model of the Rcf1 protein will be discussed.

The results presented here highlight the importance of the QRRQ motif of Rcf1 for its interaction with complex IV and molecular environment with AAC. How does the QRRQ motif influence the molecular interactions of the Rcf1 protein? The results from

this dissertation study present a number of interesting possibilities that could explain the role of the QRRQ motif.

First, several lines of evidence support a role of the QRRQ motif in influencing the structural conformation of the Rcf1 protein. The mutation of R67 (and R65, results not shown) of the QRRQ motif to alanine result in a strong decrease in the ability of Rcf1 to form the MBS-facilitated cross-linking adduct with AAC. Mutational analysis of C28 and C38, residues that were predicted to be located in the IMS/TM1 region of Rcf1 but recently have been shown to be located in the TM1/matrix region (FIGURE 35), demonstrated that MBS cross-linking between Rcf1 and AAC is dependent upon these cysteines. In the 2 transmembrane helices model of Rcf1, the predicted matrix/TM2-localized R65 and R67 residues of Rcf1 are located a substantial distance from the critical AAC cross-linking region of Rcf1 (i.e. R65 and R76 are located on the opposite side of the membrane bilayer and in a different TM region of the Rcf1 protein from the C28 and C38 residues) (FIGURE 35). In the 5 transmembrane helices Rcf1 model, these domains are also located in opposite mitochondrial compartments, except that the QRRQ motif is predicted to be located in the IMS and C28/C38 near the matrix (Figure 35). Thus, in both models, the ability of QRRQ motif residues, R65 and R67, to influence the proximity of the Rcf1 C28 and C38 to AAC, suggests that residues of the QRRQ motif might contain the ability to influence the structural conformation of the Rcf1 protein. In support of this assertion are results demonstrating that the mutation of R67 (to alanine,

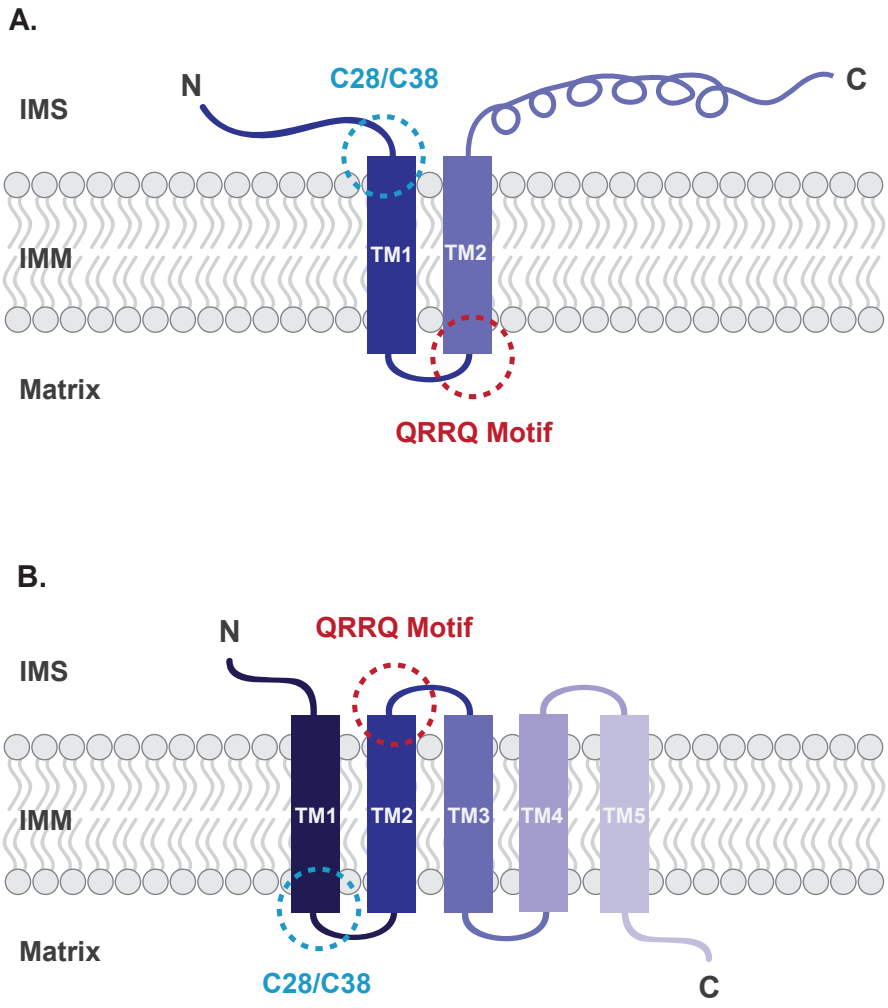

Figure 35. Predicted Model and NMR Structure of the *S. cerevisiae* Rcf1 Protein. **(A).**The predicted topology of Rcf1 in an N_{out}-C_{out} orientation within the inner mitochondrial membrane (IMM) and containing 2 transmembrane domains (TM1 and TM2). The predicted locations of C28 and C38 (cyan) and the QRRQ motif (red) are indicated. **(B).**The NMR structure of Rcf1 in an N_{out}-C_{in} orientation, and containing 5 trasnmembrane domains (TM1-TM5). The locations of C28 and C38 (cyan) and the QRRQ motif (red) are indicated The solution NMR structure of Rcf1 was obtained by Dr. Peter Brzezinski and Dr. Pia Ädelroth (Stockholm University). Following expression in *E.Coli,* the yeast Rcf1 protein was denatured and re-folded from inclusion bodies. (unpublished results, personal communication between R. Stuart and P. Brzezinski).

glutamine or histidine, but not lysine or glutamic acid) confers a novel cross-link adduct between Rcf1 and the Cox2 protein. While the cross-linking between Rcf1 mutant derivatives and Cox2 requires further characterization, this result independently suggests that the molecular environment of Rcf1 is influenced by R67 of the QRRQ motif. Therefore, the QRRQ motif might function to influence the assembly or maturation of OXPHOS complexes, including complex IV and AAC, by controlling the structural conformation of the Rcf1 protein, thereby influencing the molecular environment of Rcf1 and partner proteins, including AAC and the catalytically critical complex IV subunit, Cox2. Moreover, Rcf1 might potentially function as a wedge that regulates the assembly or modification of lipids within complex IV or AAC. In this regard, it is envisioned that the QRRQ motif might regulate the physical constraints of the matrix (or IMS) loop, resulting in a level of torsion that would be predicted to control the position of the Rcf1 transmembrane regions relative to each other. Thus, the position of the Rcf1 transmembrane regions are speculated to confer an 'open' or 'closed' conformation of the Rcf1 wedge that serves to regulate the lipid composition of OXPHOS complexes by controlling the access of lipid synthases (or modifying enzymes) to lipid-associated proteins of the Rcf1 interactome (i.e. Cox3, Cytc_1, AAC) (FIGURE 36). Furthermore, the possibility that structural changes in the Rcf1 protein may be dependent upon the protonation state of the R67 residue (suggested by the ability of glutamine and histidine, but not lysine or glutamic acid resides to promote the formation of the Rcf1-Cox2 adduct) suggest a potential mode of regulation, whereby the bioenergetic state of the mitochondria might influence the protonation state of Rcf1 R67 via changes in the pH of the mitochondrial matrix. The ability of wild-type Rcf1 to be cross-linked to AAC

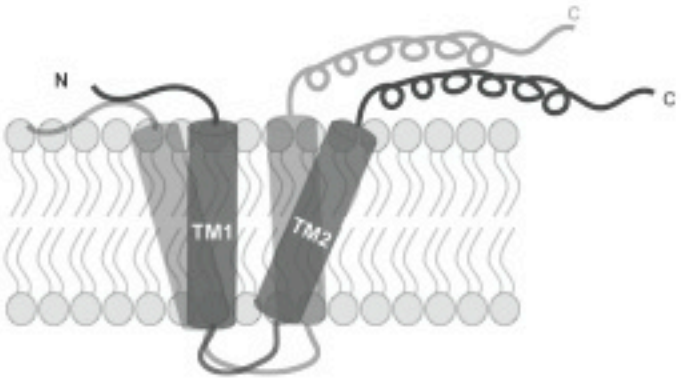

Figure 36. Proposed role of the QRRQ motif in influencing the conforma - tion of Rcf1. The QRRQ motif potentially influences the molecular environment of Rcf1 and partner proteins, (i.e. AAC, Cox3 Cytc_1) by affecting the position of the transmembrane segments TM1 and TM2.

progressively decreased as the bioenergetic status of the mitochondria changed (FIGURE 31). The decrease in the ability of Rcf1 to be cross-liked to AAC during state 3 respiration (i.e. when the AAC activity level is predicted to be elevated) suggests that either the activity of the translocase, or bioenergetic activity dependent changes in the pH of the mitochondrial compartments (matrix or IMS) influence the ability of Rcf1 to be cross-linked to AAC. Future experiments will be important for characterizing whether the bioenergetic status of the mitochondria affects the association of Rcf1 with partner proteins or enzyme complexes.

Second, evidence is presented here that suggests Rcf1 can form a homo-dimer. The mutational insertion of a cysteine in the QRRQ motif (V68C), results in the enhanced formation (or stability) of the observed Rcf1-Rcf1 homo-dimer. In contrast, Rcf1 mutant derivatives harboring mutations in conserved QRRQ residues displayed a strong reduction in the homo-dimer (R65A, R67A, Q61A/R65A, R67A/Q71A). It is important to note that the mutation of both Q residues (seen in the Q61A/Q71A Rcf1 mutant derivative) did not negatively impact the formation of the Rcf1-Rcf1 homo-dimer, and suggests that the R65 and R67 residues of the QRRQ motif might be involved in the formation or stability of an Rcf1 homo-dimer. Whether Rcf1 functions as a dimer remains unknown. Evidence presented in chapter 3 indicates that Rcf1 can associate with complex III subunits (Cytc_1 and Qcr6) in the absence of fully assembled complex III or complex IV (ρ^0 mitochondria), and supports the findings that Rcf1 can associate with complex III independent of assembled complex IV (Strogolova et al., 2012), or the Cox3 protein (Chen et al., 2012; Garlich and Stuart unpublished results). Thus, it could be speculated that individual Rcf1 proteins within an Rcf1-Rcf1 homo-dimer could

independently associate with complex III and complex IV, and thereby support the correct assembly (i.e. the lipid content) of individual enzyme complexes in a manner that influences their organization into supercomplexes. A number of recent findings support this speculation, and include the altered organization of III-IV supercomplexes in the absence of Rcf1 (and Rcf2), where there is a reduction in the III_2-IV_2 species and an increase in the III_2-IV (Chen et al., 2012; Strogolova et al., 2012; Vukotic et al., 2012), and the reported role of Rcf1 in mediating electron transfer between complex III and IV by securing a tightly-bound cytochrome *c* (Rydström Lundin et al., 2016). Notably, the Cox12 protein, together with Cox2, defines the cytochrome *c* binding site within complex IV. It was previously shown that the correct assembly of Cox12 is negatively impacted by the absence of Rcf1 (and Rcf2) (Strogolova et al., 2012). Additionally, the Cox12 protein has been shown to interact with cardiolipin (Arnarez et al., 2013; Sedlák and Robinson, 2015; Sedlák et al., 2006; Shinzawa-Itoh et al., 2007; Yoshikawa et al., 2012). Thus an Rcf1 dimer might support the assembly and structural organization of respiratory enzyme complexes by facilitating the correct lipid integration into individual complexes. Further characterization of the functional significance of Rcf1-Rcf1 homo-dimer, and the role of the QRRQ motif in its formation (or maintenance) should be addressed in future experiments.

Finally, a notable feature of the QRRQ motif that appears to be conserved among Hig1-type 2 proteins are Q/R pairs that co-align when the QRRQ motif is analyzed in an α-helical plot, i.e. the R67 residue co-aligns with the Q71 residue, and the R65 residue is adjacent to the Q61 residue (FIGURE 16A). Mutational analysis of the Q/R pairs suggests that either pair is independently critical for the stability of the Rcf1 protein,

where the stability of the Rcf1 protein is negatively impacted by the mutation of either pair, and observed to be marginally more detrimental in the Q71A/R65A mutant derivative (FIGURE 16B). Furthermore, the mutation of either Q/R pair resulted in a strong reduction in the Rcf1-Rcf1 homo-dimer. Therefore, the Q/R pairs might represent functional regions of the Rcf1 protein that could, in theory, interact with the same partner protein in a manner that is dependent on the conformation of the Rcf1 protein. As discussed above, the strong reduction in the ability of Rcf1 to be cross-linked to AAC in the R65A and R67A mutants could be interpreted as a role of the QRRQ motif, via R65 and R67, in influencing the structural conformation of the Rcf1 protein. Thus, two Q/R pairs would allow Rcf1 to interact with the same protein partner by alternating the interaction between the respective Q/R pairs. Reciprocally, the two Q/R pairs might secure the ability of a relatively static Rcf1 protein to interact with a partner protein that undergoes dynamic structural rearrangement (potentially caused by catalytic activity), such as the transition between m- and c-states by AAC, the oxidation and reduction of cytochrome *c*, proton pumping and reduction of O_2 by the III-IV supercomplex, or the assembly (or modification) of lipids that associate with OXPHOS enzymes.

Regardless of the specific mode of interaction, this dissertation study highlights the importance of the QRRQ motif as a determinant of the dynamics of Rcf1's interaction with Cox3 and complex IV, and demonstrates that altering the QRRQ motif significantly influences the catalytic activity of the complex IV enzyme. Moreover, the ability to form an Rcf1-AAC cross-linking adduct is also affected by mutations in the QRRQ motif, suggesting that the QRRQ motif plays an important role in influencing the

molecular environment of Rcf1 and partner proteins that are critical OXPHOS components.

5.6 Comparison of Hig1-type 1 and type 2 isoforms

The Hig1 family of proteins is evolutionarily conserved from α-proteobacteria to diverse eukaryotic taxa, and can be separated into two distinct groups, -type 1 and -type 2, based on their sequences. The expression of the Hig1-type 1 isoform is induced in response to various cellular stresses, where it has been shown to play a role in maintaining mitochondrial function and cell survival during hypoxia. In contrast, the -type 2 isoform appears to be constitutively expressed and, importantly, is limited to α-proteobacteria and lower eukaryotes (Strogolova et al., 2012). However, similar to -type 1 proteins, several recent studies suggest that –type 2 proteins may also function to protect the functional integrity of mitochondria from oxidative damage during hypoxia.

What then, is the significance of the variations between –type1 and –type2 isoforms, including: the divergent QRRQ motif sequences between type 1 and type 2 isoforms, their differential expression patterns (hypoxia-induced vs. constitutive), and the differences in their taxonomic distribution (-type 2 isoforms found exclusively in α-proteobacteria and lower eukaryotes? Furthermore, how are these differences reconciled with the apparent overlapping function of Hig1 proteins in the maintenance of mitochondrial function during cellular stress, and the proposed role of the Hig1-type 2 protein Rcf1 in the modification of the complex IV enzyme?

The Hig1-type 2 [Q]-$(X)_3$-R-X-R-$(X)_3$-[Q] motif is noticeably different from the Hig1-type 1 stress-induced isoforms that contain a [I/V]-HLIHM-R-$(X)_3$-[Q] motif. The results presented here suggest that differences in this motif between Hig1-type1 and

Hig1-type2 isoforms may influence a dynamic relationship between Hig1 proteins and complex IV, as evidenced by the reduced amount of complex IV that was found to co-purify with Hig1-type1$_{His}$ as compared with Hig1-type2$_{His}$ (and compared to the yeast type 2 protein, Rcf1$_{His}$). One possibility is that the differences in these motifs may reflect the need for differential modifications to complex IV that allow the enzyme to function optimally under stress conditions, such as during hypoxia. In this capacity, it is speculated that Rcf1 would function to secure a specific lipid composition within complex IV (i.e. the integration or remodeling of specific PG or CL species that associate with complex IV) that results in an altered (potentially enhanced) efficiency of O_2 uptake to the heme a_3-Cu_B center of the enzyme. Alternatively, it is possible that differences in these motifs underlie distinct dynamic interactions with complex IV that are divergent between type1 and type2 isoforms, where type 1 proteins display a "loose/rapid" interaction with complex IV and type 2 proteins display a relatively "tight/slow" association. A "loose/rapid" interaction between the Hig1-type1 isoform and complex IV may be advantageous (over the "tight/slow" association of type2) during hypoxia, where the need for rapid modifications to complex IV is critical to minimizing ROS and promoting survival.

Another apparent difference between Hig1-type 1 and type 2 isoforms is that the expression of Hig1-type 1 proteins is induced by cellular stress, whereas type 2 proteins appear to be constitutively expressed. What accounts for the differences in the expression of Hig1 isoforms?

Under conditions of limiting O_2 (hypoxia), the incomplete reduction of O_2 can lead to the production of damaging superoxide radicals, resulting in mitochondrial

dysfunction. Thus, the ability of mitochondria to continue to function under low O_2 conditions is critical for efficient energy production and the survival of the organism. Hypoxic-induced isoforms of complex IV (Cox5b), cytochrome *c* (iso-2-cytochrome *c*) and AAC (Aac3) collectively represent components that alter the composition of respiratory enzyme complexes and associated proteins to enhance ATP production by OXPHOS and maintain mitochondrial function under low O_2 conditions (Hodge et al., 1989; Kwast et al., 1999; Sabová et al., 1993). Therefore, the hypoxia-induced Hig1-type 1 isoform could represent a sub-group of Hig1 proteins that contain the unique ability (to that of the Hig1-type 2 isoform) to recognize or interact with hypoxia-induced OXPHOS isoforms (i.e. Cox5b, iso-2-cytochrome *c*, and Aac3), and thereby maintain the regulation of OXPHOS by Hig1 proteins under low O_2 conditions.

It is possible that Hig-type 1 proteins confer a modification to complex IV that is different from that of Hig1-type 2 proteins, and that allows the enzyme to function optimally during hypoxia. Alternatively, type 1 proteins might enhance the activity of OXPHOS enzymes by the same function that is proposed for type 2 proteins (including Rcf1) (i.e. facilitating the assembly or modification of associated lipids). Thus, in addition to the presence of constitutively expressed Hig1-type 2 protein, the induction of the hypoxia-induced type 1 isoform would be predicted to increase the abundance of Hig1 proteins that are functionally identical, and thereby secure optimal OXPHOS function under low O_2 conditions by significantly increasing the proportion of Hig1-modified (catalytically enhanced) OXPHOS enzymes.

While Hig1-type 2 proteins are found in many bacteria and lower eukaryotes, the type 1 isoform appears to be exclusively present in higher eukaryotes. If Hig1 proteins

(type 1 and type 2) share a common underlying function, such as facilitating the modification of lipids that are associated with OXPHOS complexes, their divergent taxonomic distribution might reflect differences in the type of lipids that associate with OXPHOS enzymes between bacteria and higher eukaryotes. While the lipid binding sites of Cox3/subunit III have been shown to be extensively conserved from bacteria to mammals, the specific type of lipid that binds to the Cox3/subunit III are different between bacteria and mammals (Varanasi et al., 2006). It is also possible that the hypoxia-induced type 1 isoform may represent an additional level of regulation that has been acquired exclusively by higher eukaryotes, that provides an enhanced efficiency of O_2 transfer under low O_2 conditions, either by the increased abundance of Hig1 proteins or through a different function (i.e. different type of enzyme modification) than the type 2 isoform.

5.7 The Role of Hig1 proteins in hypoxia and stress conditions

What is the relationship between the speculated role of Rcf1 in the lipid integration or remodeling of OXPHOS complexes presented here and the reported involvement of Rcf1/Hig1 proteins in the mediation of hypoxic and oxidative damage? A number of recent independent studies have implicated Rcf1 (and Hig1 homologs from various eukaryotic taxa) in the mitigation of ROS production and oxidative damage (Ameri et al., 2015; Chen et al., 2012; Fischer et al., 2016; Vukotic et al., 2012). Two of these studies presented evidence that suggests Rcf1/Hig1 proteins are required for growth under hypoxic conditions (Vukotic et al., 2012) and maintenance of lifespan (Fischer et al., 2016). Furthermore, it was recently shown that the binding of a Hig1 family protein (Higd1a) to complex IV positively regulates complex IV activity through structural

changes in the enzyme, and the authors speculate that Higd1a –associated structural changes may be important for the reported Higd1a-dependent survival during hypoxia (Hayashi et al., 2015). Here, it has been proposed that Rcf1, in a dynamic manner that is influenced by the Hig1-type 2 QRRQ motif, associates with Cox3- containing complex IV, possibly during assembly, and affects the stability and catalytic properties of the enzyme by securing the correct maturation of the enzyme and its associated lipids. The altered level of complex IV inhibition by DCCD that was observed in *rcf1*$_{\text{His}}^{\text{R67A}}$ mitochondria suggests that Rcf1 may affect the stability and enzymatic activity of complex IV by influencing the assembly or modification of Cox3-associated lipids that are reported to regulate the O_2 uptake pathway of the complex IV enzyme.

The reported regulation of the complex IV O_2 path by Cox3-associated lipids was proposed by Shinzawa-Itoh et al., to occur through changes in the conformation of the PG tail ends that are induced by the introduction of O_2 molecules into the pathway, or potentially through long-range interactions with the redox active center of the enzyme, and that are predicted to control the O_2 supply to the a_3-Cu_B oxygen reduction site (Shinzawa-Itoh et al., 2007). In support of this speculation are reports that subunit 3 of *Rhodobacter sphaeroides* aa_3-type cytochrome *c* oxidase, homologous to the Cox3 protein of mitochondrial complex IV, protects the structural integrity of the heme a_3-Cu_B active center from suicide inactivation in a lipid-dependent manner through long range interactions with the active center (Bratton et al., 1999; Varanasi et al., 2006). The regulation of the complex IV O_2 path by Cox3-associated lipids was found to be strongly dependent on the composition of the Cox3-associated PG molecules, suggesting that the specificity of the Cox3-associated PG species may be a critical determinant in the level of

regulation of the complex IV O_2 path (Shinzawa-Itoh et al., 2007). Therefore, it is possible that the association between Rcf1 and newly-synthesized Cox3 may be important for securing the integration of specific lipid species into complex IV that confer a unique level of regulation.

Furthermore, the reported roles of Rcf1 in the mediation of oxidative damage and ROS production, and the required presence of Rcf1 for hypoxic growth and lifespan maintenance, suggest that Rcf1 –modified complex IV species may be critical for OXPHOS under sub-optimal conditions such as hypoxia. Thus, Rcf1-dependent modifications to complex IV are proposed to result in a complex IV species that is capable of optimal function under hypoxic conditions, resulting in decreased ROS production that minimizes oxidative damage (including lipid peroxidation) and supports OXPHOS, thereby maintaining normal lifespan under hypoxic conditions. In agreement, the results of this dissertation study support the speculation that Rcf1/Hig1-type 2 proteins, through a transient and dynamic interaction with newly-synthesized Cox3 protein that is dependent on the QRRQ motif, function to modulate the catalytic properties of the complex IV enzyme, potentially through Cox3-associated lipids that potentially result in long-range structural changes near heme a_3-Cu_B. Furthermore, it is speculated here that the proposed Rcf1-dependent complex IV structural changes modulate the access of O_2 to the redox-active heme a_3-Cu_B center, thereby mitigating the production of, or damage from, reactive oxygen species during hypoxia (FIGURE 37).

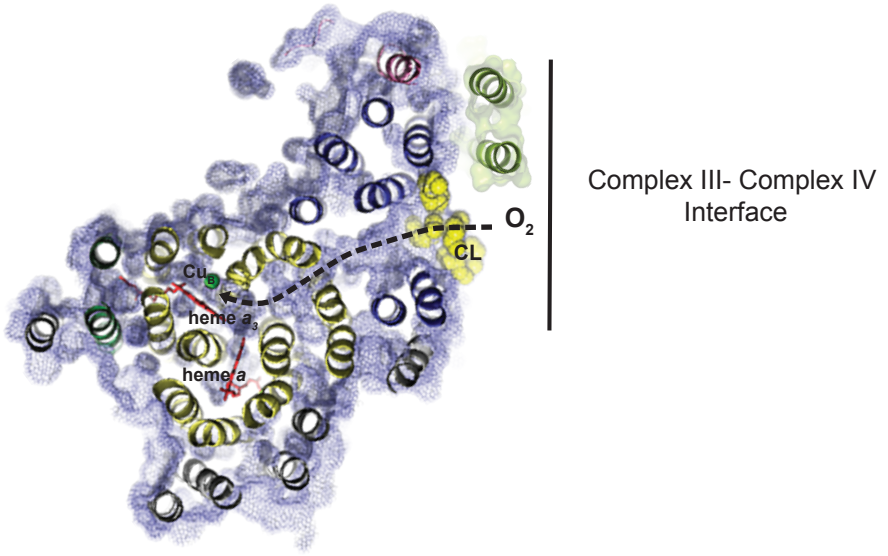

Figure 37. Proposed Rcf1-Complex IV interface It is speculated that Rcf1 (depicted here in green), through a transient and dynamic interaction with newly-synthesized Cox3 (Blue) that is influenced by the Rcf1 QRRQ motif, functions to modulate the catalytic properties of the complex IV enzyme, potentially through Cox3 lipids that result in long-range structural changes that affect the heme a_3-Cu_B center, thereby modulating access of the access of O_2 to the redox center.

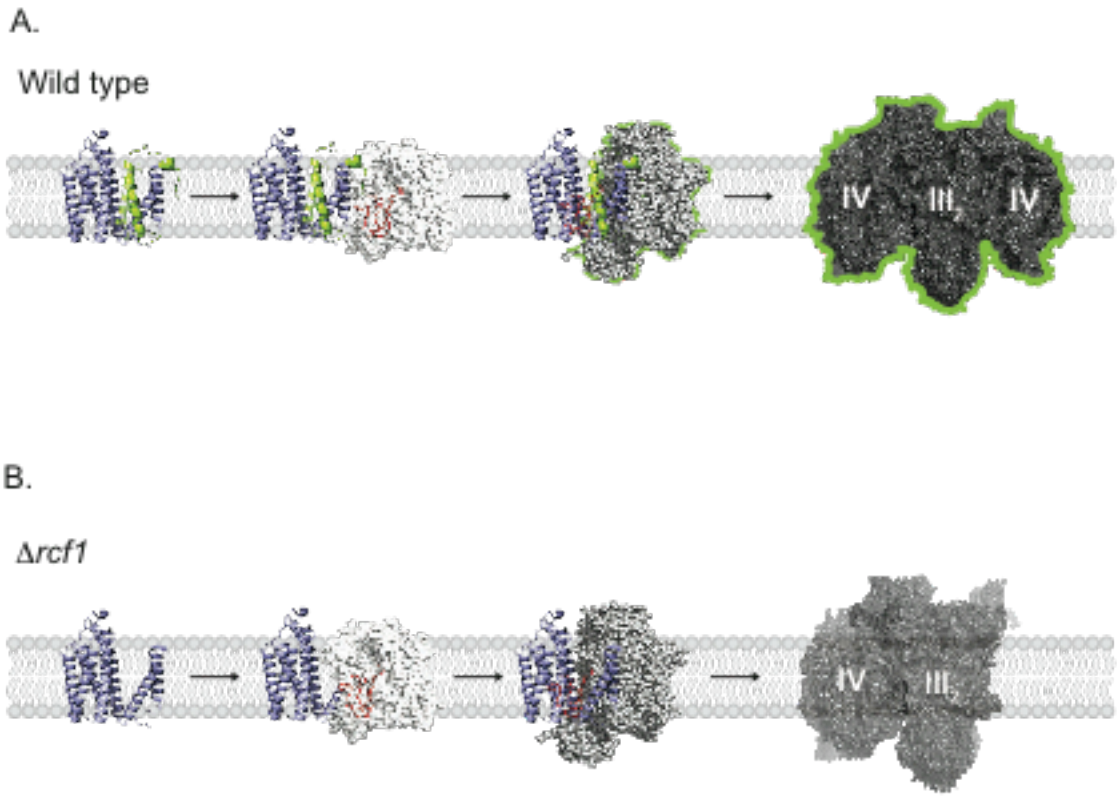

Figure 38. Model of speculated Rcf1 function. (A) Rcf1 (green) associates with newly-synthesized Cox3 (slate blue) and facilitates the integration or modification of Cox3 associated lipids (red) by maintaining Cox3 in a lipid integration/modification competent structural conformation that allows a lipid synthase or modifying enzyme (white) access to Cox3 for the insertion or modification of specific lipid species. The Rcf1-associated Cox3 is then integrated into a complex IV assembly intermediate (grey) prior to full assembly of a complex IV sub-population (green outline) that contains Rcf1's molecular "imprint", and can therefore function optimally during hypoxia.
(B) In Rcf1 deficient mitochondria (Δ*rcf1*), the absence of the complex IV sub-population containing Rcf1's molecular imprint results in reduced complex IV heterogeneity and mitochondria that are susceptible to hypoxia (i.e. lack the complex IV sub-population that can function optimally during hypoxia.

5.8 Model of the proposed role of Rcf1/Hig1 proteins

Based on the results of this dissertation study, a model is proposed in which the Rcf1 protein, through its association with newly synthesized Cox3, functions to regulate the catalytic properties of the complex IV enzyme by facilitating the integration (or modification) of Cox3-associated lipids that modulate the O_2 pathway to the heme a_3-Cu_B catalytic center. Moreover, it is speculated that Rcf1 contributes to the heterogeneity of the complex IV enzyme population within the mitochondria by modifying the O_2 uptake efficiency of a subpopulation of complex IV, thereby securing a subpopulation of complex IV that functions optimally during hypoxia, thereby mitigating the production of, or damage from, reactive oxygen species, the absence of this complex IV subpopulation in Δ*rcf1* mitochondria results in yeast that are more susceptible to hypoxia-induced mitochondrial dysfunction and oxidative damage (FIGURE 38).

In conclusion, the results presented in this dissertation study highlight the importance of Rcf1 in the regulation of aerobic cellular energy production via OXPHOS, and a common mechanism of Hig1 proteins is proposed here, where Rcf1/Hig1 proteins influence OXPHOS through the assembly of respiratory enzyme complexes that are adapted to function optimally under stress.

REFERENCES

Acín-Pérez, R., Fernandez-Silva, P., Peleato, M.L., Pérez-Martos, A., and Enríquez, J.A. (2008). Respiratory active mitochondrial supercomplexes. Mol. Cell *32*, 529–539.

Althoff, T., Mills, D.J., Popot, J.-L., and Kühlbrandt, W. (2011). Arrangement of electron transport chain components in bovine mitochondrial supercomplex I1III2IV1. Embo J. *30*, 4652–4664.

Ameri, K., Jahangiri, A., Rajah, A.M., Tormos, K.V., Nagarajan, R., Pekmezci, M., Nguyen, V., Wheeler, M.L., Murphy, M.P., Sanders, T.A., et al. (2015). HIGD1A Regulates Oxygen Consumption, ROS Production, and AMPK Activity during Glucose Deprivation to Modulate Cell Survival and Tumor Growth. CellReports *10*, 891–899.

An, H.-J., Cho, G., Lee, J.-O., Paik, S.-G., Kim, Y.S., and Lee, H. (2013). Higd-1a interacts with Opa1 and is required for the morphological and functional integrity of mitochondria. Proc. Natl. Acad. Sci. U.S.a. *110*, 13014–13019.

An, H.-J., Shin, H., Jo, S.-G., Kim, Y.J., Lee, J.-O., Paik, S.-G., and Lee, H. (2011). Biochimica et Biophysica Acta. BBA - Molecular Cell Research *1813*, 2088–2098.

Aquila, H., Eiermann, W., Babel, W., and Klingenberg, M. (1978). Isolation of the ADP/ATP translocator from beef heart mitochondria as the bongkrekate-protein complex. Eur. J. Biochem. *85*, 549–560.

Arnarez, C., Marrink, S.J., and Periole, X. (2013). Identification of cardiolipin binding sites on cytochrome c oxidase at the entrance of proton channels. Sci. Rep. *3*.

Arnold, I., Pfeiffer, K., Neupert, W., Stuart, R.A., and Schägger, H. (1998). Yeast mitochondrial F1F0-ATP synthase exists as a dimer: identification of three dimer-specific subunits. Embo J. *17*, 7170–7178.

Arnold, K., Bordoli, L., Kopp, J., and Schwede, T. (2006). The SWISS-MODEL workspace: a web-based environment for protein structure homology modelling. Bioinformatics *22*, 195–201.

Barrientos, A., and Ugalde, C. (2013). I function, therefore I am: overcoming skepticism about mitochondrial supercomplexes. Cell Metab. *18*, 147–149.

Barrientos, A., Barros, M.H., Valnot, I., Rötig, A., Rustin, P., and Tzagoloff, A. (2002). Cytochrome oxidase in health and disease. Gene *286*, 53–63.

Barrientos, A., Fontanesi, F., and Díaz, F. (2009). Evaluation of the mitochondrial respiratory chain and oxidative phosphorylation system using polarography and spectrophotometric enzyme assays. Curr Protoc Hum Genet *Chapter 19*, Unit19.3.

Barrientos, A., Zambrano, A., and Tzagoloff, A. (2004). Mss51p and Cox14p jointly regulate mitochondrial Cox1p expression in Saccharomyces cerevisiae. EMBO J. *23*, 3472–3482.

Barros, M.H., Carlson, C.G., Glerum, D.M., and Tzagoloff, A. (2001). Involvement of mitochondrial ferredoxin and Cox15p in hydroxylation of heme O. FEBS Lett. *492*, 133–138.

Bedo, G., Vargas, M., Ferreiro, M.-J., Chalar, C., and Agrati, D. (2005). Characterization of hypoxia induced gene 1: expression during rat central nervous system maturation and evidence of antisense RNA expression. Int. J. Dev. Biol. *49*, 431–436.

Beyer, K., and Klingenberg, M. (1985). ADP/ATP carrier protein from beef heart mitochondria has high amounts of tightly bound cardiolipin, as revealed by 31P nuclear magnetic resonance. Biochemistry *24*, 3821–3826.

Bloch, D., Belevich, I., Jasaitis, A., Ribacka, C., Puustinen, A., Verkhovsky, M.I., and Wikström, M. (2004). The catalytic cycle of cytochrome c oxidase is not the sum of its two halves. Proc. Natl. Acad. Sci. U.S.A. *101*, 529–533.

Boekema, E.J., and Braun, H.-P. (2007). Supramolecular structure of the mitochondrial oxidative phosphorylation system. J. Biol. Chem. *282*, 1–4.

Bordoli, L., Kiefer, F., Arnold, K., Benkert, P., Battey, J., and Schwede, T. (2009). Protein structure homology modeling using SWISS-MODEL workspace. Nat Protoc *4*, 1–13.

Bradford, M.M. (1976). A rapid and sensitive method for the quantitation of microgram quantities of protein utilizing the principle of protein-dye binding. Analytical Biochemistry *72*, 248–254.

Brand, M.D. (2005). The efficiency and plasticity of mitochondrial energy transduction. Biochem. Soc. Trans. *33*, 897–904.

Brandner, K., Mick, D.U., Frazier, A.E., Taylor, R.D., Meisinger, C., and Rehling, P. (2005). Taz1, an outer mitochondrial membrane protein, affects stability and assembly of inner membrane protein complexes: implications for Barth Syndrome. Mol. Biol. Cell *16*, 5202–5214.

Brandolin G., Doussiere, J., Gulik, A., Gulik-Krzywicki, T., Lauquin, G.J.M., Vignais, P.V. (1980) Kinetic, binding and ultrastructural properties of the beef heart adenine nucleotide carrier protein after incorporation into phospholipid vesicles. Biochim. Biophys. Acta. *592*(3), 592–614.

Brandt, U and Trumpower, B.L. (1994) The protonmotive Q cycle in mitochondria and bacteria. Crit. Rev. Biochem. Mol. Biol. *29*, 165-197

Bratton, M.R., Pressler, M.A., and Hosler, J.P. (1999). Suicide inactivation of cytochrome c oxidase: catalytic turnover in the absence of subunit III alters the active site. Biochemistry *38*, 16236–16245.

Bratton, M., Mills, D., Castleden, C.K., Hosler, J., and Meunier, B. (2003). Disease-related mutations in cytochrome c oxidase studied in yeast and bacterial models. Eur. J. Biochem. *270*, 1222–1230.

Chance, B., Estabrook, R.W., and Lee, C.P. (1963). Electron Transport in the Oxysome. Science *140*, 379–380.

Chen (1995). Specific mutations in α- and γ-subunits of F_1-ATPase affect mitochondrial genome integrity in the petite negative yeast *Kluyveromyces lactis*. EMBO J. *14*, 3277–3286.

Chen, X.J., Clark-Walker G.D. (1996) The Mitochondrial Genome Integrity Gene, MGI1, of *Kluyveromyces lactis* Encodes the β-Subunit of F_1-ATPase. Genetics *144* (4), 1445-145.

Chen, X.J. (2004). Sal1p, a calcium-dependent carrier protein that suppresses an essential cellular function associated With the Aac2 isoform of ADP/ATP translocase in *Saccharomyces cerevisiae*. Genetics *167*, 607–617.

Chen, Y.-C., Taylor, E.B., Dephoure, N., Heo, J.-M., Tonhato, A., Papandreou, I., Nath, N., Denko, N.C., Gygi, S.P., and Rutter, J. (2012). Identification of a protein mediating respiratory supercomplex stability. Cell Metab. *15*, 348–360.

Cobine, P.A., Pierrel, F., and Winge, D.R. (2006). Copper trafficking to the mitochondrion and assembly of copper metalloenzymes. Biochim. Biophys. Acta *1763*, 759–772.

Costanzo, M.C., Seaver, E.C., and Fox, T.D. (1986). At least two nuclear gene products are specifically required for translation of a single yeast mitochondrial mRNA. Embo J. *5*, 3637–3641.

Cruciat, C.M., Brunner, S., Baumann, F., Neupert, W., and Stuart, R.A. (2000). The cytochrome bc_1 and cytochrome *c* oxidase complexes associate to form a single supracomplex in yeast mitochondria. J. Biol. Chem. *275*, 18093–18098.

Cui, F., Cole, H.A., Clark, D.J., and Zhurkin, V.B. (2012). Transcriptional activation of yeast genes disrupts intragenic nucleosome phasing. Nucleic Acids Res. *40*, 10753–10764.

D'Aurelio, M., Gajewski, C.D., Lenaz, G., and Manfredi, G. (2006). Respiratory chain supercomplexes set the threshold for respiration defects in human mtDNA mutant cybrids. Hum. Mol. Genet. *15*, 2157–2169.

Das, J., Miller, S.T., and Stern, D.L. (2004). Comparison of diverse protein sequences of the nuclear-encoded subunits of cytochrome C oxidase suggests conservation of structure underlies evolving functional sites. Mol. Biol. Evol. *21*, 1572–1582.

Daum, G., Gasser, S.M., and Schatz, G. (1982). Import of proteins into mitochondria. Energy-dependent, two-step processing of the intermembrane space enzyme cytochrome b2 by isolated yeast mitochondria. J. Biol. Chem. *257*, 13075–13080.

Demaurex, N., Poburko, D., and Frieden, M. (2009). Regulation of plasma membrane calcium fluxes by mitochondria. Biochim. Biophys. Acta *1787*, 1383–1394.

Denko, N., Schindler, C., Koong, A., Laderoute, K., Green, C., and Giaccia, A. (2000). Epigenetic regulation of gene expression in cervical cancer cells by the tumor microenvironment. Clin. Cancer Res. *6*, 480–487.

Dienhart, M.K., and Stuart, R.A. (2008). The yeast Aac2 protein exists in physical association with the cytochrome bc_1-COX supercomplex and the TIM23 machinery. Mol. Biol. Cell *19*, 3934–3943.

Dudkina, N.V., Heinemeyer, J., Keegstra, W., Boekema, E.J., and Braun, H.-P. (2005). Structure of dimeric ATP synthase from mitochondria: an angular association of monomers induces the strong curvature of the inner membrane. FEBS Lett. *579*, 5769–5772.

Dudkina, N.V., Kudryashev, M., Stahlberg, H., and Boekema, E.J. (2011). Interaction of complexes I, III, and IV within the bovine respirasome by single particle cryoelectron tomography. Proc. Natl. Acad. Sci. U.S.a. *108*, 15196–15200.

Endres, M., Neupert, W., and Brunner, M. (1999). Transport of the ADP/ATP carrier of mitochondria from the TOM complex to the TIM22.54 complex. Embo J. *18*, 3214–3221.

Enríquez, J.A. (2015). Supramolecular Organization of Respiratory Complexes. Annu. Rev. Physiol. *78*, 533–561.

Eubel, H., Jänsch, L., and Braun, H.-P. (2003). New insights into the respiratory chain of plant mitochondria. Supercomplexes and a unique composition of complex II. Plant Physiol. *133*, 274–286.

Fernyhough, P., Roy Chowdhury, S.K., and Schmidt, R.E. (2010). Mitochondrial stress and the pathogenesis of diabetic neuropathy. Expert Rev Endocrinol Metab *5*, 39–49.

Ferreira R, Vitorino R, Alves RM, Appell HJ, Powers SK, Duarte JA, (2010) Subsarcolemmal and intermyofibrillar mitochondria proteome differences disclose functional specializations in skeletal muscle. Proteomics *10*, 3142–54

Fischer, F., Filippis, C., and Osiewacz, H.D. (2015). RCF1-dependent respiratory supercomplexes are integral for lifespan-maintenance in a fungal ageing model. Sci. Rep. 1–13.

Fiumera, H.L., Broadley, S.A., and Fox, T.D. (2007). Translocation of mitochondrially synthesized Cox2 domains from the matrix to the intermembrane space. Mol. Cell. Biol. *27*, 4664–4673.

Fontanesi, F., Clemente, P., and Barrientos, A. (2011). Cox25 teams up with Mss51, Ssc1, and Cox14 to regulate mitochondrial cytochrome *c* oxidase subunit 1 expression and assembly in Saccharomyces cerevisiae. Journal of Biological Chemistry *286*, 555–566.

Fontanesi, F., Soto, I.C., and Barrientos, A. (2008). Cytochrome *c* oxidase biogenesis: new levels of regulation. IUBMB Life *60*, 557–568.

Fornuskova, D., Stiburek, L., Wenchich, L., Vinsova, K., Hansikova, H., and Zeman, J. (2010). Novel insights into the assembly and function of human nuclear-encoded cytochrome c oxidase subunits 4, 5a, 6a, 7a and 7b. Biochem. J. *428*, 363–374.

Gallas, M.R., Dienhart, M.K., Stuart, R.A., and Long, R.M. (2006). Characterization of Mmp37p, a Saccharomyces cerevisiae mitochondrial matrix protein with a role in mitochondrial protein import. Mol. Biol. Cell *17*, 4051–4062.

Gawaz, M., Douglas, M.G., and Klingenberg, M. (1990). Structure-function studies of adenine nucleotide transport in mitochondria. II. Biochemical analysis of distinct AAC1 and AAC2 proteins in yeast. J. Biol. Chem. *265*, 14202–14208.

Giraud, M.F., and Velours, J. (1997). The absence of the mitochondrial ATP synthase delta subunit promotes a slow growth phenotype of rho- yeast cells by a lack of assembly of the catalytic sector F_1. Eur. J. Biochem. *245*, 813–818.

Gracey, A.Y., Troll, J.V., and Somero, G.N. (2001). Hypoxia-induced gene expression profiling in the euryoxic fish Gillichthys mirabilis. Proc. Natl. Acad. Sci. U.S.a. *98*, 1993–1998.

Green DE, Tzagoloff A. (1966). The mitochondrial electron transfer chain. Arch. Biochem. Biophys *116*(1), 293–304.

HackenbrockCR. (1977). Molecular organization and the fluid nature of the mitochondrial energy transducing membrane. Struct. Biol. Membr. *34*, 199–234.

Hackenbrock CR, Chazotte B, Gupte SS. (1986) The random collision model and a critical assessment of diffusion and collision in mitochondrial electron transport. J. Bioenerg. Biomembr. *18*(5), 331–68

Hatefi, Y. (1985). The mitochondrial electron transport and oxidative phosphorylation system. Annu. Rev. Biochem. *54*, 1015–1069.

Hatefi, Y., Haavik, A.G., Fowler, L.R., and Griffiths, D.E. (1962). Studies on the electron transfer system. XLII. Reconstitution of the electron transfer system. J. Biol. Chem. *237*, 2661–2669.

Hayashi, T., Asano, Y., Shintani, Y., Aoyama, H., Kioka, H., Tsukamoto, O., Hikita, M., Shinzawa-Itoh, K., Takafuji, K., Higo, S., et al. (2015). Higd1a is a positive regulator of cytochrome coxidase. Proc. Natl. Acad. Sci. U.S.a. *112*, 1553–1558.

Helbig, A.O., de Groot, M.J.L., van Gestel, R.A., Mohammed, S., de Hulster, E.A.F., Luttik, M.A.H., Daran-Lapujade, P., Pronk, J.T., Heck, A.J.R., and Slijper, M. (2009). A three-way proteomics strategy allows differential analysis of yeast mitochondrial membrane protein complexes under anaerobic and aerobic conditions. Proteomics *9*, 4787–4798.

Hell, K., Neupert, W., and Stuart, R.A. (2001). Oxa1p acts as a general membrane insertion machinery for proteins encoded by mitochondrial DNA. Embo J. *20*, 1281–1288.

Hell, K., Tzagoloff, A., Neupert, W., and Stuart, R.A. (2000). Identification of Cox20p, a novel protein involved in the maturation and assembly of cytochrome oxidase subunit 2. J. Biol. Chem. *275*, 4571–4578.

Herrmann, J.M., Stuart, R.A., Craig, E.A., and Neupert, W. (1994). Mitochondrial heat shock protein 70, a molecular chaperone for proteins encoded by mitochondrial DNA. J. Cell Biol. *127*, 893–902.

Herrmann, J.M., and Funes, S. (2005). Biogenesis of cytochrome oxidase-sophisticated assembly lines in the mitochondrial inner membrane. Gene *354*, 43–52.

Hess, D.C., Myers, C.L., Huttenhower, C., Hibbs, M.A., Hayes, A.P., Paw, J., Clore, J.J., Mendoza, R.M., Luis, B.S., Nislow, C., et al. (2009). Computationally driven, quantitative experiments discover genes required for mitochondrial biogenesis. PLoS Genet. *5*, e1000407.

Hodge, M. R., Kim, G., Singh, K., Cumsky, M. G. (1989) Inverse regulation of the yeast *COX5* genes by oxygen and heme. Mol. Cell. Biol. *9*:1958–1964.

Horan, S., Bourges, I., Taanman, J.-W., and Meunier, B. (2005). Analysis of COX2 mutants reveals cytochrome oxidase subassemblies in yeast. Biochem. J. *390*, 703–708.

Hunte, C., Koepke, J., Lange, C., Rossmanith, T., and Michel, H. (2000). Structure at 2.3 A resolution of the cytochrome bc(1) complex from the yeast Saccharomyces cerevisiae co-crystallized with an antibody Fv fragment. Structure *8*, 669–684.

Iwata, S., Ostermeier, C., Ludwig, B., and Michel, H. (1995). Structure at 2.8 A resolution of cytochrome *c* oxidase from Paracoccus denitrificans. Nature.

Jan, P.S., Esser, K., E. Pratje, E., Michaelis, G. (2000) Som1, a third component of the yeast mitochondrial inner membrane peptidase complex that contains Imp1 and Imp2. Mol. Gen. Genet. *263* (3), 483-491

Jarrett, S.G., Lewin, A.S., and Boulton, M.E. (2010). The importance of mitochondria in age-related and inherited eye disorders. Ophthalmic Res. *44*, 179–190.

Jia, L., Dienhart, M.K., and Stuart, R.A. (2007). Oxa1 directly interacts with Atp9 and mediates its assembly into the mitochondrial F1Fo-ATP synthase complex. Mol. Biol. Cell *18*, 1897–1908.

Jia, L., Kaur, J., and Stuart, R.A. (2009). Mapping of the Saccharomyces cerevisiae Oxa1-mitochondrial ribosome interface and identification of MrpL40, a ribosomal protein in close proximity to Oxa1 and critical for oxidative phosphorylation complex assembly. Eukaryotic Cell *8*, 1792–1802.

Jiang, F., Rizavi, H.S., and Greenberg, M.L. (1997). Cardiolipin is not essential for the growth of Saccharomyces cerevisiae on fermentable or non-fermentable carbon sources. Mol. Microbiol. *26*, 481–491.

Jiang, F., Ryan, M.T., Schlame, M., Zhao, M., Gu, Z., Klingenberg, M., Pfanner, N., and Greenberg, M.L. (2000). Absence of Cardiolipin in the crd1 Null Mutant Results in Decreased Mitochondrial Membrane Potential and Reduced Mitochondrial Function. Journal of Biological Chemistry *275*, 22387–22394.

Kawamata, H., and Manfredi, G. (2010). Mitochondrial dysfunction and intracellular calcium dysregulation in ALS. Mech. Ageing Dev. *131*, 517–526.

Keilin, D., and Hartree, E.F. (1937). Preparation of pure cytochrome c from heart muscle and some of its properties.

Klingenberg, M. (1989) Molecular aspects of the adenine nucleotide carrier from mitochondria. Archives of biochemistry and biophysics *270*, 1–14.

Klingenberg, M. (2008). The ADP and ATP transport in mitochondria and its carrier. Biochimica Et Biophysica Acta (BBA) - Biomembranes *1778*, 1978–2021.

Klingenberg, M. (2009). Cardiolipin and mitochondrial carriers. Biochimica et Biophysica Acta. BBA - Biomembranes *1788*, 2048–2058.

Kloeckener-Gruissem, B., and McEwen, J.E. (1988). Identification of a third nuclear protein-coding gene required specifically for posttranscriptional expression of the mitochondrial COX3 gene in *Saccharomyces cerevisiae*. Journal of Bacteriology *170*, 1399-1402.

Kolarov, J., Kolarova, N., and Nelson, N. (1990). A third ADP/ATP translocator gene in yeast. J. Biol. Chem. *265*, 12711–12716.

Kones, R. (2010). Parkinson's disease: mitochondrial molecular pathology, inflammation, statins, and therapeutic neuroprotective nutrition. Nutr Clin Pract *25*, 371–389.

Krämer, R., Klingenberg, M. (1980) Modulation of the reconstituted adenine nucleotide exchange by membrane potential. Biochemistry *19*(3):556-60.

Krause, K., Lopes de Souza, R., Roberts, D.G.W., and Dieckmann, C.L. (2004). The mitochondrial message-specific mRNA protectors Cbp1 and Pet309 are associated in a high-molecular weight complex. Mol. Biol. Cell *15*, 2674–2683.

Kwast, K. E., Burke, P. V., Staahl, B. T., Poyton, R. O. (1999) Oxygen sensing in yeast: evidence for the involvement of the respiratory chain in regulating the transcription of a subset of hypoxic genes. Proc. Natl. Acad. Sci. U.S.A. *96*, 5446–5451

Kyhse-Andersen, J., (1984) Electroblotting of multiple gels: a simple apparatus without buffer tank for rapid transfer of proteins from polyacrylamide to nitrocellulose. J Biochem. Biophys. Methods *10*, 203–209.

Laemmli, U.K., (1970) Cleavage of Structural Proteins during the Assembly of the Head of Bacteriophage T4. Nature *227*, 680-685.

Lane, N., and Martin, W. (2010). The energetics of genome complexity. Nature *467*, 929–934.

Lange, C., Nett, J.H., Trumpower, B.L., and Hunte, C. (2001). Specific roles of protein-phospholipid interactions in the yeast cytochrome bc_1 complex structure. EMBO J. *20*, 6591–6600.

Lawson, J.E., and Douglas, M.G. (1988). Separate genes encode functionally equivalent ADP/ATP carrier proteins in *Saccharomyces cerevisiae*. Isolation and analysis of *AAC2*. Journal of Biological Chemistry *263*, 14812-14818.

Lawson, J.E., Gawaz, M., and Klingenberg, M. (1990). Structure-function studies of adenine nucleotide transport in mitochondria. I. Construction and genetic analysis of yeast mutants encoding the ADP/ATP carrier protein of mitochondria. Journal of Biological Chemistry *265*, 14195-14201.

Lenaz, G., and Genova, M.L. (2009). Structural and functional organization of the mitochondrial respiratory chain: a dynamic super-assembly. Int. J. Biochem. Cell Biol. *41*, 1750–1772.

Lill, R., and Mühlenhoff, U. (2008). Maturation of iron-sulfur proteins in eukaryotes: mechanisms, connected processes, and diseases. Annu. Rev. Biochem. *77*, 669–700.

Lindert, S., Maslennikov, I., Chiu, E.J.C., Pierce, L.C., McCammon, J.A., and Choe, S. (2014). Biochemical and Biophysical Research Communications. Biochemical and Biophysical Research Communications *445*, 724–733.

Lucas, M.F., Rousseau, D.L., and Guallar, V. (2011). Electron transfer pathways in cytochrome c oxidase. Biochim. Biophys. Acta *1807*, 1305–1313.

McKenzie, M., Lazarou, M., Thorburn, D.R., and Ryan, M.T. (2006). Mitochondrial respiratory chain supercomplexes are destabilized in Barth Syndrome patients. J. Mol. Biol. *361*, 462–469.

Mick, D.U., Fox, T.D., and Rehling, P. (2011). Inventory control: cytochrome *c* oxidase assembly regulates mitochondrial translation. Nat. Rev. Mol. Cell Biol. *12*, 14–20.

Mick, D.U., Wagner, K., van der Laan, M., Frazier, A.E., Perschil, I., Pawlas, M., Meyer, H.E., Warscheid, B., and Rehling, P. (2007). Shy1 couples Cox1 translational regulation to cytochrome c oxidase assembly. EMBO J. *26*, 4347–4358.

Mileykovskaya, E., Zhang, M., and Dowhan, W. (2005). Cardiolipin in energy transducing membranes. Biochemistry Mosc. *70*, 154–158.

Mileykovskaya, E., and Dowhan, W. (2014). Chemistry and Physics of Lipids. Chemistry and Physics of Lipids *179*, 42–48.

Mileykovskaya, E., Penczek, P.A., Fang, J., Mallampalli, V.K.P.S., Sparagna, G.C., and Dowhan, W. (2012). Arrangement of the respiratory chain complexes in Saccharomyces cerevisiae supercomplex III2IV2 revealed by single particle cryo-electron microscopy. Journal of Biological Chemistry *287*, 23095–23103.

Mitchell, P. (1961) Nature (London) *191*, 144-148.

Mitchell, P. (1966) Chemiosmotic Coupling in Oxidative and Photosynthetic Phosphorylation, Glynn Research, Bodmin

Mitchell, P. (1968) Chemiosmotic Coupling and Energy Transduction, Glynn Research, Bodmin

Mulero, J.J., and Fox, T.D. (1993). Alteration of the Saccharomyces cerevisiae COX2 mRNA 5'-untranslated leader by mitochondrial gene replacement and functional interaction with the translational activator protein PET111. Mol. Biol. Cell *4*, 1327–1335.

Nunnari, J., Fox, T.D., and Walter, P. (1993). A mitochondrial protease with two catalytic subunits of nonoverlapping specificities. Science *262*, 1997–2004.

Nunnari, J., and Suomalainen, A. (2012). Mitochondria: In Sickness and in Health. Cell *148*, 1145–1159.

Nury, H., Dahout-Gonzalez, C., Trézéguet, V., Lauquin, G.J.-M., Brandolin, G., and Pebay-Peyroula, E. (2006). Relations between structure and function of the mitochondrial ADP/ATP carrier. Annu. Rev. Biochem. *75*, 713–741.

O'Malley, K., Pratt, P., Robertson, J., Lilly, M., and Douglas, M.G. (1982). Selection of the nuclear gene for the mitochondrial adenine nucleotide translocator by genetic complementation of the op1 mutation in yeast. J. Biol. Chem. *257*, 2097–2103.

Ogunjimi, E.O., Pokalsky, C.N., Shroyer, L.A., and Prochaska, L.J. (2000). Evidence for a conformational change in subunit III of bovine heart mitochondrial cytochrome *c* oxidase. J. Bioenerg. Biomembr. *32*, 617–626.

Palmieri, F. (2013). The mitochondrial transporter family SLC25: identification, properties and physiopathology. Mol. Aspects Med. *34*, 465–484.

Paumard, P., Vaillier, J., Coulary, B., Schaeffer, J., Soubannier, V., Mueller, D.M., Brèthes, D., di Rago, J.-P., and Velours, J. (2002). The ATP synthase is involved in generating mitochondrial cristae morphology. Embo J. *21*, 221–230.

Pebay-Peyroula, E., and Brandolin, G. (2004). Nucleotide exchange in mitochondria: insight at a molecular level. Curr. Opin. Struct. Biol. *14*, 420–425.

Pebay-Peyroula, E., Dahout-Gonzalez, C., Kahn, R., Trézéguet, V., Lauquin, G.J.-M., and Brandolin, G. (2003). Structure of mitochondrial ADP/ATP carrier in complex with carboxyatractyloside. Nature *426*, 39–44.

Pfanner, N., Tropschug, M., and Neupert, W. (1987). Mitochondrial protein import: nucleoside triphosphates are involved in conferring import-competence to precursors. Cell *49*, 815-823.

Pfeiffer, K., Gohil, V., Stuart, R.A., Hunte, C., Brandt, U., Greenberg, M.L., and Schägger, H. (2003). Cardiolipin Stabilizes Respiratory Chain Supercomplexes. Journal of Biological Chemistry *278*, 52873–52880.

Pineau, B., Bourge, M., Marion, J., Mauve, C., Gilard, F., Maneta-Peyret, L., Moreau, P., Satiat-Jeunemaître, B., Brown, S.C., De Paepe, R., et al. (2013). The importance of cardiolipin synthase for mitochondrial ultrastructure, respiratory function, plant development, and stress responses in Arabidopsis. Plant Cell *25*, 4195–4208.

Poutre, C.G., and Fox, T.D. (1987). PET111, a *Saccharomyces cerevisiae* nuclear gene required for translation of the mitochondrial mRNA encoding cytochrome *c* oxidase subunit II. Genetics *115*, 637–647.

Reinders, J., Zahedi, R.P., Pfanner, N., Meisinger, C., Sickmann, A., (2006) Toward the complete yeast mitochondrial proteome: multidimensional separation techniques for mitochondrial proteomics. J Proteome Res. *5*, 1543–1554.

Ren, J., Pulakat, L., Whaley-Connell, A., and Sowers, J.R. (2010). Mitochondrial biogenesis in the metabolic syndrome and cardiovascular disease. J. Mol. Med. *88*, 993–1001.

Riccio, P., Aquila, H., Klingenberg, M., (1975) Purification of the carboxy-atractylate binding protein from mitochondria. FEBS Lett. *56*(1), 133–138.

Rich, P.R., and Marechal, A. (2013). Functions of the hydrophilic channels in protonmotive cytochrome c oxidase. Journal of the Royal Society Interface *10*, 20130183–20130183.

Rosswell, D.F. and White, E. H., (1978) The chemiluminescence of luminol and related hydrazides. Meth. Enzymol. *57*, 409.

Ruprecht, J.J., Hellawell, A.M., Harding, M., Crichton, P.G., McCoy, A.J., and Kunji, E.R.S. (2014). Structures of yeast mitochondrial ADP/ATP carriers support a domain-based alternating-access transport mechanism. Proc. Natl. Acad. Sci. U.S.A. *111*, E426–E434.

Ryan, M.T., Müller, H., and Pfanner, N. (1999). Functional staging of ADP/ATP carrier translocation across the outer mitochondrial membrane. J. Biol. Chem. *274*, 20619–20627.

Rydström Lundin, C., Ballmoos, von, C., Ott, M., Ädelroth, P., and Brzezinski, P. (2016). Regulatory role of the respiratory supercomplex factors in *Saccharomyces cerevisiae*. Proc. Natl. Acad. Sci. U.S.A. *113*, E4476–E4485.

Sabová, L., Zema, I., Supek, F., Kolarov, J., **(**1993) Transcriptional control of AAC3 gene encoding mitochondrial ADP/ATP translocator in *Saccharomyces cerevisiae* by oxygen, heme and ROX1 factor. Eur. J. Biochem. *213*: 547–553.

Saddar, S., Dienhart, M.K., and Stuart, R.A. (2008). The F_1F_O-ATP synthase complex influences the assembly state of the cytochrome bc_1-cytochrome oxidase supercomplex and its association with the TIM23 machinery. J. Biol. Chem. *283*, 6677–6686.

Saiki, K., Mogi, T., Hori, H., Tsubaki, M., and Anraku, Y. (1993). Identification of the functional domains in heme O synthase. Site-directed mutagenesis studies on the cyoE gene of the cytochrome bo operon in *Escherichia coli.* J. Biol. Chem. *268*, 26927–26934.

Sambrook, J., Fritschi, E.F., and Maniatis, T., (1989) Molecular cloning: a laboratory manual, Cold Spring Harbor Laboratory Press, New York.

Santo-Domingo, J., and Demaurex, N. (2012). The renaissance of mitochondrial pH. J Gen Physiol *139*, 415–423.

Saraste, M. (1999). Oxidative phosphorylation at the fin de siècle. Science *283*, 1488–1493.

Sas, K., Párdutz, Á., Toldi, J., and Vécsei, L. (2010). Dementia, stroke and migraine--some common pathological mechanisms. J. Neurol. Sci. *299*, 55–65.

Schäfer, E., Seelert, H., Reifschneider, N.H., Krause, F., Dencher, N.A., and Vonck, J. (2006). Architecture of active mammalian respiratory chain supercomplexes. J. Biol. Chem. *281*, 15370–15375.

Schägger, H., and Pfeiffer, K. (2000). Supercomplexes in the respiratory chains of yeast and mammalian mitochondria. EMBO J. *19*, 1777–1783.

Schägger, H. (2002). Respiratory chain supercomplexes of mitochondria and bacteria. Biochim. Biophys. Acta *1555*, 154–159.

Scheffler, I.E. (2001). Mitochondria make a come back. Adv. Drug Deliv. Rev. *49*, 3–26.

Sedlák, E., and Robinson, N.C. (2015). Destabilization of the Quaternary Structure of Bovine Heart Cytochrome cOxidase upon Removal of Tightly Bound Cardiolipin. Biochemistry *54*, 5569–5577.

Sedlák, E., Panda, M., Dale, M.P., Weintraub, S.T., and Robinson, N.C. (2006). Photolabeling of Cardiolipin Binding Subunits within Bovine Heart Cytochrome *c* Oxidase. Biochemistry *45*, 746–754.

Shen, C., Nettleton, D., Jiang, M., Kim, S.K., and Powell-Coffman, J.A. (2005). Roles of the HIF-1 hypoxia-inducible factor during hypoxia response in Caenorhabditis elegans. J. Biol. Chem. *280*, 20580–20588.

Shingú-Vázquez, M., Camacho-Villasana, Y., Sandoval-Romero, L., Butler, C.A., Fox, T.D., and Pérez-Martínez, X. (2010). The carboxyl-terminal end of Cox1 is required for feedback assembly regulation of Cox1 synthesis in Saccharomyces cerevisiae mitochondria. J. Biol. Chem. *285*, 34382–34389.

Shinzawa-Itoh, K., Aoyama, H., Muramoto, K., Terada, H., Kurauchi, T., Tadehara, Y., Yamasaki, A., Sugimura, T., Kurono, S., Tsujimoto, K., et al. (2007). Structures and physiological roles of 13 integral lipids of bovine heart cytochrome c oxidase. Embo J. *26*, 1713–1725.

Sickmann, A., Reinders, J., Wagner, Y., Joppich, C., Zahedi, R., Meyer, H.E., Schönfisch, B., Perschil, I., Chacinska, A., Guiard, B., et al. (2003). The proteome of Saccharomyces cerevisiae mitochondria. Proc. Natl. Acad. Sci. U.S.A. *100*, 13207–13212.

Soto, I.C., Fontanesi, F., Liu, J., and Barrientos, A. (2012). Biogenesis and assembly of eukaryotic cytochrome c oxidase catalytic core. Biochim. Biophys. Acta *1817*, 883–897.

Stiburek, L., Vesela, K., Hansikova, H., Pecina, P., Tesarova, M., Cerna, L., Houstek, J., and Zeman, J. (2005). Tissue-specific cytochrome *c* oxidase assembly defects due to mutations in SCO2 and SURF1. Biochem. J. *392*, 625–632.

Strecker, V., Kadeer, Z., Heidler, J., Cruciat, C.-M., Angerer, H., Giese, H., Pfeiffer, K., Stuart, R.A., and Wittig, I. (2016). Biochimica et Biophysica Acta. BBA - Molecular Cell Research *1863*, 1643–1652.

Strogolova, V., Furness, A., Robb-McGrath, M., Garlich, J., and Stuart, R.A. (2012). Rcf1 and Rcf2, Members of the Hypoxia-Induced Gene 1 Protein Family, Are Critical Components of the Mitochondrial Cytochrome bc_1-Cytochrome *c* Oxidase Supercomplex. Mol. Cell. Biol. *32*, 1363–1373.

Stuart, R.A. (2008). Supercomplex organization of the oxidative phosphorylation enzymes in yeast mitochondria. J. Bioenerg. Biomembr. *40*, 411–417.

Suthammarak, W., Yang, Y.-Y., Morgan, P.G., and Sedensky, M.M. (2009). Complex I function is defective in complex IV-deficient *Caenorhabditis elegans*. J. Biol. Chem. *284*, 6425–6435.

Tamura, Y., Harada, Y., Nishikawa, S.-I., Yamano, K., Kamiya, M., Shiota, T., Kuroda, T., Kuge, O., Sesaki, H., Imai, K., et al. (2013). Tam41 Is a CDP-Diacylglycerol Synthase Required for Cardiolipin Biosynthesis in Mitochondria. Cell Metab. *17*, 709–718.

Tiranti, V., Corona, P., Greco, M., Taanman, J.W., Carrara, F., Lamantea, E., Nijtmans, L., Uziel, G., and Zeviani, M. (2000). A novel frameshift mutation of the mtDNA COIII gene leads to impaired assembly of cytochrome *c* oxidase in a patient affected by Leigh-like syndrome. Hum. Mol. Genet. *9*, 2733–2742.

Tsukihara, T., Aoyama, H., Yamashita, E., Tomizaki, T., Yamaguchi, H., Shinzawa-Itoh, K., Nakashima, R., Yaono, R., and Yoshikawa, S. (1995). Structures of metal sites of oxidized bovine heart cytochrome *c* oxidase at 2.8 Å. Science *269*, 1069–1074.

Tsukihara, T., Aoyama, H., Yamashita, E., Tomizaki, T., Yamaguchi, H., Shinzawa-Itoh, K., Nakashima, R., Yaono, R., and Yoshikawa, S. (1996). The whole structure of the 13-subunit oxidized cytochrome *c* oxidase at 2.8 Å. Science *272*, 1136–1144.

Tzagoloff, A., Nobrega, M., Gorman, N., Sinclair, P. (1993) On the functions of the yeast COX10 and COX11 gene products. Biochem. Mol. Biol. Int. *31*(3), 593-598

Varanasi, L., Mills, D., Murphree, A., Gray, J., Purser, C., Baker, R., and Hosler, J. (2006). Altering conserved lipid binding sites in cytochrome *c* oxidase of Rhodobacter sphaeroides perturbs the interaction between subunits I and III and promotes suicide inactivation of the enzyme. Biochemistry *45*, 14896–14907.

Vukotic, M., Oeljeklaus, S., Wiese, S., Vögtle, F.N., Meisinger, C., Meyer, H.E., Zieseniss, A., Katschinski, D.M., Jans, D.C., Jakobs, S., et al. (2012). Rcf1 mediates cytochrome oxidase assembly and respirasome formation, revealing heterogeneity of the enzyme complex. Cell Metab. *15*, 336–347.

Waldbaum, S., and Patel, M. (2010). Mitochondrial dysfunction and oxidative stress: a contributing link to acquired epilepsy? J. Bioenerg. Biomembr. *42*, 449–455.

Wallace, D.C. (2005). A mitochondrial paradigm of metabolic and degenerative diseases, aging, and cancer: a dawn for evolutionary medicine. Annu. Rev. Genet. *39*, 359–407.

Wang, J., Cao, Y., Chen, Y., Chen, Y., Gardner, P., and Steiner, D.F. (2006). Pancreatic beta cells lack a low glucose and O_2-inducible mitochondrial protein that augments cell survival. Proc. Natl. Acad. Sci. U.S.a. *103*, 10636–10641.

Wikstrom, M.K. (1977). Proton pump coupled to cytochrome *c* oxidase in mitochondria. Nature *266*, 271–273.

Yoshikawa, S., Muramoto, K., and Shinzawa-Itoh, K. (2011). Proton-pumping mechanism of cytochrome *c* oxidase. Annu Rev Biophys *40*, 205–223.

Yoshikawa, S., Muramoto, K., Shinzawa-Itoh, K., and Mochizuki, M. (2012). Structural studies on bovine heart cytochrome *c* oxidase. Biochimica et Biophysica Acta. BBA - Bioenergetics *1817*, 579–589.

Zhang, M., Mileykovskaya, E., and Dowhan, W. (2002). Gluing the Respiratory Chain Together. Cardiolipin is required for supercomplex formation in the inner mitochondrial membrane. J. Biol. Chem. *277*, 43553–43556.

Zhang, M., Mileykovskaya, E., and Dowhan, W. (2005). Cardiolipin is essential for organization of complexes III and IV into a supercomplex in intact yeast mitochondria. J. Biol. Chem. *280*, 29403–29408.